HELSINGIN YLIOPISTO
HELSINGFORS UNIVERSITET
UNIVERSITY OF HELSINKI

Master's thesis

Hydrogeology and Environmental geology study track

Retention of sediment and nutrients in cultivated mineral soil and organic soil catchments on two-stage channels in southern Finland

Jani Wikström

2023

Supervisors: Tom Jilbert and Kaisa Västilä

Master's Programme in Geology and Geophysics

Faculty of Science

Tiedekunta – Fakultet – Faculty Faculty of Science	Koulutusohjelma – Utbildningsprogram – Degree programme Master's Programme in Geology and Geophysics

Opintosuunta – Studieinrikting – Study track
Hydrogeology and Environmental Geology

Tekijä – Författare – Author
Jani Wikström

Työn nimi – Arbetets titel – Title
Retention of sediment and nutrients in cultivated mineral soil and organic soil catchments on two-stage channels in southern Finland

Työn laji – Arbetets art – Level	Aika – Datum – Month and year	Sivumäärä – Sidoantal – Number of pages
Master's Thesis	11/2023	78 pp. + 2 appendices

Tiivistelmä – Referat – Abstract

Agricultural nutrient inputs to surface waters play a major role in eutrophication and the decrease in water quality in downstream waters. Two-stage channel is a water management practice designed to reduce flooding in agricultural fields but has been shown to reduce nutrient losses from upstream catchment by nutrient rich sediment deposition and providing suitable conditions for soluble reactive phosphorus sorption and precipitation. Fresh sediment deposition from three contrasting two-stage channel floodplains in southern Finland was used to study sediment accumulation and associated nutrient dynamics. Total of 32 sediment traps were installed by Valumavesi project (Finnish Environment Institute) between summer and fall in 2021 and retrieved in the summer of 2022 and analysed for sediment accumulation, geochemical composition, and nutrient content, and phosphorus speciation.

Cultivated mineral soils experienced more sediment transport (2.5–6.4 kg m^{-2} a^{-1}) than organic soils (0.2 kg m^{-2} a^{-1}) that controlled the nutrient retention in floodplains. In one of the mineral soil sites this estimated 3–4 % of stream total suspended sediment load (2.3–3.2 tons of sediment deposition) over 223 day measuring period along 250 m floodplain. Implementation of vegetation management methods could increase the retention efficiency to 3.3–4.7 % of stream load. Spatial variability in sediment deposition was controlled by topography, inundation extent and frequency, channel stability, and vegetation management.

Most of the variability in study sites geochemistry was explained by minerogenic and organic matter associated with catchment surficial soils. Independent of soil type, manganese explained horizontal variability between sediment trap samples and vertical variability in core samples from previous studies. Changes in redox sensitive manganese and iron concentrations often coincided with changes in phosphorus concentration and speciation. This was used to interpret phosphorus dynamics. Iron bound phosphorus was the dominant species in cultivated mineral soil and forested peatland catchments. Ther former soils had more detrital apatite minerals associated with less weathered Littorina Sea clays, while organic soils were associated with phosphorus in non-reducible metals that precipitate in more anoxic conditions.

Floodplain soil phosphorus saturation was not observed but could affect the two-stage channel management in the future as more nutrients accumulate to the floodplains. Regardless, all two-stage channels were able to retain nutrient rich sediments to floodplains that should have a positive influence on reducing nutrient loads from agricultural streams in downstream waters.

Avainsanat – Nyckelord – Keywords
Eutrophication, Phosphorus, Phosphorus speciation, Sediment, Two-stage channel, Nutrient loading, Floodplain

Säilytyspaikka – Förvaringställe – Where deposited
University of Helsinki e-thesis platform (HELDA)

Muita tietoja – Övriga uppgifter – Additional information

32 figures and 11 tables

Tiedekunta – Fakultet – Faculty Matemaattis-luonnontieteellinen tiedekunta	Koulutusohjelma – Utbildningsprogram – Degree programme Geologian ja geofysiikan maisteriohjelma

Opintosuunta – Studieinrikting – Study track
Hydro- ja ympäristögeologian opintosuunta

Tekijä – Författare – Author
Jani Wikström

Työn nimi – Arbetets titel – Title
Sedimentin ja ravinteiden pidättyminen eteläsuomalaisilla kaksitasouomilla viljellyissä kivennäismaissa, sekä turvemaan valuma-alueella

Työn laji – Arbetets art – Level	Aika – Datum – Month and year	Sivumäärä – Sidoantal – Number of pages
Maisterintutkielma	11/2023	78 s. + 2 liitteet

Tiivistelmä – Referat – Abstract

Maatalouden ravinnekuormituksella on suuri vaikutus viljelysmaiden alapuolisten vesistöjen rehevöitymiseen ja veden laatuun. Kaksitasouomat on suunniteltu viljelysmaiden tulvavesien hallintaan, mutta ne myös vähentävät ravinteiden huuhtoutumista yläjuoksun valuma-alueilta, kun virran kuljettamat sedimentit kertyvät tulvatasanteille. Tulvatasanteet tarjoavat myös suotuisat olosuhteet liukoisen fosforin sorptiolle sekä saostumiselle. Sedimentin ja siihen liittyvää ravinteiden kertymistä tulvatasanteille seurattiin kolmelta toisistaan erottuvalta eteläsuomalaiselta kaksitasouomalta niiden keskinäisen dynamiikan tutkimiseen. Suomen ympäristökeskuksen Valumavesi projekti asensi 32 keräintä kaksitasouoman tulvatasanteille 2021 kesän ja syksyn aikana, jotka kerättiin vuoden 2022 kesällä ja niistä analysoitiin sedimenttikertymä, geokemiallinen koostumus, ravinnepitoisuudet sekä fosforin eri fraktiot.

Sedimenttikertymä oli suurempaa viljellyillä kivennäismailla (2.5–6.4 kg m^{-2} a^{-1}), kuin orgaanisilla viljelysmailla (0.2 kg m^{-2} a^{-1}), mikä vaikutti merkittävästi tulvatasanteiden ravinnekertymään. Yhdellä tutkimusalueella tämä tarkoitti 3–4 % uoman kiintoaineksen määrästä (2.3–3.2 tonnin sedimenttikertymää) 250 m tulvatasanteelle 223 päivän aikana. Jos tulvatasanteen kasvillisuuden niitto olisi laajennettu koskemaan koko tulvatasannetta, olisi sedimentin pidätyskyky kasvanut 3.3–4.7 % uoman kiintoaineskuormasta. Sedimenttikertymän paikkakohtaiseen vaihteluun vaikuttivat pinnan topografia, tulvinnan laajuus, tulvimistiheys, uoman vakaus ja kasvillisuuden hoitomenetelmät.

Tutkimusalueiden geokemiallisen koostumuksen vaihtelu selittyi enimmäkseen sedimenttien kivennäis- ja orgaanisen aineksen määrällä, joka juontui valuma-alueen maaperästä. Maaperästä riippumattomat mangaanipitoisuudet selittivät tutkimusalueiden paikallista horisontaalista vaihtelua sedimenttikeräin näytteissä ja vertikaalista vaihtelua aikaisempien tutkimuksien sedimenttiprofiileissa. Redox-herkän mangaanin ja fosforifraktioiden vaihtelu tapahtui usein samanaikaisesti, jota käytettiin fosforidynamiikan tutkimiseen. Rautasidonnainen fosfori oli merkittävin fosforifraktio viljellyillä mineraali ja orgaanisilla mailla. Kivennäismailla oli enemmän detritaalista apatiittia vähän rapautuneista Litorinanmeren aikaisista savikoista, kun taas orgaanisilla mailla oli enemmän fosforia kiinnittyneenä ei-redusoituviin metalleihin, jotka muodostuvat hapettomammissa olosuhteissa.

Tulvatasanteille kertyneet sedimentit eivät olleet kyllästyneet fosforista, mutta se on mahdollista ravinnerikkaiden sedimenttien edelleen kertyessä, jolla voi olla vaikutusta kaksitasouoman kunnostusmenetelmiin tulevaisuudessa. Kaikki tutkitut kaksitasouomat pidättivät ravinnerikkaita sedimenttejä, jonka tulisi näkyä pienempänä ravinnekuormituksena alajuoksun vesistöissä.

Avainsanat – Nyckelord – Keywords
Rehevöityminen, Fosfori, Fosfori fraktiot, Sedimentti, Kaksitasouoma, Ravinnekuormitus, Tulvatasanne

Säilytyspaikka – Förvaringställe – Where deposited
Helsingin yliopisto opinnäytetietokanta HELDA

Muita tietoja – Övriga uppgifter – Additional information

32 kuvaa ja 11 taulukkoa

CONTENTS

1. INTRODUCTION

1.1. Soil nutrients and eutrophication

Increasing demand for agricultural products has indirectly led to a decrease in surface water quality. Agricultural soils lack of sufficient crop nutrients is commonly supplemented by use of fertilizers. Biotic and abiotic nutrient cycles ensure that unused fertilizer nutrients are transported into surface water bodies and coastal areas, causing eutrophication, and creating continuous need for new fertilizer additions. Excess nutrients in water bodies increase the aquatic vegetation growth that will consume oxygen from the water as it decays. Lack of oxygen and change in the water quality by excess nutrients and increased turbidity can lead to change in biota and reduced biodiversity (e.g., Smith 2003, Smith et al. 2006). The Finnish Baltic Sea coastal area has long suffered from the excess nutrient transport and even with vast efforts has yet to reach good water quality status. Recent reports by HELCOM state that in 2017, the nutrient load to Baltic Sea was dominated by riverine transport, where agriculture and managed forests had large contributions to the loads (HELCOM 2022). Finnish inland surface water quality has been improved using various methods such as raising lake water level, river restoration, removal of phosphorus saturated soils, and building wetlands and settling pools (Aho et al. 1999). Agricultural management practices have been developed to make land use more sustainable with less fertilizer inputs and improved water management practices. These include gypsum amendments (e.g., Uusitalo et al. 2012), constructed wetlands (Laakso et al. 2017), buffer zones, or two-stage channels (TSCs), all of which aim to reduce nutrient runoff and thus limit eutrophication.

Constructed TSCs are built to resemble natural river floodplain systems with a narrow main channel (MC) and vegetated floodplain (FP) on either or both sides of the MC that were developed to reduce overbank flooding to the fields during high water stages and reduce maintenance requirements (Powell et al. 2007). Two-stage channels morphology is designed to keep water in the MC during base flow conditions with low stream sediment transport and nutrient loads, but water level rises to the floodplains during high loads (Figure 1). Flooding frequency and duration can be controlled by TSC sizing (Powell et al. 2007, Västilä et al. 2016). Further benefits for TSCs have been found in nutrient and sediment transport management (e.g. Kallio 2010, Roley et al. 2012a, Roley et al. 2012b, Mahl et al. 2015, Västilä et al. 2016, Hodaj et al. 2017, Trentman et al. 2020). Floodplains under changing drying-wetting cycles enhance nitrogen removal via denitrification (Roley et al. 2012a, Dee and Tank 2020), retention of carbon, nutrients, and metals via sediment accumulation together with plant up-take and sorption to sediment surfaces (Davis et al. 2015, Hodaj et al. 2017, Kindervater and Steinman 2019, Nifong and Taylor 2021). Floodplains and associated vegetation decrease stream flow velocity, increasing the water retention time that enhances nutrient and sediment retention capability (Nifong and Taylor 2021). Phosphorus (P) cycling in floodplains are closely linked to that of iron (Fe). For example, low P sorption in floodplains has been linked to iron bound P (Fe-P) saturation in topsoil (Baldan et al. 2021). A key question in TSC research is to what extent TSCs can limit P transport and potentially reduce P loads to surface waters. Studies have recognized the release of iron associated P during reducing conditions but also resorption of P if enough free Fe or Al surfaces are available (Sah and Mikkelsen 1986, Jensen et al. 1992, Heiberg et al. 2012, Forsmann and Kjaergaard 2014). Some soils, such as sandy peatland, may maintain high P sorption capacity even in anoxic conditions (Heiberg et al. 2012). Humic substances have also been reported to decrease Fe-P release during anoxia (Tammeorg et al. 2022).

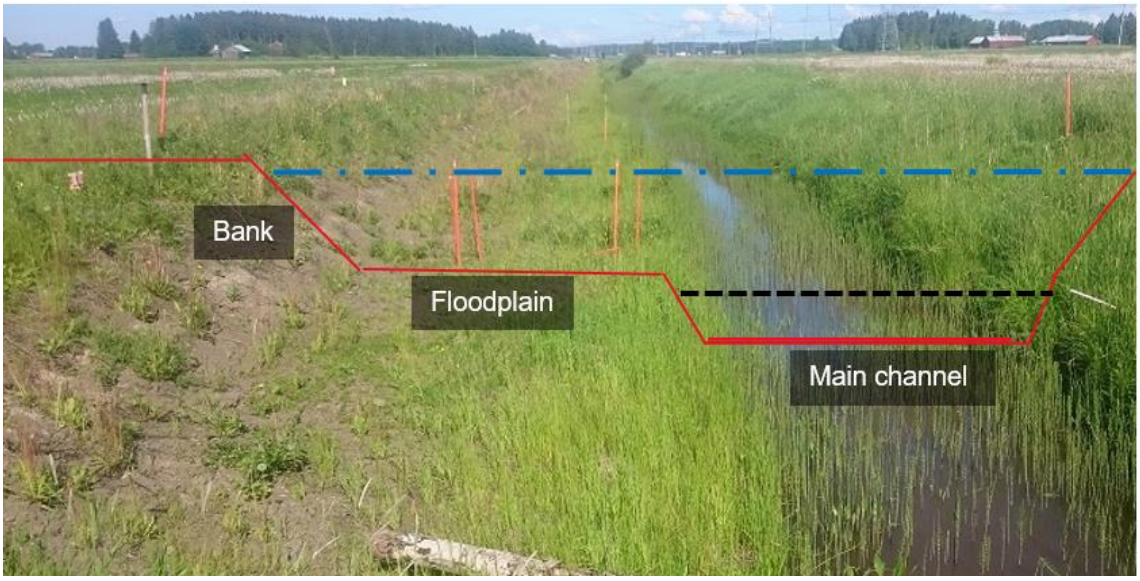

Figure 1. Uuhikonoja two-stage channel cross sectional view before growth season in June 2022, displaying the excavated morphology with bank, floodplain, and main channel. Black dashed line indicating the low water stage (baseflow) conditions visible in the figure and blue dash-dotted line the high-water stage (also referred as bankfull or stormflow) conditions. Picture: Jani Wikström.

In this project, three contrasting TSCs in southern Finland were studied for floodplain sediment transport and retention using geochemical analyses of material captured in sediment traps. Major and trace elements in digested samples, including P and Fe, were studied using inductively coupled plasma mass spectrometry (ICP-MS), while carbon (C) and nitrogen (N) were determined by thermal combustion. Nutrient (C, N, P) accumulation rates were calculated, and a closer inspection of P speciation was achieved using a tailored sequential extraction scheme (modified SEDEX). The primary goals of the thesis were 1) to quantify fresh sediment accumulation on TSC floodplains, 2) to identify and explain differences in geochemical compositions between the study catchments sedimentation on TSC floodplains, 3) to identify factors affecting sediment and nutrient retention with closer focus on P speciation. Results are compared using statistical analyses and connected to existing literature to identify nutrient retention dynamics, and the potential of TSCs in each study area to reduce catchments nutrient loads to water bodies.

1.2. Phosphorus bioavailability and mobility

The forms of P in soil are not equal when it comes to enhancing eutrophication. Different forms of P are studied using sequential extraction methods (SEDEX, e.g., Ruttenberg 1992) to determine how P is bound in the environment. Inorganic P forms include apatite rocks and secondary phases of iron or aluminium oxides, to which P is bound via sorption or co-precipitation (Lahermo et al. 1996). Apatite P released by weathering enters the soil solution in the form of soluble reactive phosphorus (SRP), from which it can be bio-assimilated into organic P-bearing molecules in plants (e.g., Richardson and Simpson 2011). During plant decay, P is again released into the dissolved phase but may be sorbed to soil Fe- or Al-oxides (e.g., Kaila 1963, Dieter et al. 2015), influencing its further bioavailability. A decrease in oxidation-reduction potential (redox) due to sediment burial or inundation by floodwaters, together with loading of degradable organic matter, enable P remobilization into the dissolved phase and thus transport to surface waters, potentially enhancing eutrophication in downstream areas. This is especially harmful in agricultural streams and lakes rich in C and N, where aquatic vegetation growth is limited mainly by P availability (e.g., Wyant et al. 2013, Ryan 2014).

A plethora of P fractionation methods have been published over the last few decades, that according to (Barrow et al. 2021) are all related to an original fractionation scheme by (Chang and Jackson 1957). Sequential extraction results must be interpreted with caution, due to the difficulty of separating each P-species into their own fractions without dissolving the subsequent fractions or loss of sample material (Ruban et al. 1999). The used extraction solutions are also not officially standardized, making the comparison between studies difficult. Barrow et al. (2021) reported that in some cases sequential extraction schemes could extract P from targeted species even without the discrete element present in the sample. Similarly, Kaila (1963) found some contradictory results from Finnish soil P-speciation results relative to literature but states that various complex processes control P-speciation that can affect the results significantly.

2. GEOLOGIC SETTING AND CLIMATE

2.1. Catchment characteristics and geology

Three study sites in southern Finland with TSC constructed for agriculture or forestry are located in Sipoo, Tammela, and Loppi (Figure 2) with catchment size, land use, average elevation in Table 1. TSCs next to Ritobäcken (Sipoo) and Uuhikonoja (Tammela) represent agricultural sites with mineral soil, while Pipakallionsuo (Loppi) catchment represents forested peatland with organic and till dominated surficial soils.

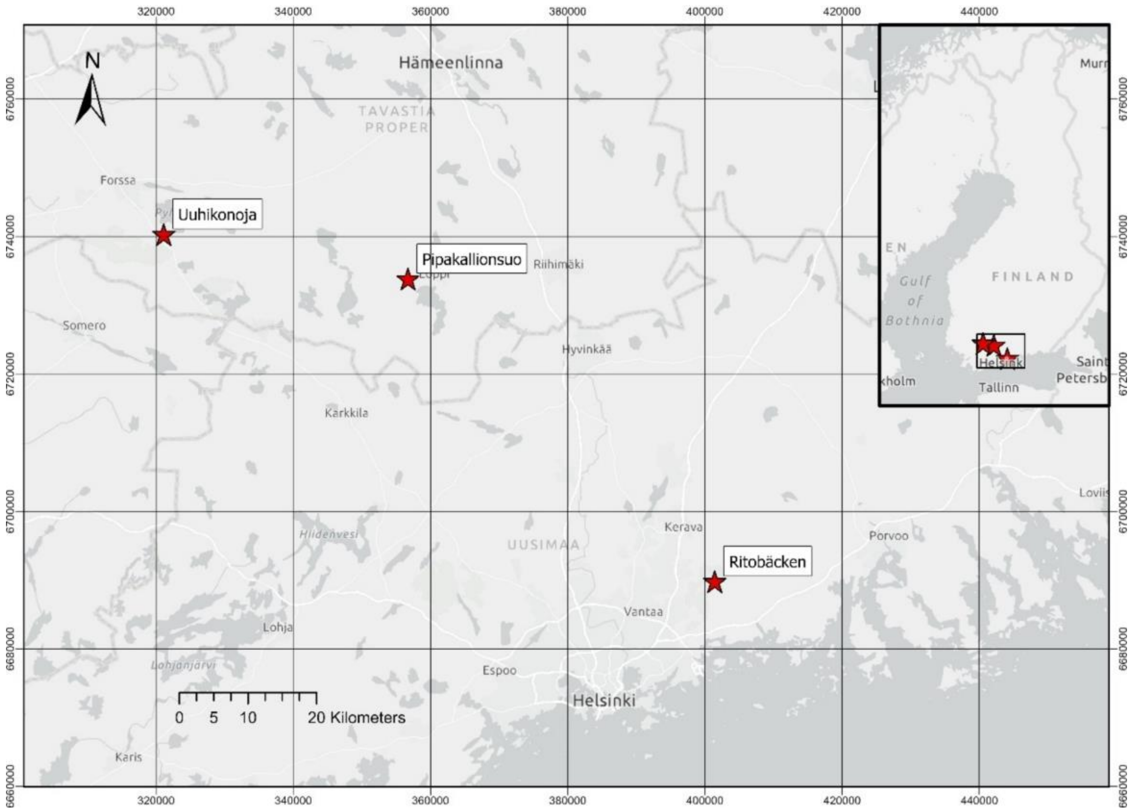

Figure 2. Each study site location in southern Finland. Modified Base map by Esri and National Land Survey of Finland (2023).

Table 1. Study site catchment characteristics including constructed two-stage channel length and sampled channel length, catchment size, average elevation level, and land use (Finnish Environmental Institute 2018).

Site and TSC excavation year	TSC length (sampled reach length)	Average elevation (N2000)*	Water shed area	Arable land (% land use)	Forest or rock outcrops (% land use)	Urban area (% land use)	Water bodies (% land use)	Inland marshes (% land use)
	m	m	ha	ha	ha	ha	ha	ha
Ritobäcken, 2010	850.0 (250)	43.0	770.0	104.0 (13.5 %)	600.0 (77.9 %)	17.0 (5.2 %)	25.0 (3.2 %)	2.0 (0.2 %)
Pipakallionsuo, 2016	250.0 (200)	128.0	140.0	6.0 (4.3 %)	130.0 (93.4 %)	3.0 (2.3 %)	0.1 (0.1%)	0.0 (0.0 %)
Uuhikonoja, 2020	2000.0 (850)	106.0	541.0	261.0 (48.2 %)	241.0 (44.5 %)	39.0 (7.2 %)	0.3 (0.1 %)	0.0 (0.0 %)

*Average elevation calculated as average elevation in catchment area from the National Landsurvey of Finland digital elevation model.

In the Corine 2018 land use dataset level 1 (Finnish Environmental Institute 2018), Pipakallionsuo peatlands are classified as forests, while forests and rock outcrops share the same classification. Consequently, Ritobäcken and Pipakallionsuo appear similar in land use (Table 1), but clear differences between these sites are seen in soil maps (Figure 3 and Figure 4).

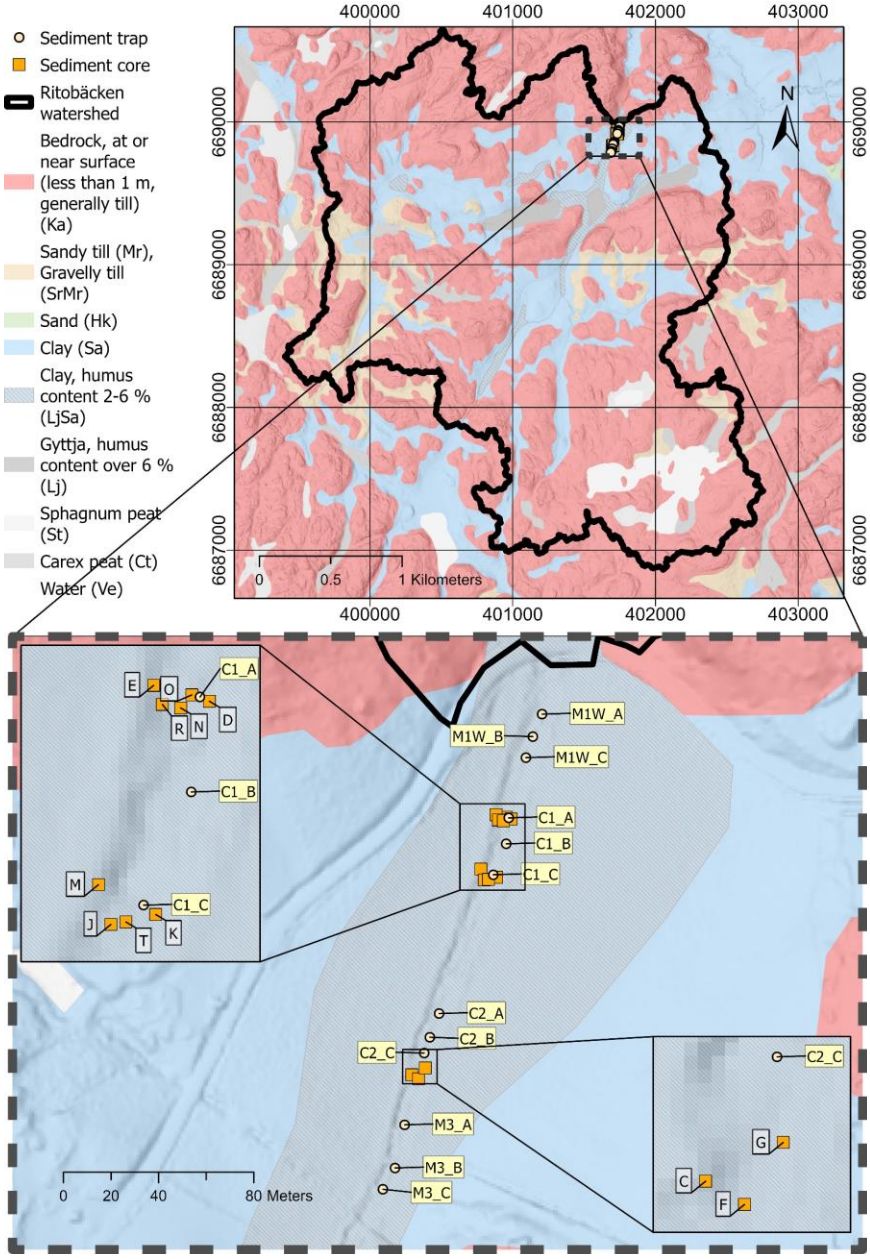

Figure 3. Ritobäcken (Sipoo) catchment (black line), surficial soil, and inset map of the studied two-stage channel (TSC). The inset map shows the locations of the sediment traps (this thesis) and sediment cores (Andelin 2019). Inset maps in bottom figure displays sediment cores different sampling locations across the TSC, including main channel (cores N, J, and C), ditch bank (cores M, E, and R), and floodplain (cores J, T, K, O, D, G, and F). Soil map data for superficial deposits (1:20 000) layer (GTK Hakku 2021). Topographic relief with four times vertical exaggeration from hill shaded map layer created from LiDAR (0.5 points per square meter) dataset (National Land Survey of Finland 2023).

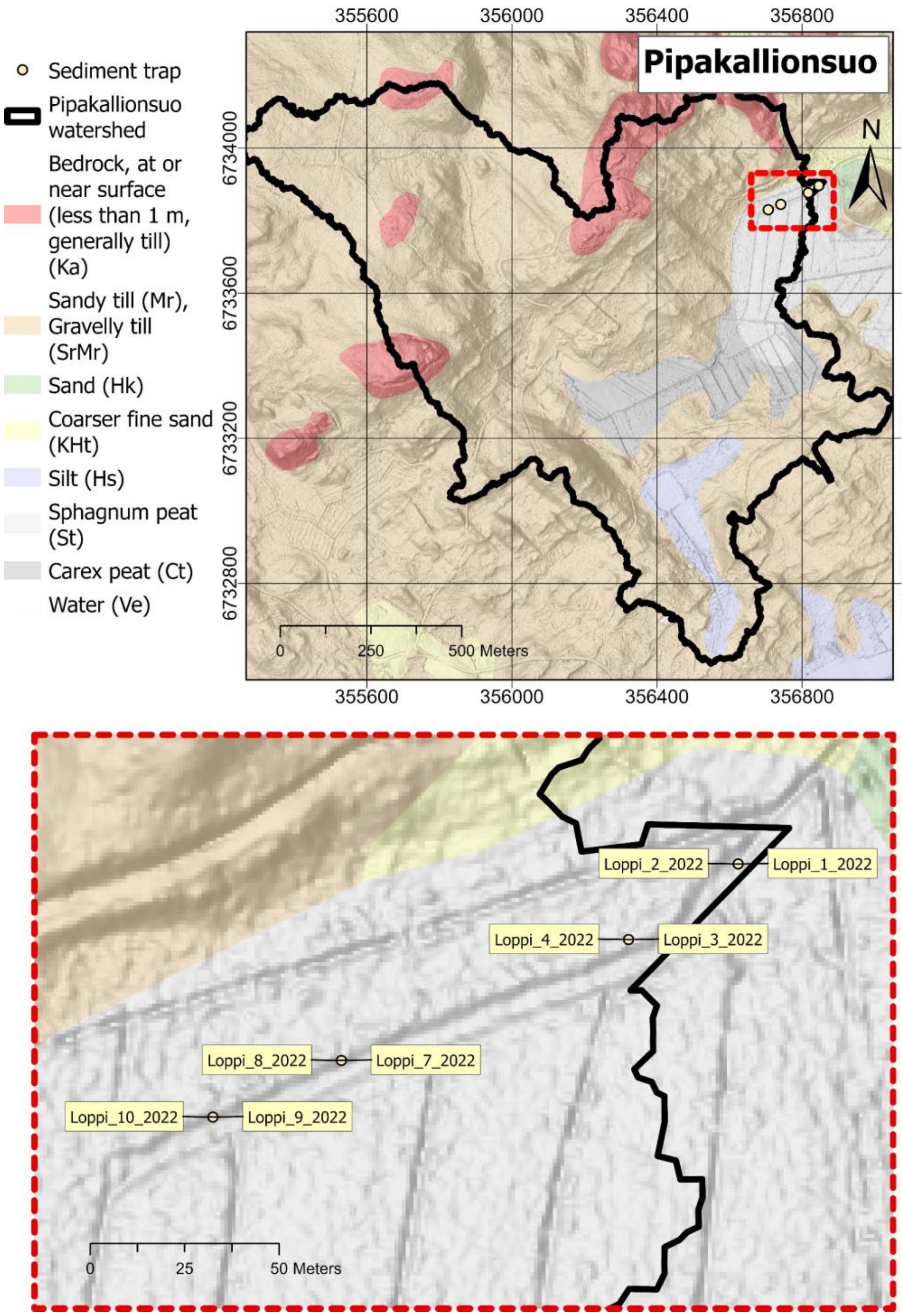

Figure 4. Pipakallionsuo (Loppi) catchment (black line), surficial soil deposits and inset map of the TSC study area with sediment traps (dashed red line). Sediment traps are placed in pairs that are 1.5 m apart from each other with odd numbered traps closer to the main channel and even numbered traps further from the main channel. Soil map data for superficial deposits (1:20 000) layer (GTK Hakku 2021). Topographic relief with four times vertical exaggeration from hill shaded map layer created from LiDAR (0.5 points per square meter) dataset (National Land Survey of Finland 2023).

All study site catchments have mostly granitic bedrock, while surficial sediment deposits were either dominated by clay-silt rich sediment or till (Geological Survey of Finland

Hakku service, GTK Hakku). Sediment deposits in southern Finland are products of the Weichselian glaciation and its deglaciation that submerged most of southern Finland under water on various occasions (e.g., Tikkanen and Oksanen 2002). In submerged conditions the past Baltic Sea stages accumulated vast clay and silt deposits in southern Finland (e.g., Haavisto-Hyvärinen et al. 1990b, Saarnisto 2000, Lunkka et al. 2021). During Baltic Ice Lake, Yoldia Sea, and Ancylus Lake stages all study sites have been submerged, but during the latest stage of Litorina Sea, Loppi and Tammela sites were supra-aquatic (Aho et al. 1999), while Sipoo depressions between revealed bedrock outcrops were submerged (Figure 3). These differences are reflected in the modern soil composition as determined in this study.

The glacial till dominated Pipakallionsuo catchment is located between the First and Second Salpausselkä ridges and has the highest average elevation of the study sites. Some of the glacial formations are well preserved and the areas began to swamp over 9000 years ago (Haavisto-Hyvärinen et al. 1990a, Saarnisto 2000). Peat thickness in the study area is generally over 1 m and at most 3.5 m in northeast areas that are beyond the investigated study site (Moisanen 2014). Being at higher elevation, Pipakallionsuo has preserved large till deposits relative to lower elevation Uuhikonoja and Ritobäcken sites, where till is eroded or buried underneath the clay and silt layers. Pipakallionsuo marginal moraines have been reported to be diamicton-dominated sediments that deposited in under 20 m water depth (Figure 4, Palmu 1999), indicating deposition early in the postglacial period, when the area was submerged.

Uuhikonoja is approximately 40 km to the west of the Salpausselkä II and Pipakallionsuo site, in a clay-silt dominated agricultural area. Uuhikonoja catchment is clay dominated with higher elevated areas having till deposits. Organic peatlands visible in the catchment were formed as past Baltic Sea stages water level lowered and water in closed depressions was overgrown into peatlands like in Pipakallionsuo, but most of these are beyond the studied catchment area (Figure 5). The gravel ridge in the southern edge of the catchment is an esker formation and adjacent silt deposits are littoral deposits that have been washed from the esker during submerged conditions (Palmu 1999), providing a source of different sediment composition within the catchment.

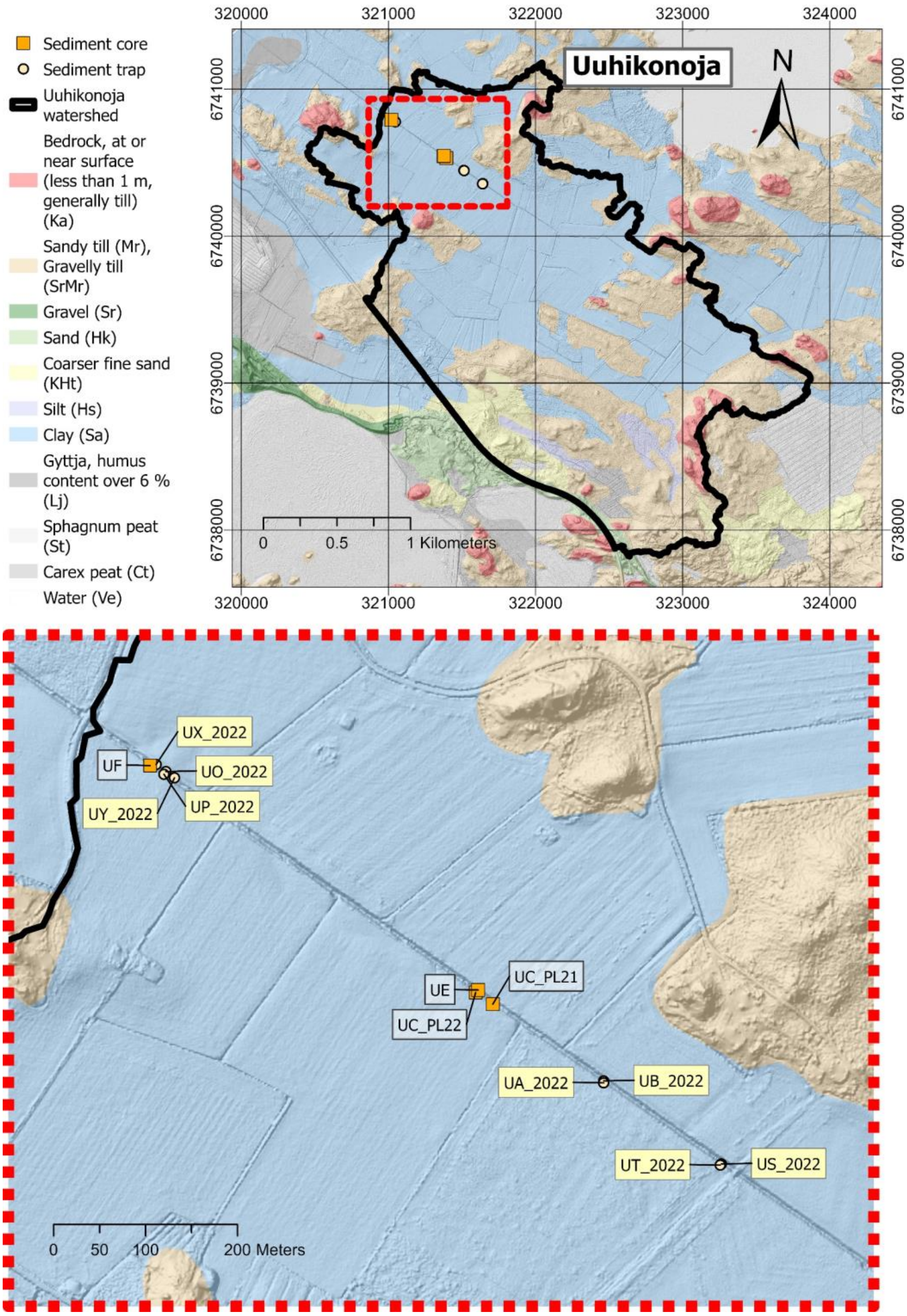

Figure 5. Uuhikonoja (Tammela) catchment (blackline), surficial soil deposits, and inset map of the TSC study area. Sediment traps (this thesis) and sediment cores sampled in 2020 locations marked on the map. Soil map data for superficial deposits (1:20 000) layer (GTK Hakku 2023). Topographic relief with four times vertical exaggeration from hill shaded map layer created from LiDAR (0.5 points per square meter) dataset (National Land Survey of Finland, 2023).

Ritobäcken catchment, approximately 10 km from the current Baltic Sea shoreline, was submerged during the Baltic Ice Lake stage, during which clay and silt deposits accumulated that were later washed out during Yoldia Sea stage due to land uplift associated abrasion and revealed bedrock outcrops underneath (Kielosto et al. 1998, Aho et al. 1999). Vast submerged areas got thin till cover as the waves also redistributed the higher elevated areas into depression valleys carved by glacier meltwaters (Kielosto et al. 1998). Before Littorina Sea shoreline retreated in 2500 BP the iron sulphide rich sediments accumulated in the submerged depressions and after the retreat non-sulfidic sediments started accumulating (Yli-Halla et al. 1999). When the buried sulphide rich layers are disturbed, for example by building agricultural drainage networks, the disturbed sulphide soils become oxidized (e.g., Yli-Halla et al. 1999). Oxidized sulphide soils increase the soil acidity and leach metals from sediments (Sohlenius and Öborn 2004), affecting the local sediment and surface water geochemistry.

2.2. Climate in southern Finland during study period

Helsinki-Vantaa airport weather station was considered to represent southern Finland temperature and precipitation and was compared between the study period (2021-2022) and Finnish Meteorological Institutes (FMI) reference period from 1991-2020 (Figure 6). During the study period December was colder and drier than the reference period, while the spring and early summer of 2022 had more frequent precipitation, but temperatures remain close to the reference period. Higher resolution weather observation data from Helsinki-Vantaa airport show that Southern-Finland had snow cover from late December 2021 until late April 2022 (Figure 7).

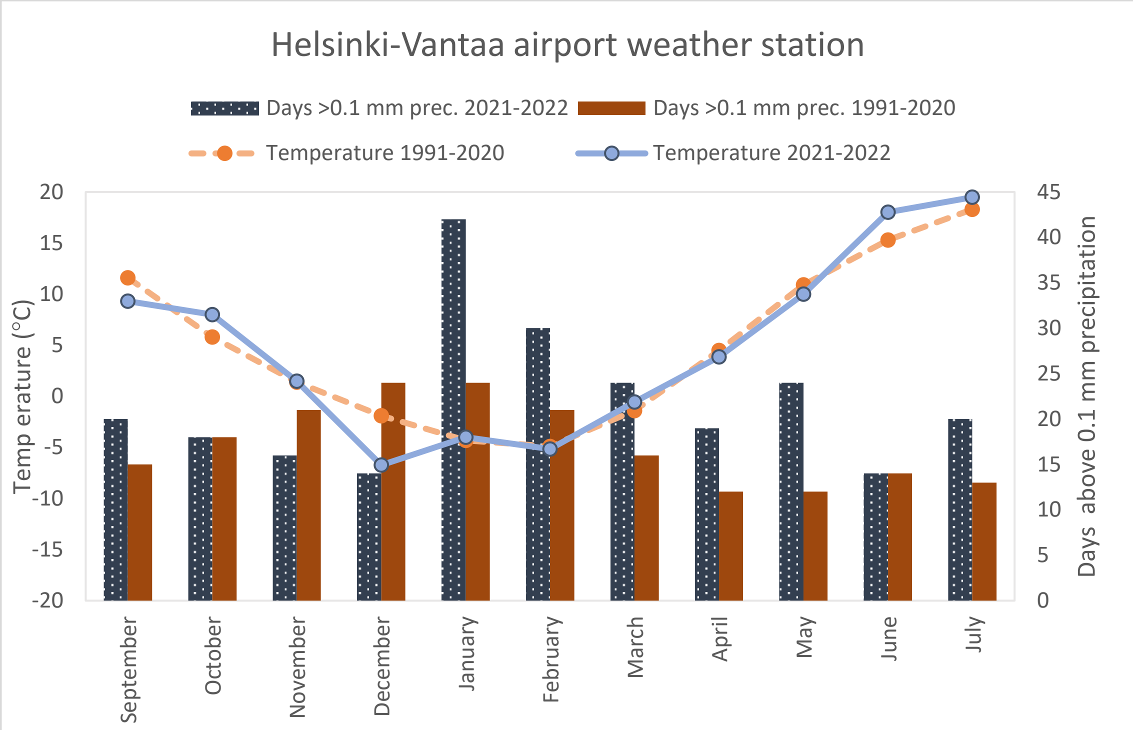

Figure 6. Helsinki-Vantaa airport weather station observations for monthly average temperatures and number of days with above 0.1 mm precipitation between study period and the FMI reference period 1991-2020.

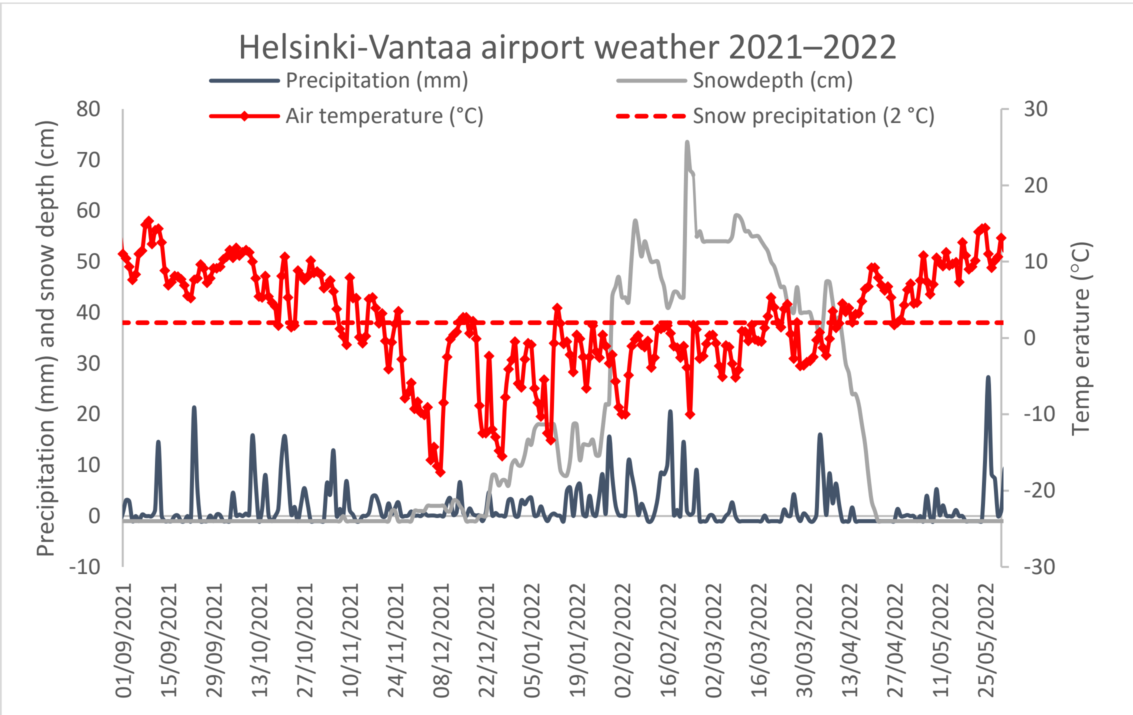

Figure 7. Climate observations over the study period 1.9.2021–25.5.2022 from closest weather station to Ritobäcken (Helsinki-Vantaa airport). Dashed red line estimates the air temperature when precipitation occurs as snowfall (2 °C).

3. MATERIALS AND METHODS

3.1. Sediment trap sampling, preparation, and sediment accumulation

To study the fresh sediment accumulated in TSCs, the Valumavesi project (SYKE) installed a total of 32 sediment traps across three Finnish TSC floodplains in 2021. When stream water level rises above the floodplain, the suspended sediments can deposit on the floodplains (Roley et al. 2012a) and become captured by the sediment traps. Sample locations for each study site are presented in Figure 3, Figure 4, and Figure 5 together with produced surface soil and shaded relief maps (GTK, Superficial deposits 1:20 000), while Table 2 shows the sample coordinates, sample installation and collection dates. For this thesis, 28 new sediment traps were collected and processed for geochemical analyses. Additionally, four sediment traps were collected by colleagues within the Valumavesi project and made available for geochemical analyses (section 3.2.).

Table 2. Sediment traps collected for the thesis and the coordinates (ETRS-TM35FIN), elevation (N2000), installation and sampling dates for each study site.

	Sediment trap sample	Easting (ETRS-TM35FIN)	Northing (ETRS-TM35FIN)	Elevation (m, N2000)	Installation date	Sampling date
Ritobäcken	M1W_A_2021**	401753.4	6689984.3	16.61	14/10/2021	16/12/2021
Ritobäcken	M1W_A_2022	401753.4	6689984.3	16.61	16/12/2021	25/05/2022
Ritobäcken	M1W_B_2021**	401749.5	6689974.9	16.60	14/10/2021	16/12/2021
Ritobäcken	M1W_B_2022	401749.5	6689974.9	16.60	16/12/2021	25/05/2022
Ritobäcken	M1W_C_2022	401746.6	6689966.1	16.57	14/10/2021	25/05/2022
Ritobäcken	C1A_2021**	401739.3	6689940.8	16.68	14/10/2021	16/12/2021
Ritobäcken	C1_A_2022	401739.3	6689940.8	16.68	16/12/2021	25/05/2022
Ritobäcken	C1B_2021**	401738.3	6689929.9	16.70	14/10/2021	16/12/2021
Ritobäcken	C1_B_2022	401738.3	6689929.9	16.70	16/12/2021	25/05/2022
Ritobäcken	C1_C_2022	401732.6	6689916.9	16.72	14/10/2021	25/05/2022
Ritobäcken	C2_A_2022	401710.1	6689858.5	16.79	03/09/2021	25/05/2022
Ritobäcken	C2_B_2022	401706.2	6689848.6	16.83	03/09/2021	25/05/2022
Ritobäcken	C2_C_2022	401703.9	6689841.9	16.81	03/09/2021	25/05/2022
Ritobäcken	M3_A_2022	401695.6	6689811.8	16.94	03/09/2021	25/05/2022
Ritobäcken	M3_B_2022	401691.6	6689793.7	16.93	03/09/2021	25/05/2022
Ritobäcken	M3_C_2022	401686.5	6689784.7	16.99	03/09/2021	25/05/2022
Pipakallionsuo*	Loppi_1_2022	356846.0	6733897.0	No data	06/2021	07/06/2022

Table 2. Continuing.

	Sediment trap sample	Easting (ETRS-TM35FIN)	Northing (ETRS-TM35FIN)	Elevation (m, N2000)	Installation date	Sampling date
Pipakallionsuo*	Loppi_2_2022	356846.0	6733897.0	No data	06/2021	07/06/2022
Pipakallionsuo*	Loppi_3_2022	356817.0	6733877.0	No data	06/2021	07/06/2022
Pipakallionsuo*	Loppi_4_2022	356817.0	6733877.0	No data	06/2021	07/06/2022
Pipakallionsuo*	Loppi_7_2022	356741.0	6733845.0	No data	06/2021	07/06/2022
Pipakallionsuo*	Loppi_8_2022	356741.0	6733845.0	No data	06/2021	07/06/2022
Pipakallionsuo*	Loppi_9_2022	356707.0	6733830.0	No data	06/2021	07/06/2022
Pipakallionsuo*	Loppi_10_2022	356707.0	6733830.0	No data	06/2021	07/06/2022
Uuhikonoja	UO_2022	321037.6	6740784.0	97.94	09/10/2021	21/06/2022
Uuhikonoja	UX_2022	321027.0	6740791.5	98.08	09/10/2021	21/06/2022
Uuhikonoja	UY_2022	321047.0	6740777.1	98.07	09/10/2021	21/06/2022
Uuhikonoja	UP_2022	321035.6	6740781.0	98.26	09/10/2021	21/06/2022
Uuhikonoja	UA_2022	321513.8	6740445.1	98.88	09/10/2021	21/06/2022
Uuhikonoja	UB_2022	321513.75	6740447.2	98.80	09/10/2021	21/06/2022
Uuhikonoja	UT_2022	321640.56	6740355.5	99.00	09/10/2021	21/06/2022
Uuhikonoja	US_2022	321641.76	6740356.8	98.91	09/10/2021	21/06/2022

*Traps are split to four pairs that share coordinates. Odd numbered sediment traps are closer to the main channel and the even numbered are 1.5m away from odd numbered traps further from the main channel. No elevations measured for Pipakallionsuo. Sediment traps collected by Tiina Ronkainen (Valumavesi project, Tapio Oy).

** Sediment traps collected and processed by Kaisa Västilä (Valumavesi project)

Sediment traps were flat square-shaped mats of dimensions 20 cm × 20 cm (Pipakallionsuo) and 30 cm × 30 cm with addition of steel plate bottom (Ritobäcken and Uuhikonoja), made of artificial grass, to simulate the riparian vegetation capturing sediment on natural floodplains. During installation the sediment traps were hooked to the floodplain with four steel pins from each corner to avoid floodwaters moving the trap during measuring period. During sampling, the steel pins were carefully removed, and sediment trap bottom was cleaned with paper towel moistened with deionized water to avoid any contamination with accumulated sediment and placed in re-closable plastic bags (Amergrip Maxi).

In the laboratory, sediment traps were moved to rinsing vessel and large visible vegetation was removed and placed into pre-dried and weighed oven-proof vessel for drying (not used in this thesis). Any material or water in the plastic bag was added to the rinsing vessel together with the sediment trap. Deionized water was added to the rinsing vessel to submerge the trap, and trapped sediment was resuspended by rinsing and brushing

(Justman brush 149-0210, VWR International). The sediment-water mixture was carefully poured into pre-dried and weighed oven proof vessels (aluminium tray 1.5–2 L) and oven dried in 45 °C. Rinsing and brushing was continued until all sediment was removed from the sediment trap, which usually took 3–8 rinsing rounds. Any easily removable vegetation pieces found during brushing and rinsing were removed and placed into their respective oven-proof vessel. An exception in the process was made for Uuhikonoja sample UT_2022, which had an approximately 8 cm thick sediment layer over the trap in the field. For UT_2022, sediment that could be collected by hand was first removed into a plastic bucket and weighed for wet weight. The remaining sediment was rinsed by a similar method as for other sediment traps. A total of 8.06 kg wet weight of sediment was removed by hand and 10% of this mass (806 g) was used for sample processing. All data were recalculated to the full 100% original mass.

The rinsing vessel used and sediment traps from Ritobäcken (Figure 8A) and Uuhikonoja (Figure 8B), show clear difference in deposited material. Figure 8C shows the brushed and rinsed sediment trap free of sediment. The vessels with sediment-water mixture were oven dried at 45 °C and weighed together with oven vessels until their weight stabilized. To preserve organic phosphorus phases for phosphorus speciation analysis, the drying temperature was set to be under 60 °C (Ruban et al. 2001). Total sedimentation for each sediment trap was calculated by adding together each respective trap's drying vessel weights (equation 1).

$$\mathrm{TS_{trap}} = \frac{\sum(\mathrm{VS_n} - \mathrm{V_n})}{\mathrm{T_{area}}} \tag{1}$$

Where TS_{Trap} is the total sediment accumulated by the sediment trap (kg m^{-2}), VS_n is the dry weight (kg) of oven vessel and dried sediment, and V_n is the empty vessel weight (kg). T_{area} is the surface area of the trap (m^2). Oven vessels were reused after rinsing with deionized water, drying, and weighing, to remove any possible residual sample material. Dry sediment-water mixture forms silt-clay sheet (Figure 8D). Dried sediments were scraped into re-closable plastic bags (Amergrip) from the vessels using disposable plastic spoons, and gently broken down to fine grained powder by pressing over the bag or using mortar and pestle for hard silt and clay rich samples. Sediment samples were used in chemical analyses for geochemical composition, carbon and nitrogen content, organic matter content, and phosphorus speciation analysis.

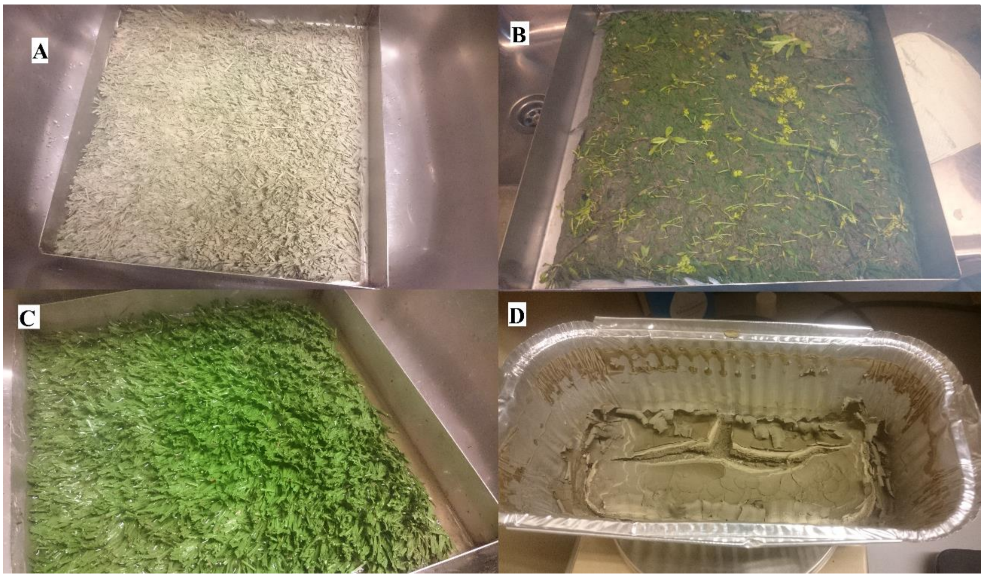

Figure 8. A) Sediment trap from Ritobäcken before rinsing, B) Sediment trap that was partly inundated during sample collection from Uuhikonoja, C) Rinsed and brushed Sediment trap D) Ovenproof vessel with dried sediment-water mixture that has formed a hard silt and clay sheet. Figures are not to scale. Clear difference in deposited material can be seen between A and B.

3.2. Laboratory analyses

3.2.1. Microwave assisted acid digestion

The sediment trap samples were analyzed using a microwave assisted digestion method (EPA3051A, Link et al. 1998). Microwave assisted digestion using strong nitric acid extracts the acid soluble metals, leaving insoluble material such as many silicate minerals relatively undigested (Lahermo et al. 1996). A total of 48 samples were analyzed for 24 elements, calcium (Ca), sodium (Na), magnesium (Mg), aluminum (Al), potassium (K), titanium (Ti), phosphorus (P), sulfur (S), vanadium (V), chromium (Cr), iron (Fe), cobalt (Co), nickel (Ni), copper (Cu), zinc (Zn), manganese (Mn), strontium (Sr), zircon (Zr), arsenic (As), molybdenum (Mo), selenium (Se), cadmium (Cd), lead (Pb), and uranium (U), with 32 sediment traps, four lab replicates, eight reference materials, and four blank samples. Samples were prepared by measuring 250 mg of dry weight sample into Teflon tubes lined with disposable Teflon liners. Static electricity was dampened from Teflon tubes prior to sample placement using Static Eliminator (Cola-Parmer-Labs 800-AS/SPI). Each tube was treated with 10 ml of 67% nitric acid (HNO_3), closed with pressure releasing screw cap, and placed into CEM Mars 6 microwave. The microwave could hold 32 tubes at once, so the samples were split into two batches, with four reference samples, two lab replicates and two blank samples each for quality control. The microwave program for EPA3051A heats up and holds the temperature at 175°C for 10 minutes to digest the acid soluble components. Tubes were allowed to cool overnight and tube caps were opened carefully to allow possible residual pressure inside to release.

The acid solutions were transferred from Teflon tubes into 15 ml vials and diluted 100-fold before analysis in Helsinki Geoscience Laboratories HelLabs with Agilent 7900 ICP-QQQ inductively coupled plasma spectrometer (ICP-MS). The simplified operation principle of ICP-MS is that the sample is ionized using plasma in high temperature, after which mass-charge ratio is measured using multiple mass analysers (e.g., Hoffman et al. 2009). Mass analysers and detectors convert measurements to electric signals and element concentration values. More detailed description of ICP-MS analysis can be found in literature (e.g., Howard 2001, Hoffmann 2007).

3.2.2. Loss on ignition, carbon, and nitrogen content

Soil organic matter (SOM) content was measured with loss-on-ignition (LOI) method in University of Helsinki HelLabs using thermogravimetric analyzer (TGA701, LECO) following a standard protocol (SFS3008 1981). For analysis, two grams of sample was weighed into desiccated crucibles that were placed into the device, which then starts the heating the samples first to 105 °C to remove any moisture, and then heated to 550 °C for organic matter ignition. TGA 701 automatically weighs the samples inside the furnace until the weight stops decreasing, indicating the weight lost on ignition in set method temperature. Samples moisture and soil organic content is calculated by the TGA701 with equations 2 and 3 respectively. SOM can be converted to soil organic carbon (SOC) by using conventional conversion factor of 0.58, but in agricultural topsoil this factor has been found to overestimate the SOC (Jensen et al. 2018). In this study, sediment samples were analysed for carbon and nitrogen content by University of Helsinki EcoEnv labs, Viikki. Accurate measurements for SOC allow estimation of floodplain sediment carbon retention and comparison with the conventional conversion factor for SOC at our study sites.

$$Moisture = \frac{(M_1 - M_2)}{M_1} \times 100\ (\%) \tag{2}$$

$$SOM = \frac{M_2 - M_3}{M_2} \times 100\ (\%) \tag{3}$$

Where *Moisture* is the amount of moisture content removed from sample (%), M_1 is the initial mass of sample (g) and M_2 is the mass after 105 °C drying (g). *SOM* is soil organic matter removed from sample (%), M_3 is the sample mass after 550 °C combustion (g).

3.2.3. Phosphorus speciation (Tailored SEDEX, UV-VIS, and ICP-MS)

Phosphorus is bound in sediments in inorganic and organic phases that can be extracted using different sequential extraction schemes (Ruban et al. 1999). Phosphorus speciation was determined for fractions of easily exchangeable P, reactive Fe-bound P, Al bound P, residual inorganic P, and residual organic P by a tailored sequential extraction method. The method follows closely the same procedure as was done with previous samples provided by Valumavesi project (section 3.2.). A total of 44 samples were analyzed, including 32 sediment trap samples, four lab replicates, four reference materials, and four blanks for quality assurance.

The methodology is a tailored version of SEDEX by Ruttenberg (1992) for phosphorus speciation in marine sediments, and Ruban et al. (1999) for lake sediments. In SEDEX the samples are mixed with extraction solution which dissolves the targeted phosphorus species from solid sediment sample to the supernatant which is then analyzed with ultraviolet-visible spectroscopy (UV-VIS, SFS6878 2004) or ICP-MS. After each extraction step, the solid residual sample is continuously used to sequentially extract new target P-species with new extractant solution until all targeted species are extracted. Extractant steps used were 1) 1M ammonium chloride (NH_4Cl) for exchangeable P (referred as Ex-P), 2) citrate-dithionite-bicarbonate (CDB) for Fe-P, 3) 1M sodium hydroxide (NaOH), followed by acidification with 3.5M hydrochloric acid (HCl) for Al-P, 4) 1M HCl for residual inorganic-P (Ca-P), 5) residue dry combusted in 550 ℃ and ashes extracted with 1M HCl for residual organic P (Res.Org-P). Citrate-dithionite-bicarbonate solution was made according to Ruttenberg (1992) by mixing 0.3M Na_3-citrate and 1M $NaHCO_3$ with 0.25 g of NaS_2O_4 per 10 ml of solution. Total phosphorus was calculated from the sum of all extracted P species (TP-SEDEX). Magnetic stirrer was used to help dissolution in extractant mixing process. Detailed steps for sequential extraction scheme were as follows (Table 3).

Table 3.Tailored sequential extraction (SEDEX) scheme used for different phosphorus speciation extraction.

Step	Sample	Extract (volume)	Rinsing time	Centri-fuge	Extra steps		Analysis	Phase extracted
1. Ex-P	0.1 g dry weight	1M NH_4Cl (10 ml)	2 h	15 min (2000 rpm)			UV-VIS	Exchange-able P (Ex-P)
2. Fe-P	Residue (step 1)	CDB* (10 ml)	8 h	15 min (2000 rpm)	Store in freezer until analysis		ICP-MS	Reductible P, Fe-P
3A	Residue (step 2)	1 M NaOH (10 ml)	16 h	15 min (2000 rpm)	Continue to step 3B			
3B Al-P	5 ml step 3A super-natant	3.5 M HCl (2 ml)		Shake by hand	Precipitate forms?	Yes	Add 0.5 ml of 67% HNO3, Blockheat (100 °C) for 2-3 h**	P in non-reducible metals, Al-(hydr)oxides, Al-P
						No	ICP-MS	
4. Ca-P	Residue (step 3A)	1 M HCl (10 ml)	55h*** (18 h)	15 min (2000 rpm)			ICP-MS	Detrital apatite minerals, Ca-P
5A	Residue (step 4)	Ashing at 550°C for 4 h			Continue to step 5B			
5B Res.Org-P	Residue (step 5A)	1 M HCl (10 ml)	16h	15 min (2000 rpm)			ICP-MS	Residual organic P

*CDB stands for Citrate dithionite bicarbonate solution made by mixing 0.3 M Na_3-citrate and 1M $NaHCO_3$ with 0.25 g of NaS_2O_4 per 10 ml of solution.

**If sample volume lost to evaporation, add pure water (Milli-Q) to 7 ml total volume.

***Samples were left to shake over the weekend, normally 18 h rinsing time is used.

The NH_4Cl extracted phosphorus solution prepared in stage 1 of sequential extraction was measured using UV-VIS (Hach-Lange 5000), following standard SFS-EN ISO 6878:2004 for determination of orthophosphate. The method is based on orthophosphate ions reacting with added molybdate and antimony ions to the sample solution which changes the solution colour based on the concentration of reactive orthophosphate ions, in this case orthophosphates extracted with NH_4Cl solution. UV-VIS measures the absorbance of ultraviolet in the blue tint solution and determines the concentration of orthophosphate ions. UV-VIS measurement was done by taking 5 ml of sample from step 1 vials in 25 ml bottles instead of the standard 50 ml to avoid over diluting the samples. For each sample 0.5 ml of ascorbic acid and 1 ml of molybdate was added to form the blue coloured molybdate complex for measurement. Phosphorus species for SEDEX steps 2–5 were analysed using ICP-MS (Agilent 7900 ICP-QQQ).

3.3. Materials from other studies and open data sources

Additional samples for the study sites were provided by Valumavesi project, including four sediment cores for Uuhikonoja and 8 sediment traps for Pipakallionsuo. Additional sediment core samples for Ritobäcken are from Andelin (2019) thesis project, which presented a method to distinguish Ritobäcken's TSC excavation depth based on sediment core profiles geochemistry and examined if different sediment sample processing methods affect nutrient content in chemical analyses. Sample locations are shown in Figure 3, Figure 4, and Figure 5, while analyses performed for each sample are displayed in Table 4. For this thesis the sediment core profiles and known excavation depths from Andelin (2019) thesis were compared to sediment trap samples of fresh sediment accumulation. Sediment trap samples from Pipakallionsuo were available for two years and were used to see if the P-species distribution has remained constant in consecutive samplings. P-speciation for Uuhikonoja's sediment cores were compared with fresh sediment trap P-speciation despite different sampling locations along the TSC reach.

Due to the disparity in sample analyses done between sites, Ritobäcken will be covered in more detail for site-specific comparisons. Valumavesi project has also provided continuous water level monitoring observations, streams discharge (Q) and suspended solids data for total suspended solids (TSS), total nitrogen (TN), total phosphorus (TP) at the Ritobäcken site. Additionally open-source databases from Karttapaikka (National Land Survey of Finland), Finnish Environmental Institute (SYKE), Finnish

Meteorological Institute (FMI), and Hakku services (GTK) are used to study sites soil, bedrock, land use, and topography.

Table 4. Samples available from previous studies and performed geochemical analyses. Sample location implies the position in TSC, where MC = main channel, FP = floodplain, Bank = unexcavated stream bank.

Site	Sample type	Sample	Sample location	P-species	Geochemistry	C, N	Source
Ritobäcken	Sediment core	C	MC		x	x	Andelin (2019)
Ritobäcken	Sediment core	D	FP		x		
Ritobäcken	Sediment core	E	Bank		x	x	
Ritobäcken	Sediment core	F	FP	x*	x		
Ritobäcken	Sediment core	G	FP		x		
Ritobäcken	Sediment core	J	MC	x*	x	x	
Ritobäcken	Sediment core	K	FP		x		
Ritobäcken	Sediment core	M	FP		x	x	
Ritobäcken	Sediment core	N	MC	x*	x	x	
Ritobäcken	Sediment core	O	FP	x*	x	x	
Ritobäcken	Sediment core	R	FP		x	x	
Ritobäcken	Sediment core	T	FP		x		
Uuhikonoja	Sediment core	UF	FP	x*			NBS-VEGE-NUTRI project
Uuhikonoja	Sediment core	UC PL22	FP	x*			
Uuhikonoja	Sediment core	UC PL21	FP	x*			
Uuhikonoja	Sediment core	UE	FP	x*			
Pipakallionsuo	Sediment trap	Loppi_1_2021	FP	x*		x*	Valumavesi project and Tapio Oy
Pipakallionsuo	Sediment trap	Loppi_2_2021	FP	x*		x*	
Pipakallionsuo	Sediment trap	Loppi_3_2021	FP	x*		x*	
Pipakallionsuo	Sediment trap	Loppi_4_2021	FP	x*		x*	
Pipakallionsuo	Sediment trap	Loppi_7_2021	FP	x*		x*	
Pipakallionsuo	Sediment trap	Loppi_8_2021	FP	x*		x*	
Pipakallionsuo	Sediment trap	Loppi_9_2021	FP	x*		x*	
Pipakallionsuo	Sediment trap	Loppi_10_2021	FP	x*		x*	

*P-species analysed by Aino Syrjänen (research assistant in Valumavesi project 2020-2021).

3.4. Geoinformation systems (GIS)

3.3.1. Watershed above two-stage channel

For each study site the soil, bedrock, catchment size, and land use maps were produced using ArcGIS Pro 3.0.3 (Esri Inc.) GIS desktop application. To estimate the catchment size affecting the floodplain sediment accumulation watershed area new digital elevation model (DEM) with 1m cell size was produced using National Land Survey of Finland LiDAR 0.5p that is precise enough to distinguish studied TSC floodplains and main channel. LiDAR data was classified for ground and low vegetation separately, allowing filtering for only ground surface that is converted into raster dataset (DEM). LiDAR data is converted from LAS data format to raster using ‘LAS Dataset To Raster’-tool using settings for triangulation interpolation type, with natural neighbor method and no thinning, cell size is set to 1 m.

Catchment size for each site was calculated using ‘Watershed’-function in ArcGIS Pro to account for surface flow area affecting the TSC. The watershed function calculates all raster cells that flow past a selected ’pourpoint’ based on the surface waterflow direction. Surface flow direction is calculated using ‘Flow Direction’-function that calculates flow direction from each raster cell based on the slope of the raster compared to the neighboring cells (Flow Direction function documentation, Esri 2023a). Flow direction created from DEM is not always able to identify small features like streams or features that affect water flow connectivity, such as culverts and bridges. For more accurate results the water flow connectivity was increased by filling small uneven pits from DEM using ‘Fill’-function and burning flow-disjointing features to the DEM using the ‘Raster Calculator’-tool, to reduce culverts and bridges elevation by two meters. The burned DEM was used to calculate a Flow Direction raster that can be used for ‘Flow Accumulation’ and ‘Watershed’ functions. Flow accumulation function uses the flow direction raster to visualize the stream network. Using the stream network created by Flow accumulation it is then possible to estimate the location of a pourpoint where water flow is leaving the watershed. Pourpoints were placed slightly downstream after the last sediment trap samples to estimate catchment size affecting sediment deposition for the studied TSC floodplain.

With ArcGIS Pro it is possible to change raster dataset symbology to convert DEM into shaded relief layer, which specifies the position of the light source (Sun) to simulate shadows, creating contrast between changing topography (Shaded Relief function documentation, Esri 2023b). Contrasting elevations make topography of glacial formations easier to identify, that can be used to study sites’ (de)glaciation history

(Putkinen et al. 2017). Interpreted (de)glaciation history and literature were used to explain soil formation history of the studied catchments.

3.3.2. Ritobäcken floodplain inundation

Three water level observation stations in Ritobäcken were used with measured sediment trap elevations to estimate the TSC floodplain inundation events. Figure 9 displays the observed water levels in three observation stations and four different sediment trap installment periods. Floodplain inundation estimate was done by calculating water level at each sediment trap location using linear interpolation (equation 4). The method assumes water level decreases linearly across the slope between two water level observation stations. 'Near' analysis tool in ArcGIS Pro was used to measure distances between sediment traps and water level observation stations. Interpolated water levels were used to investigate the connection between sedimentation, and the extent and evolution of inundation events.

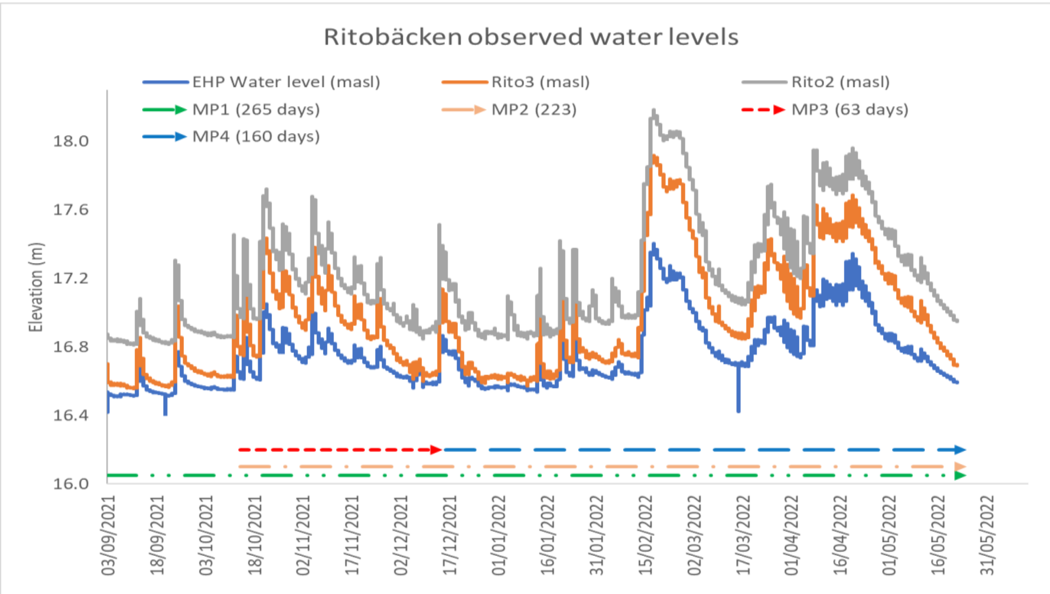

Figure 9. Ritobäcken observed water levels from observation stations (EHP Water level, Rito3, Rito2), and sediment trap measuring periods denoted as MP1–4, reflecting the time the sediment traps were installed and the overlap between the periods. Measuring period 3 sediment traps were retrieved in December 2021 and measuring period 4 sediment traps were installed in their place and retrieved together with the remaining traps in May 2022.

$$WL_x = Obs_1 \times \frac{L - D}{L} + Obs_2 \times \frac{D}{L} \tag{4}$$

Where WL_x is the interpolated water level for sediment trap x, Obs_1 is the water level (m) in closest water level observation station, Obs_2 is the water level (m) in the closest observation station located in opposite side of sediment trap (m) along the reach, D is the distance (m) between sediment trap and Obs_1, and Obs_2 and L is the distance (m) between Obs_1 and Obs_2.

The interpolated water levels for each sediment trap location were used to model the water level across the TSC, that gives insight on the potential maximum of the inundation extent. For convenience the interpolated water level dataset with 15-minute timesteps (n = 25169) was downscaled to daily average water level dataset (n = 263). The interpolated water levels for each day were then converted into water level raster layers by using Empirical Bayesian Kriging Regression Prediction model with DEM as explanatory variable. The modelled water level raster was subtracted from the DEM to visualize any raster cells where the water level was above surface level, thus producing maps for daily inundation extent.

Daily inundation extent maps were used together with shaded relief layer to limit the studied floodplain area to 250-meter reach length, while considering the area of inundated floodplain (Figure 10). The floodplain area was divided into 15 sections, where the measured elevation levels of sediment traps (Table 2) were used to determine if sediment trap and the surrounding areas were inundated (Figure 10). Floodplain sections with interpolated water level above sediment trap elevations were considered inundated and added together for inundated floodplain area. Three synthetic sections were made to account for areas without sediment traps, that were considered to be inundated if closest sediment trap either up- or downstream was inundated. This approach allows to see in which order the sediment traps inundate and to calculate the net sediment accumulation that accounts for flooding extent (equation 5), where t (days) is the time, $\overline{TStrap}$ (kg m^{-2}) is the mean sediment accumulation rate and $\overline{FP_{inundated}}$ (m^2) is the mean inundated floodplain area.

$$Total\ sediment\ accumulated\ (t) = \overline{TS_{trap}} \times \overline{FP_{inundated}} \qquad (5)$$

Using interpolated water level reduces some of the problems of simple bathtub modelling methods that are based on flat water level that overestimates the flooding extent (e.g., Williams and Lück-Vogel 2020). The applied method has uncertainties from the uneven ground, visually decided section areas, and the DEM having too coarse resolution to measure accurate geomorphology of the floodplain.

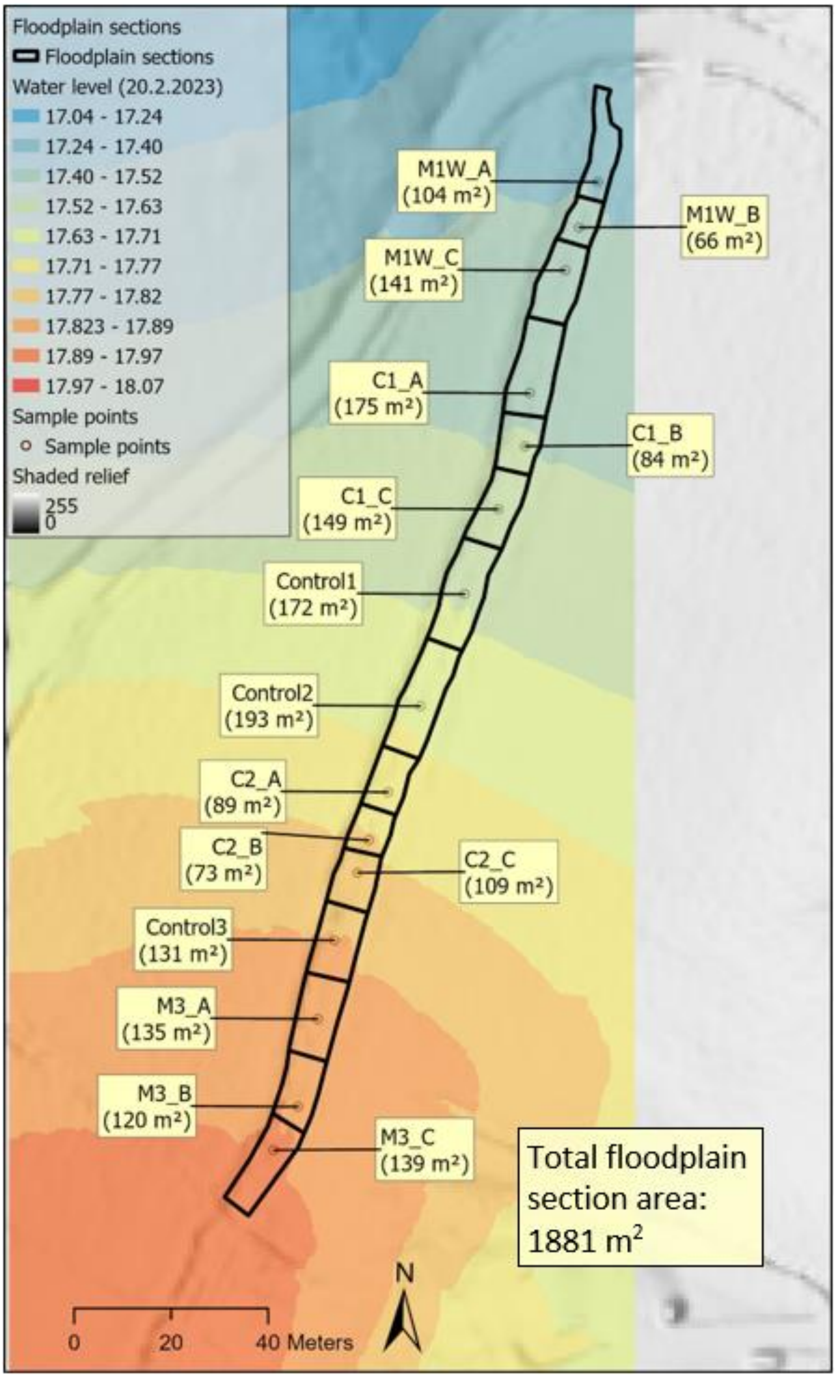

Figure 10. Example of Ritobäcken modelled water level layer for 20.3.2023 (colour gradient). Floodplain is visually divided into 15 sections, where each sediment trap locations cover a set area of the floodplain (Black line). Three synthetic areas (Control1, Control2, and Control3) were made to cover areas without sediment traps. The modelled water level is compared to sediment trap elevations to see if the respective section is inundated to calculate inundation extent.

3.5. Data processing and Statistical analyses

Measured sediment accumulation, geochemistry, nutrient content, and P fractions were explored using element scatter plots, descriptive statistics, non-parametric tests, hierarchical cluster analysis (HCA), and principal component analysis (PCA). Non-parametric tests were used due to the small sample pool, non-normal nature of geochemical data and to use categorical variables like vegetation management method. Plots and tests were done with SPSS version 28 and R version 4.3.0. (R Core Team 2023). Relative standard deviation (RSD) was used to study spatial variability of measured sediment accumulation rates within each study site (equation 6). Where RSD is the relative standard deviation (%), σ is the standard deviation and μ is the mean.

$$RSD = \frac{\sigma}{\mu} \tag{6}$$

Principal component analysis was performed in R using 'PCA' function from FactoMineR library (Lê et al. 2008) and visualized with 'fviz_pca_biplot' function from factoextra library (Kassambara and Mundt 2020). For PCA the used data was first standardized using centered-log-ratio (clr) to close the complex from unanalyzed elements (Aitchison 1986) and to center the results around common variable to make different study sites comparable. Centering makes each sample case variable sum to add up to zero. Clr was done using equation 7, where each sample cases data is a ratio between measured variable (x_i) and the compositions geometric mean (equation 8*)* that is log transformed.

$$clr(x_i) = \log\left(\frac{x_i}{\bar{g}(x_n)}\right) \tag{7}$$

$$\bar{g}(x_n) = \sqrt[n]{x_1 x_2 \ldots x_n} \tag{8}$$

Principal component analysis reduces the dimensions of the analyzed sample variables to find the principal components (PC) with maximum variance by use of eigenvalues and eigen vectors (Aitchison 1986). Use of CLR transformation standardizes the samples around geometric mean that reduces the loss of variance based on the component magnitude, that is problem with variance calculated by concentrations (Aitchison 1986). Results of PCA can be visualized with biplots that show two selected principal components (PC), displaying variable factor loadings (vectors) and observation loading scores (points). Variable factor loadings can be used to interpret the strong positive or negative correlation when they are parallel to each other, and no correlation when they are perpendicular to each other (Aitchison 1986, Grunsky 2010).

Hierarchical cluster analysis is a multivariate cluster analysis that identifies similarity between observation using suitable clustering method (Gong and Richman 1995, Grunsky 2010). Hierarchical cluster analysis assumes connection between the analyzed observations based on similarity of data.

4. RESULTS

4.1. Sediment accumulation

4.1.1. Spatial and temporal variability in sediment accumulation

Sediment traps net accumulation varied greatly between and within the study sites (Table 5 and Table 6). For comparable results between all sites the sediment accumulations were normalized to represent weight per area over one year period. Highest sediment accumulation rates were observed in Uuhikonoja with on average 17816 g m^{-2} a^{-1} including anomalous sediment accumulation in UT_2022 trap where nearby slope erosion had buried the trap under approximately 8 cm thick sediment cover. The nearby US_2022 sediment trap was not buried but still had relatively high amount of sediment accumulated when compared to sediment traps downstream. Even if UT_2022 was excluded Uuhikonoja had the highest sedimentation rates (6378.1 g m^{-2} a^{-1}) compared to Ritobäcken and Pipakallionsuo which had average annual sedimentation rates of 2474.4 g m^{-2} a^{-1} and 230.1 g m^{-2} a^{-1} respectively. Temporal variability could be observed in Ritobäcken, where sediment traps sampled in December had relatively lower annual accumulation rates compared to their May 2022 sampled counterparts, with single exception being C1_A_2021 (Figure 11). Uuhikonoja also had the highest variability in sediment accumulation with relative standard deviation (RSD) of 97.5 %, while Ritobäcken and Pipakallionsuo had 55.2 % and 74.4 %, respectively.

Table 5. Net sediment accumulation collected from each sediment trap. Net sediment accumulations were normalized to annual sediment accumulation rates by dividing them with sediment trap area and trap installation period to make results comparable.

Site	Sample	Measuring period (MP)	Sediment trap sediment accumulation (g)	Annual sediment accumulation rate (g m^{-2} a^{-1})
Ritobäcken	M1W_A_2022	MP4	85.04	2155.53
Ritobäcken	M1W_A_2021	MP3	23.14	1489.61
Ritobäcken	M1W_B_2022	MP4	237.78	6027.06
Ritobäcken	M1W_B_2021	MP3	42.85	2758.42
Ritobäcken	M1W_C_2022	MP2	190.43	3463.23
Ritobäcken	C1_A_2022	MP4	49.50	1254.69
Ritobäcken	C1_A_2021	MP3	27.15	1747.75
Ritobäcken	C1_B_2022	MP4	105.89	2684.02
Ritobäcken	C1_B_2021	MP3	24.26	1561.71
Ritobäcken	C1_C_2022	MP2	68.22	1240.67
Ritobäcken	C2_A_2022	MP1	90.83	1390.06
Ritobäcken	C2_B_2022	MP1	60.68	928.65
Ritobäcken	C2_C_2022	MP1	240.03	3673.42
Ritobäcken	M3_A_2022	MP1	251.16	3843.75
Ritobäcken	M3_B_2022	MP1	113.16	1731.80
Ritobäcken	M3_C_2022	MP1	237.84	3639.90
Pipakallionsuo	Loppi_1_2022		3.23	80.75
Pipakallionsuo	Loppi_2_2022		3.67	91.75
Pipakallionsuo	Loppi_3_2022		17.11	427.75
Pipakallionsuo	Loppi_4_2022		14.23	355.75
Pipakallionsuo	Loppi_7_2022		3.73	93.25
Pipakallionsuo	Loppi_8_2022		2.48	62.00
Pipakallionsuo	Loppi_9_2022		19.13	478.25
Pipakallionsuo	Loppi_10_2022		10.06	251.50
Uuhikonoja	UO_2022		860.77	12834.19
Uuhikonoja	UX_2022		381.50	5688.21
Uuhikonoja	UY_2022		576.41	8594.35
Uuhikonoja	UP_2022		51.49	767.72

Table 5. Continuing.

Site	Sample	Measuring period (MP)	Sediment trap sediment accumulation (g)	Annual sediment accumulation rate (g m^{-2} a^{-1})
Uuhikonoja	UA_2022		30.99	462.06
Uuhikonoja	UB_2022		44.62	665.29
Uuhikonoja	UT_2022		6565.00	97885.06
Uuhikonoja	US_2022		1048.62	15635.06

Table 6. Average sediment accumulation by sediment traps, rescaled annual accumulation rates and the minimum and maximum of each sites annual accumulation rates to show the variability.

	Sediment captured by sediment traps (g)	Annual sediment accumulation rate (g m^{-2} a^{-1})	Sediment accumulation rate, minimum-maximum (g m^{-2} a^{-1})
Ritobäcken	115.5	2474.4	928.7–6027.1
Pipakallionsuo	9.2	230.1	62.0–478.3
Uuhikonoja	1194.9	17816.5	462.1–97885.1

Ritobäcken and Uuhikonoja had higher sediment accumulation rates downstream, where surface elevations are lower (Figure 11), with exception being the traps with signs of slope erosion (UT_2022 and US_2022). Additionally, Uuhikonoja trap UB_2022 accumulated 43.9 % more sediment relative to the nearby UA_2022 trap that was two meters away and 8 cm higher in elevation. Pipakallionsuo had no measured surface elevation levels, but the sediment traps were placed as four pairs (transects) with odd numbered traps being 1.5 m apart from their even numbered counterparts that were further from the main channel. Pipakallionsuo sediment traps closer to the main channel accumulated more sediment (Figure 12, Table 5), but Mann-Whitney U test indicated that the difference was not statistically significant.

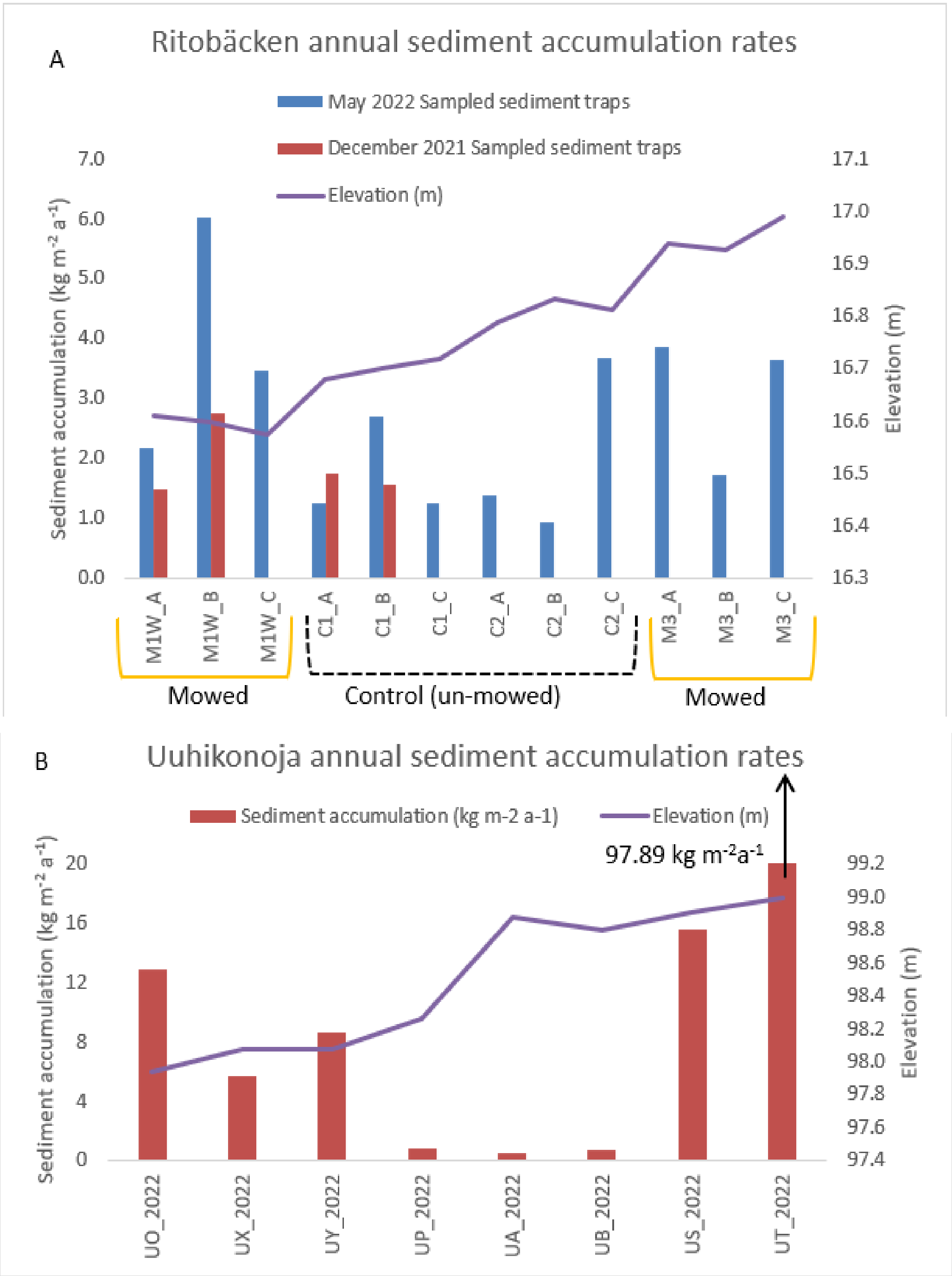

Figure 11. Annual sediment accumulation rates Ritobäcken (A) and Uuhikonoja (B) together with surface elevation of each sediment trap (purple line). Sediment traps are in order from left to right based on location on floodplain downstream to upstream. Bar colours in (A) represent the different sampling date, where red bars were sampled in December 2021 and blue bars in May 2022. Brackets under the sample labels in (A) indicate the vegetation management method, vegetation mowed to 5–10 cm length (orange line) and un-mowed (black dashed line). Uuhikonoja had no vegetation management experiment.

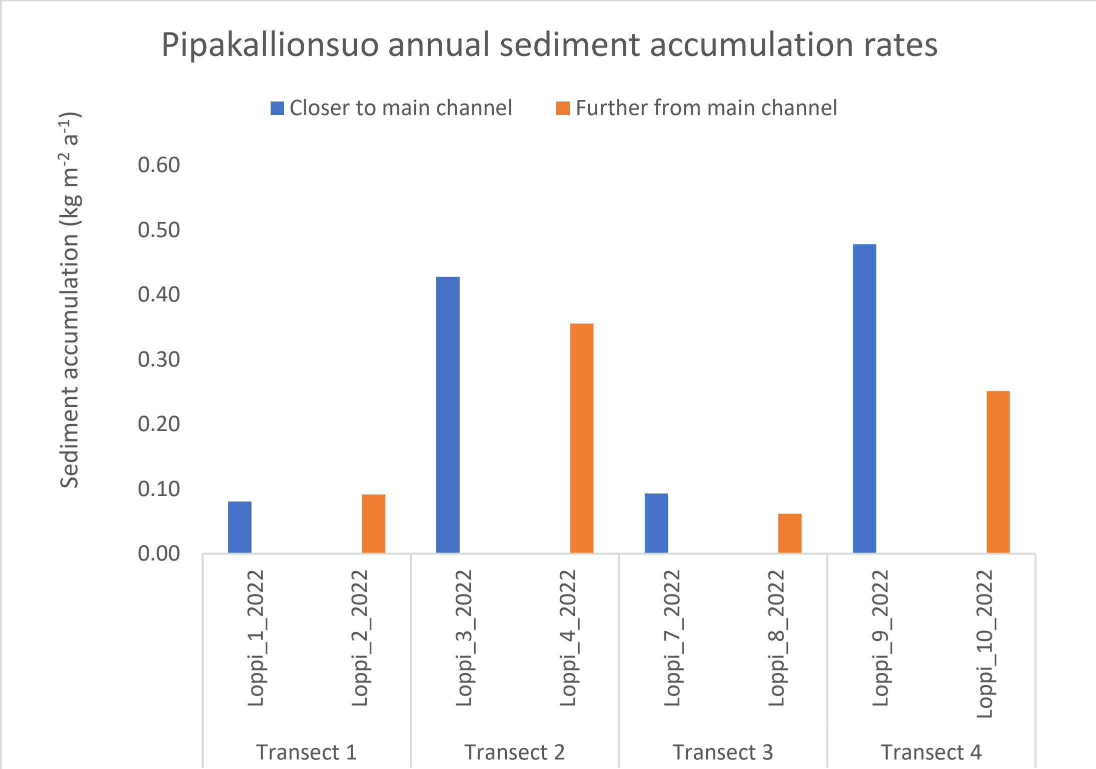

Figure 12. Pipakallionsuo sediment trap annual accumulation rates. Sediment traps were placed in four transects, where odd numbered traps were closer (blue bars) and even numbered traps further (red bars) from the main channel. The traps in each transect were approximately 1.5 m apart.

4.1.2. A closer look at Ritobäcken vegetation management, sediment accumulation, and inundation events

Ritobäcken sediment traps were part of vegetation management experiment by Valumavesi project, where samples with initial letter M had the vegetation on floodplain mowed to approximately 5–10 cm length, and traps with initial letter C were the control samples (un-mowed). On average the mowed sections annual sediment accumulation rates were 73.4 % higher compared to control sections and the difference was statistically significant using Mann-Whitney U test (Figure 13A). Sediment trap M3_B_2022 also displayed much lower sedimentation rates compared to its adjacent traps, while C2_C_2022 had much higher accumulation rates relative to other control management traps (Table 4). Average sediment accumulation rates between mowed and control sections were 2.19 kg m^{-2} and 1.23 kg m^{-2} respectively. Inundation duration between vegetation management methods were relatively similar, floodplain was inundated on average for 121 and 115 days for mowed and control sections respectively (Figure 13B).

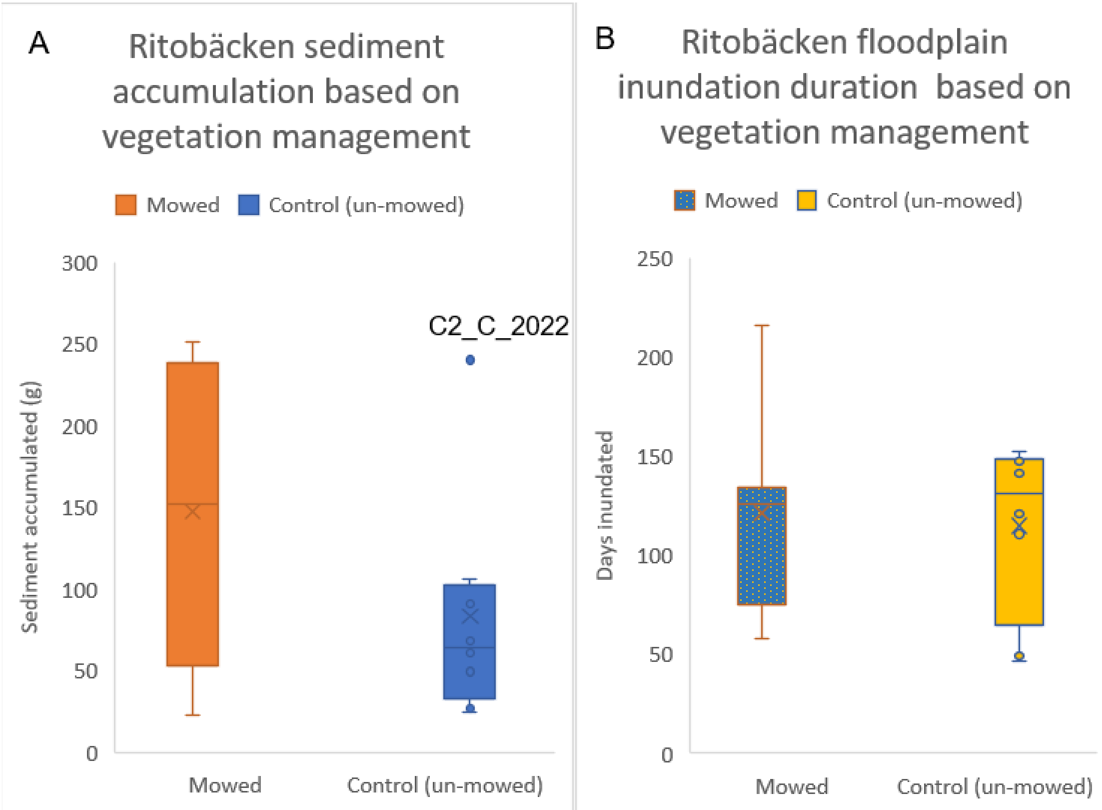

Figure 13. Comparison between Ritobäcken sediment traps based on vegetation management method, sediment accumulation (A), floodplain inundation duration (B). Mowed sections were cut to 5–10 cm length, while control sections were left unmowed. One outlier observed in (A), where sediment trap C2_C_2022 has much higher sediment accumulation relative to other control section traps, comparable sediment accumulation to highest mowed traps.

Ritobäcken floodplain inundation extent and sedimentation were estimated for a selected area of 1881 m^2, where sediment traps show differences in inundated floodplain area and total inundation duration over the four measuring periods (MP1-4, Table 7). Measuring periods were inundated for 51–85 % of the installation duration and average flooding extent varied between 1146–1345 m^2. Total sediment accumulation on the floodplain was estimated to be between the sediment accumulation over average flooding area and the maximum floodplain area (1881 m^2). For example, this estimates an average deposition of 1.89 tons and maximum deposition of 2.70 tons deposited over MP2 (Table 7). To estimate sediment accumulation rate between all Ritobäcken sediment traps, the MP3 and MP4 sediment accumulations were added together to make all measuring periods 223 or 265 days, to gain average sediment accumulation rate of 1.71 kg m^{-2}. The resulting average sediment accumulation rate estimates 2.25–3.22 tons of sediment deposition over 14.10.2021–25.5.2022 (223 days) period, which accounts for 2.62–3.71 % of the stream

TSS load. Shorter measuring period was selected due to only MP1 covers the longer 265-day time-period and its effect on sediment accumulation rates is expected to be minor due to few inundation events during 3.9.2021–14.10.2021 (Figure 14). The floodplain sediment accumulation varied between 1.48–4.64 % of the stream TSS load, with highest sediment retention efficiency measured in MP4 (Table 7). Assuming the increased sediment accumulation applies to whole floodplain, then vegetation management method would result in 2.87–4.12 and 1.62–2.32 tons of sediment deposition over the MP2 period for mowed and un-mowed method, respectively.

Table 7. Ritobäcken sediment traps sediment accumulation rates, inundation duration and the estimated total floodplain sediment accumulation over each measuring period (MP). The estimated floodplain sedimentation is based on average and maximum flooding extent and average sediment accumulation rate. Sediment retention assumes that all accumulated sediment is removed from stream load and estimated as ratio between sediment accumulation and sum of TSS and sediment accumulation. Note that the measuring periods and stream loads overlap with each other.

Measuring period (days)		Average sediment accumulation rate, kg m^{-2}	1)Sediment accumulation, 1000 kg	Average flooding area, m^2 (% flood-plain)	Days inundated (% measuring period)	2)TSS load, 1000 kg	3)Sediment retention (%)
MP1 (265)	3.9.2021-25.5.2022	1.84	2.11–3.46	1146 (60.9)	134 (50.7)	87.9	2.34–3.79
MP2 (223)	14.10.2021-25.5.2022	1.44	1.89–2.70	1314 (69.8)	184 (82.4)	83.6	2.21–3.13
MP3 (63)	14.10.2021-15.12.2021	0.33	0.44–0.61	1345 (71.5)	54 (85.2)	29.7	1.46–2.02
MP4 (160)	16.12.2021-25.5.2022	1.33	1.73–2.50	1301 (69.2)	125 (78.0)	53.9	3.11–4.43

1) Sediment accumulation on floodplain was estimated to be relative to the sediment accumulation between average flooding extent and the potential maximum flooding extent (1881 m2).

2) TSS load is the total suspended solids observed from EHP observation station.

3) Sediment retention estimated as a ratio between sediment accumulation and sum of TSS and sediment accumulation.

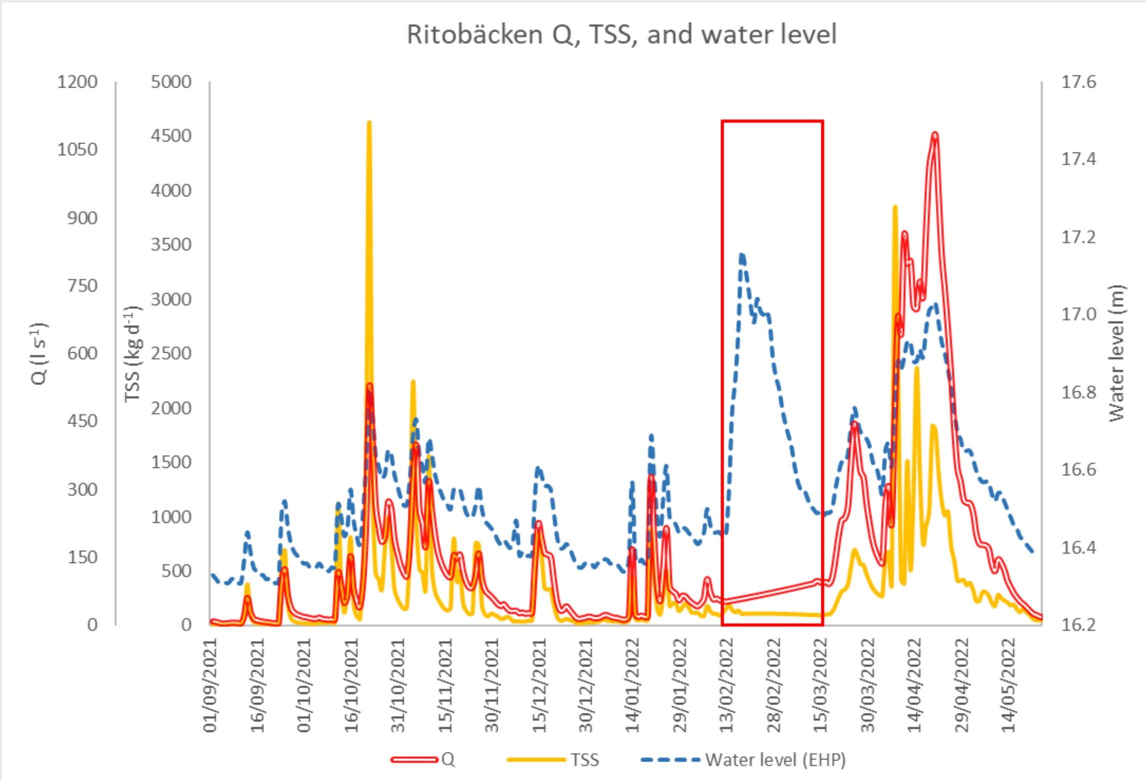

Figure 14. Discharge (Q), total suspended solids (TSS) loads, and water level measured from EHP observation station. Red rectangle displaying the period 12.2.2022–16.3.2022 when TSS, Q, and water level have a different trend.

4.1.3. Ritobäcken stream loads and climate

All water level observations station parameters (Q, TSS, TP, NO_3, TN, water level) correlated significantly with each other, while only TSS–precipitation, water level–snow depth, and snow depth–temperature shared significant correlation between weather station (Helsinki-Vantaa airport) and EHP water level observation station (Table 8). Very strong correlation exists between the TSS and water level observations. Exception to correlation was found in the period 12.2.2022–16.3.2022, when the water level rises to its peak at 17.2 m, but no major changes are observed in the discharge or TSS load (Figure 14). During this time-period the weather station data from Helsinki-Vantaa airport (Figure 7) shows the increase in precipitation, peak snow depth (73 cm), and temperatures remain below 2 °C. Snow depth decreases rapidly after temperatures rise above the 2 °C line in April with coinciding with TSS load increase.

Table 8. Correlations between EHP water level observation station parameters and Helsinki-Vantaa weather station climate parameters. Parameters and their units include, Q = Stream discharge (l s^{-1}), TSS = total suspended solids (kg d^{-1}), TP = total phosphorus (kg d^{-1}), TN = total nitrogen (kg d^{-1}), Water level = daily water level at EHP observation station (m), T = air temperature (℃), Prec. = precipitation (mm), and snow depth (cm). Significant correlations highlighted in bold.

	Q	TSS	TP	NO_3	TN	Water level	T	Prec.	Snow depth
Q	1.00	**0.67****	**0.86****	**0.89****	**0.89****	**0.69****	0.04	-0.07	0.04
TSS	**0.67****	1.00	**0.96****	**0.81****	**0.82****	**0.49****	0.07	**0.19****	-0.04
TP	**0.86****	**0.96****	1.00	**0.91****	**0.92****	**0.61****	0.07	0.10	-0.02
NO_3	**0.89****	**0.81****	**0.91****	1.00	**1.00****	**0.64****	0.11	0.04	-0.02
TN	**0.89****	**0.82****	**0.92****	**1.00****	1.00	**0.64****	0.10	0.04	-0.04
Water level	**0.69****	**0.49****	**0.61****	**0.64****	**0.64****	1.00	0.01	0.01	**0.38****
T	0.00	0.07	0.07	0.11	0.10	0.01	1.00	0.02	**-0.43****
Prec.	-0.07	**0.19****	0.10	0.04	0.04	0.01	0.02	1.00	0.02
Snow depth	0.04	-0.04	-0.02	-0.02	-0.04	**0.38****	**-0.43****	0.02	1.00

** Correlation is significant at level 0.01 (two-tailed).

4.1.4. Ritobäcken modelled water level and inundation event evolution

Interpolated flooding extent layers display how far the flooding reaches on the floodplain in different stages (Figure 15). During the base flow conditions (12.2.2022) only main channel of the stream flow is visible (Figure 15A), while during high water level (19.2.2022) there was potential of overbank flooding (Figure 15B). Interpolated flooding extent also shows the large topographical heterogeneity within the floodplain and used DEM, where floodplain is not entirely covered. Based on the modelled water level, the Ritobäcken floodplain inundation events usually start by water entering the floodplain in the lower elevation downstream sections. In February the observation periods highest water level indicates overbank flooding (Figure 15B and Figure 16A), with some disconnected sections revealing depressions that capture floodwater as the water level decreases. Inconsistency in flooded sections show potential errors caused by low resolution DEM and floodplain topographical heterogeneity.

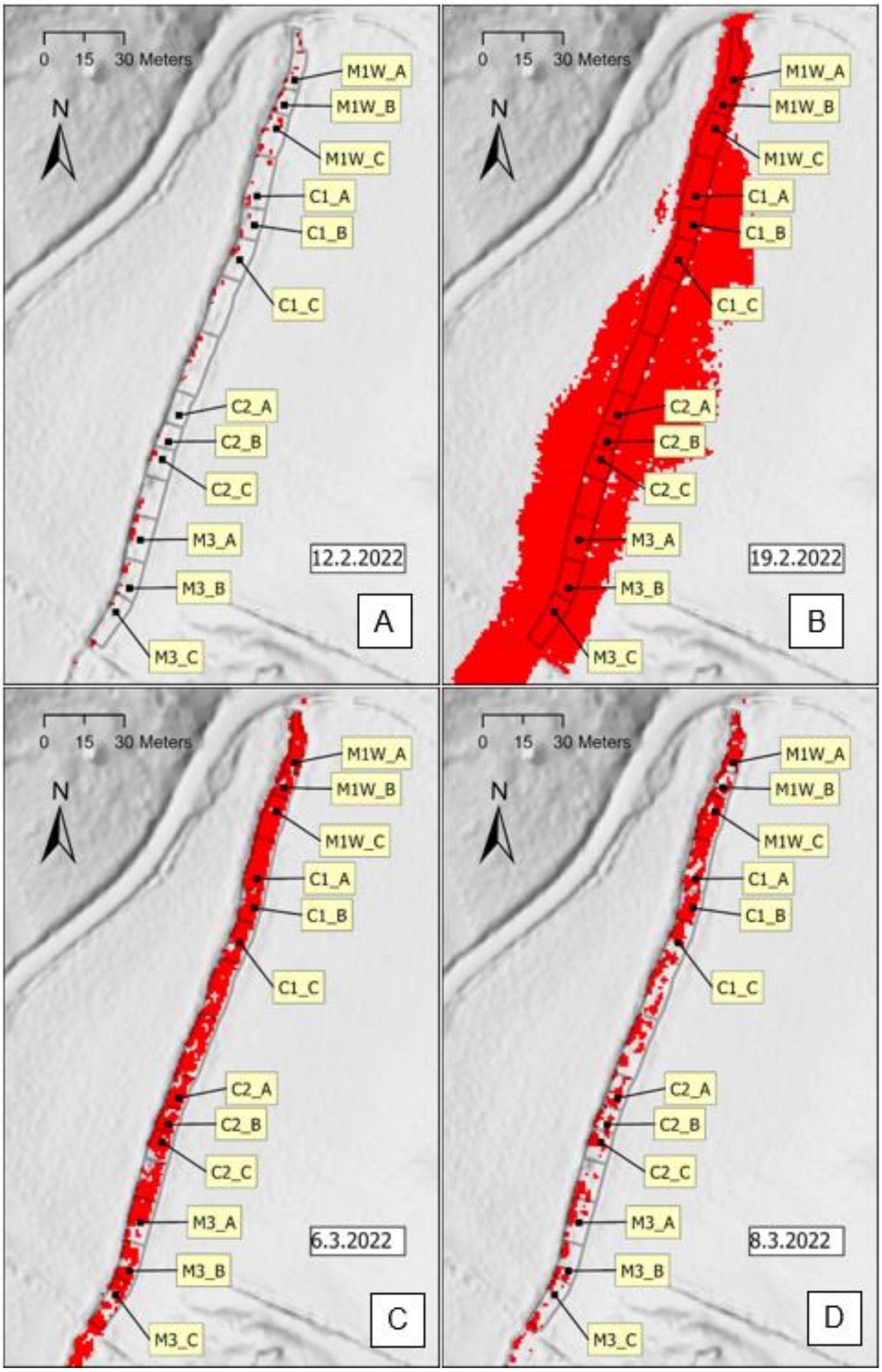

Figure 15. Ritobäcken flooding extent modelled for 12.2.-12.3.2022 flood event using Empirical Bayesian Kriging (EBK) Regression Prediction model (A–E). Water level above surface level shown in red color. Gray line indicates the visually determined floodplains maximum extent and the floodplain area studied for sediment accumulation. The models cross validation results shown for two events, 19.2.2022 and 12.3.2022 (F and G). The model overestimates high water level observations and underestimates the low water level observations displayed by difference in measured and predicted curves density. In E, the orange line indicates the cross section in Figure 16A, and blue line indicates the cross section in 16B.

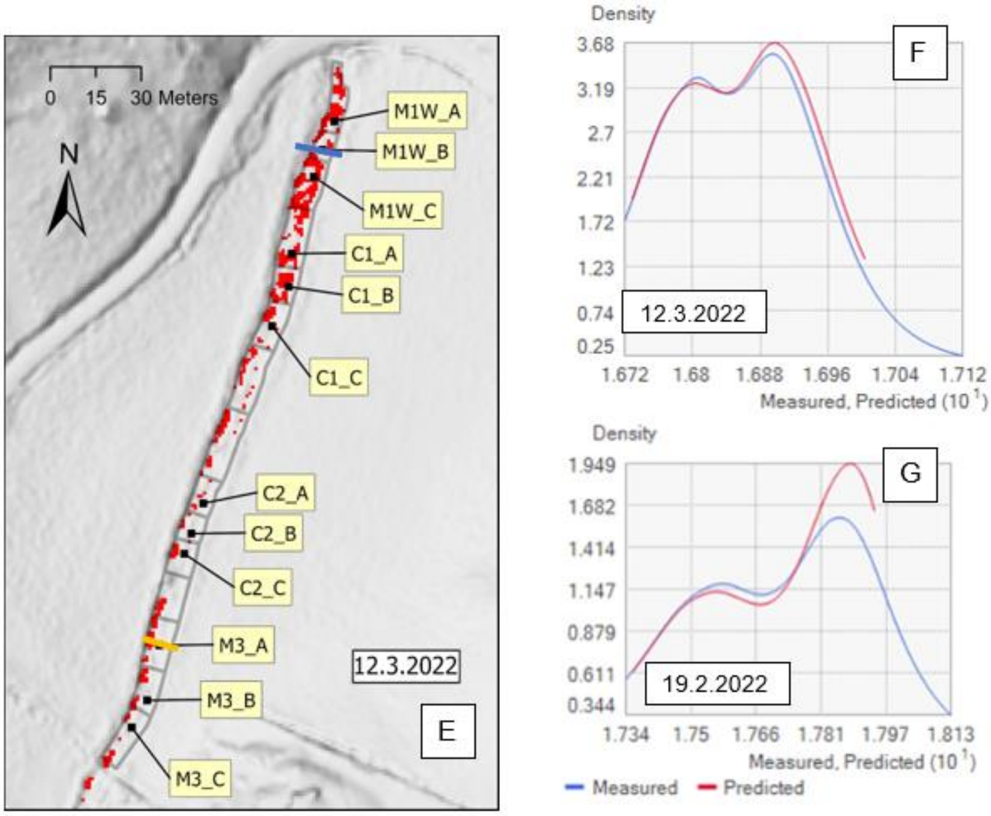

Figure 15 continues.

Cross sections made for up- and downstream sections display the spatial variability in floodplain inundation as the inundation event progresses (Figure 16). The upstream cross section at M3_A trap (Figure 16A) location experiences overbank flooding in 19.2.2022, while downstream section at M1W_B (Figure 16B) the flooding stays within the TSC limits. As the flooding dissipates within few days from near full floodplain inundation to near base flow conditions between 6.3.2022–12.3.2022 in upstream sections, the downstream sections are still flooded (Figure 15A–E and Figure 16). The downstream cross section showing the main channel at higher elevation relative to the floodplains lowest section shows the limitation of the low-resolution DEM at detecting small streams. Figure 16B). During the studied observation period downstream sediment traps are generally inundated longer closely following changes in surface elevation (Figure 17).

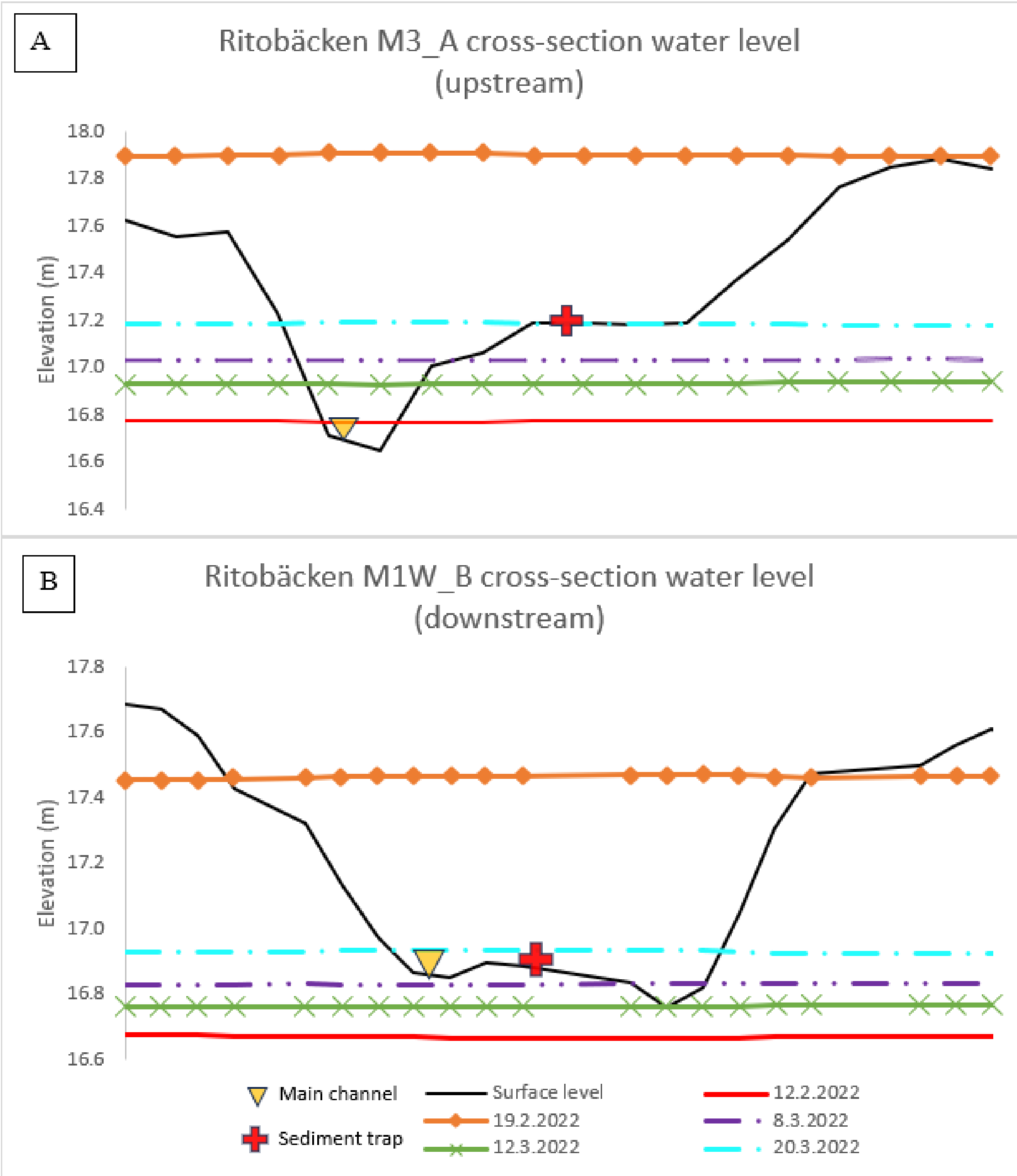

Figure 16. Ritobäcken upstream cross section from M3_A trap location (A) and downstream cross section from M1W_B trap location (B). Horizontal lines indicate the modelled water level during the 12.2.2022–12.3.2022 inundation event shown in Figure 16A-E. Cross section location and flooding extent along the TSC floodplain shown in figure 16E. Sediment trap location indicated with red cross and main channel position with yellow triangle.

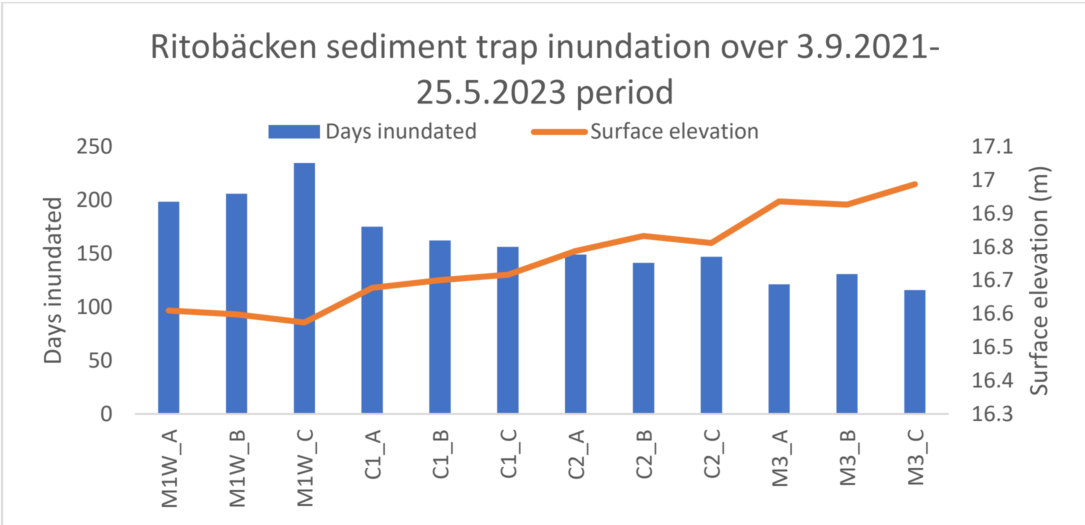

Figure 17. Ritobäcken sediment trap inundation duration over the water level observation period 3.9.2021-25.2023 and each respective traps surface elevation (orange line). Sediment traps are in order from left (downstream) to right (upstream).

4.2. Sediment geochemistry

4.2.1. Geochemistry of sediment trap material

All Ca and Se results in addition to sediment trap sample C1_B_2022 were removed from geochemical analyses due to analytical issues with ICP-MS. Specifically C1_B_2022 had values identical to blank samples that were below method detection limit. Sediment trap laboratory replicates and used reference materials had relative standard deviation (RSD) of 5.62%, including heterogeneity in Pipakallionsuo replicate with 15.28% RSD. At least one reference material was between 90–110 % recovery threshold for Na, Mg, Al, P, V, Cr, Fe, Co, Ni, Cu, Zn, Mn, As, Cd, Pb. Outside of this recovery threshold were Al, K, Ti, S, Mo, and U. Elements outside the acceptable recovery thresholds were included in the analyses due to good RSD between lab replicates but the methods poor recovery for listed elements and or the used reference materials needs to be considered. Used reference materials had no certified value for Zr, and only one reference material had a certified value for S. Samples with laboratory replicates are reported as an average between the replicates.

Uuhikonoja had generally highest average metal concentrations of the three locations (Table 9). Exceptions to this pattern are Cr, Mn, Sr, Cd, and Pb, whose concentrations were more evenly distributed between the study sites. Pipakallionsuo had the lowest concentrations in most analyzed elements, but much higher Mo concentrations, with over three-fold compared to Ritobäcken or Uuhikonoja. Analyzed element concentrations measured on average 11.33%, 32.2%, and 16.13% of total composition for Ritobäcken, Pipakallinsuo, and Uuhikonoja respectively. Elements not analyzed include oxygen and silicon, which constitute major fractions of soil material.

Table 9. Averages of sediment trap samples analysed for geochemical composition in Ritobäcken, Pipakallionsuo, and Uuhikonoja. Analyses performed with microwave assisted nitric acid digestion (EPA3051A), except for C, N, and loss on ignition (LOI, SFS3008:1981).

		Ritobäcken	Pipakallionsuo	Uuhikonoja
Measuring period (days)		63-265*	365	272
Na	ppm	339.25	128.29	619.74
Mg	ppm	8359.59	3380.25	17005.34
Al	%	2.31	1.05	4.37
K	ppm	4945.75	1494.59	9406.11
Ti	ppm	939.47	451.09	1494.01
P	ppm	646.07	1146.72	779.45
S	ppm	746.05	1969.09	228.20
V	ppm	54.44	24.64	102.38
Cr	ppm	54.75	105.16	102.59
Fe	%	3.21	2.48	6.09
Co	ppm	17.60	8.08	25.04
Ni	ppm	26.21	11.45	56.28
Cu	ppm	35.01	18.22	66.45
Zn	ppm	102.82	76.81	155.53
Mn	ppm	784.78	476.45	788.89
Sr	ppm	23.25	44.75	38.87
Zr	ppm	39.77	23.95	80.00
As	ppm	5.16	6.02	9.14
Mo	ppm	0.28	1.18	0.15
Se	ppm	0.24	0.49	0.26
Cd	ppm	0.25	0.27	0.19
Pb	ppm	17.57	11.61	20.63
U	ppm	2.63	2.61	7.89
LOI	%	10.51	50.60	7.76
C	%	3.79	26.42	2.37
N	%	0.30	1.33	0.21

*Four different measuring periods for Ritobäcken with four sediment traps for 63 days, four sediment traps for 160 days, two sediment traps for 223 days, and six sediment traps for 265 days, refer to Table 2 for details on different installation periods.

4.2.2. Manganese and iron ratio

Ritobäcken sediment traps had an average Mn:Fe ratio of 0.024 with noticeable difference in MP3 traps (M1W_A_2021, M1W_B_2021, C1A_2021, and C1B_2021) showing above average ratios up to 0.043 (Figure 18). Andelin (2019) FP and MC sediment cores from Ritobäcken also displayed high Mn:Fe ratios close to the surface that decreases with depth until reaching relatively constant ratio after 5–15 and 2–7 cm for FP and MC cores respectively (Figure 19). Pipakallionsuo sediment traps had similar variability to Ritobäcken in Mn:Fe ratio with lower ratios in Loppi_1, Loppi_7, Loppi_8, and Loppi_9, and two-fold higher ratios in Loppi_2, Loppi_3, Loppi_4, and Loppi_10 (Figure 20). Uuhikonoja sediment traps had lower Mn:Fe ratio of 0.009 in US_2022 an UT_2022 traps that were affected by slope erosion, while other traps varied between 0.013–0.016 (Figure 21). Spatial variability observed by RSD for Ritobäcken, Pipakallionsuo, and Uuhikonoja were 34.8 %, 46.8 %, and 19.31 % respectively. For most sediment traps, high P concentrations coincided with high Mn:Fe ratios, with few exceptions, such as lower Mn:Fe ratios at Uuhikonoja sediment traps UX, UO, and UX, that were inundated or wet during field sampling.

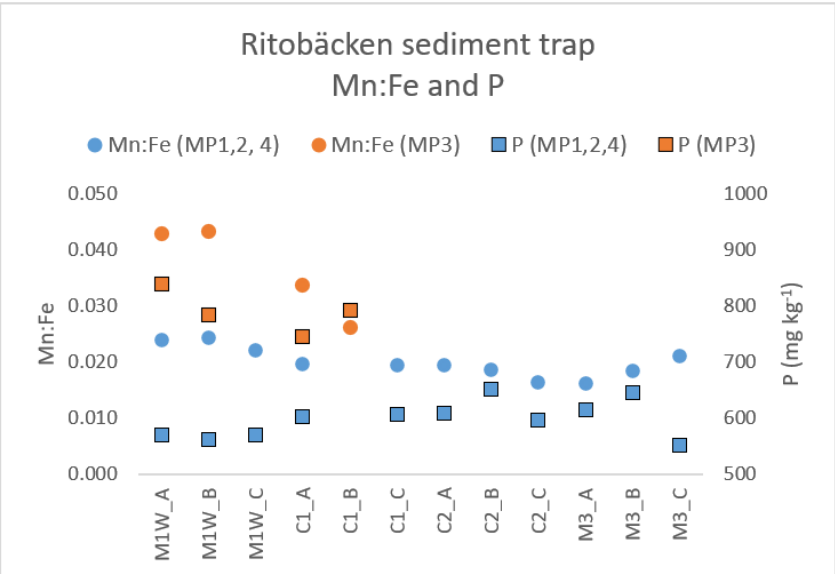

Figure 18. Ritobäcken sediment trap Mn:Fe ratio and its spatial variation along the reach and comparison to the P concentration distribution. Categories are in order of downstream (left) to upstream (right). Includes sediment traps from all measuring periods (MP1-4) which gives two results for trap locations M1W_A, M1W_B, and C1_A with blue markers (MP1, 2, and 4) and orange markers (MP3). Trap location C1_B only has results for MP3.

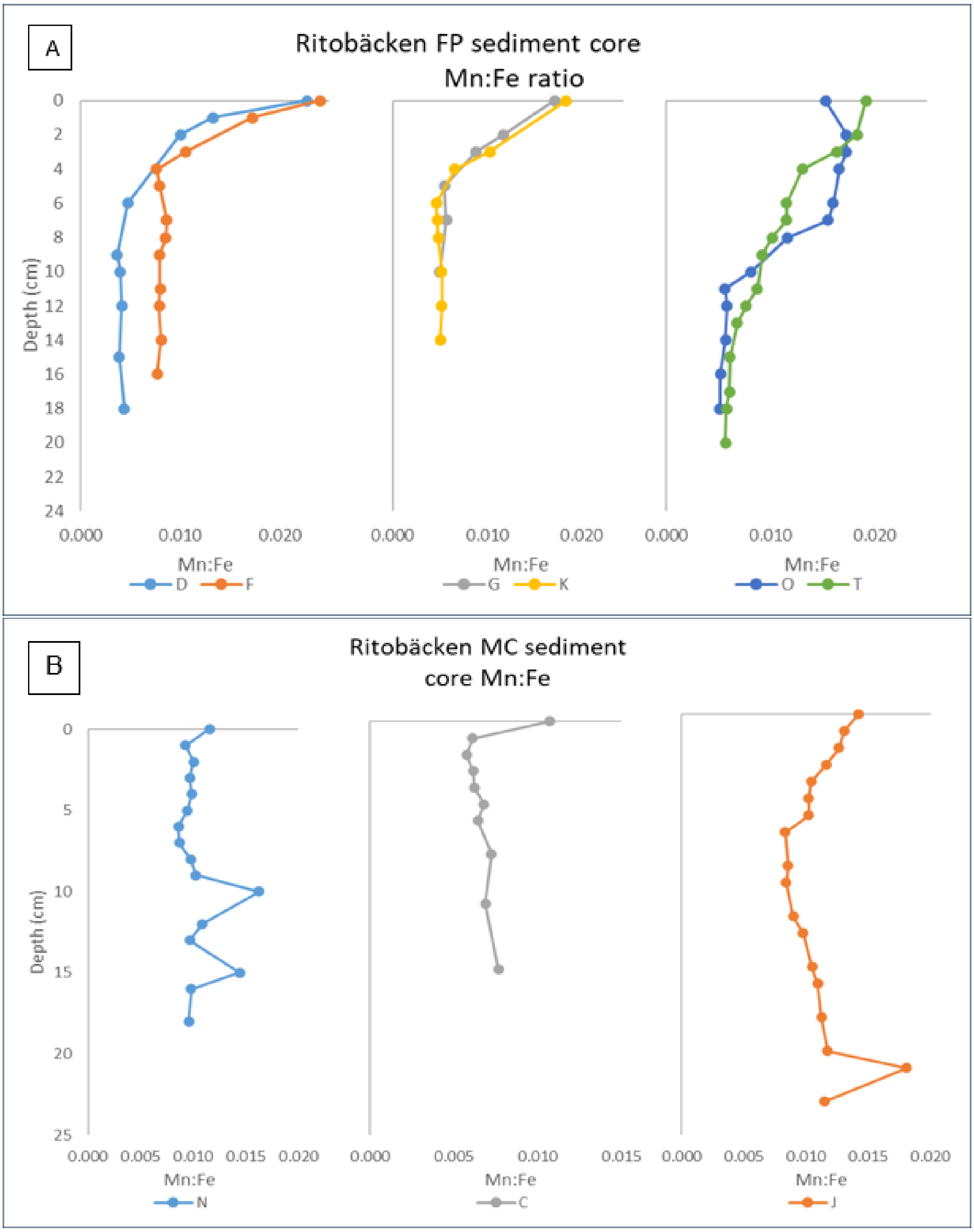

Figure 19. Ritobäcken floodplain (FP) and main channel (MC) sediment core Mn:Fe ratio profiles as an indicator of changes in oxidation conditions. Floodplain cores Mn:Fe ratio reaches constant ratio at approximately 5 cm depth (A). Main channel sediment cores Mn:Fe ratio reaches constant ratio after 1 cm for cores C and N, while core J reaches constant ratio after 7 cm (B).

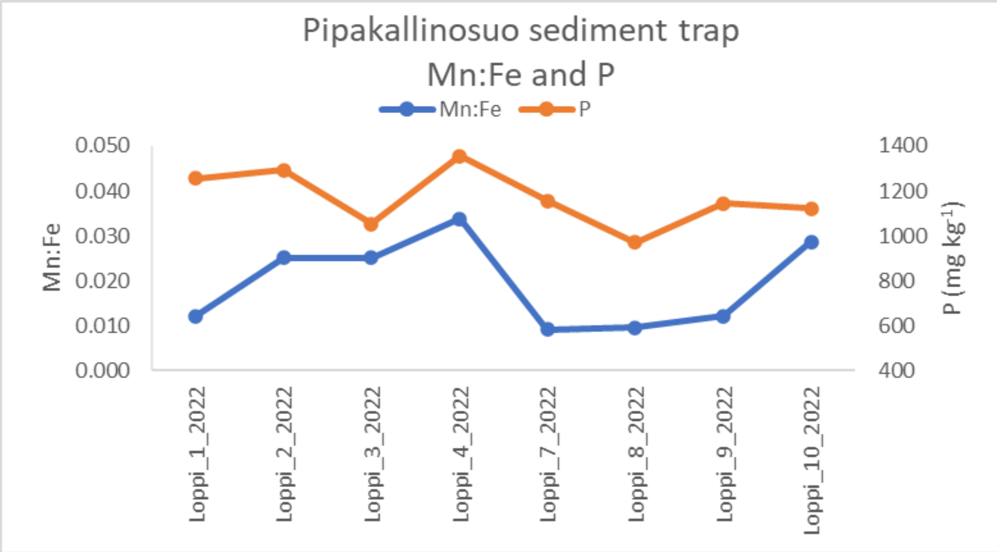

Figure 20. Pipakallionsuo sediment trap Mn:Fe ratio used as indicator for changes in oxidation conditions and its spatial variation along the reach and how it affects the P concentration distribution. Categories are in order of downstream (left) to upstream (right), with odd numbered traps closer to the MC and even numbered traps approximately 1.5 m further.

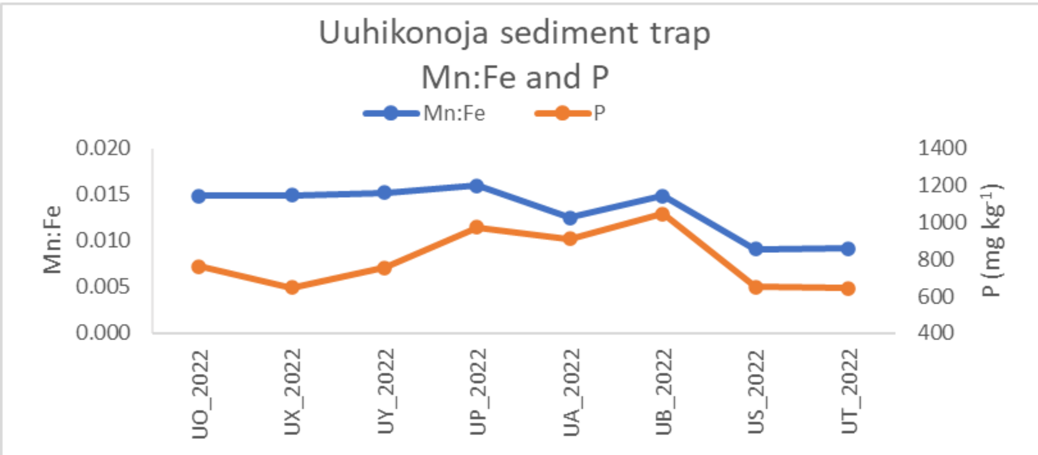

Figure 21. Uuhikonoja trap Mn:Fe ratio used as indicator for changes in oxidation conditions and its spatial variation along the reach and how it affects the P concentration distribution. Categories are in order of downstream (left) to upstream (right).

4.2.1. Sediment trap organic matter and C, N, P accumulation

Soils at the three locations contained organic matter and minerogenic material. Organic matter contents determined by LOI were highest at Pipakallionsuo (51 % of total mass) and lower at the other two locations (11 % and 8 % at Ritobäcken and Uuhikonoja, respectively, Table 9). Two Pipakallionsuo sediment traps had far above average organic matter content of 79 % and 70 % for Loppi_2_2022 and Loppi_8_2022, respectively.

Carbon, N and P contents for all sites show similar variability as expected from their presence in organic matter. Pipakallionsuo had the highest C:LOI ratio with average of 0.52 with lower ratios observed in Ritobäcken and Uuhikonoja with lower average ratios of 0.39 and 0.30 respectively. Linear regressions for C:LOI were high with R^2 of 0.996, 0.969, and 0.775 for Pipakallionsuo, Uuhikonoja, And Ritobäcken,. Sediment trap specific results for LOI, C:N, and C:LOI for all sediment traps presented in Appendix 1.

Highest nutrient accumulations for C, N, and P were observed in Uuhikonoja, followed by Ritobäcken and Pipakallionsuo (Table 10). Nutrient accumulation rates in the TSC closely follow the sediment accumulation rates for Ritobäcken and Uuhikonoja. Due to lower overall sedimentation rates, Pipakallionsuo also has low nutrient accumulation rates, which are slightly increased by higher nutrient concentrations (Figure 22, Table 9). Nutrient accumulation rates generally increased towards the downstream of each TSC, with lower elevation level and longer inundation duration, with exceptions caused by physical disturbances or local depressions. These include Ritobäcken C2_C_2022 sediment trap located in a depression and Uuhikonoja sediment traps affected by slope erosion (UT_2022 and US_2022), which show anomalously high nutrient accumulation rates following the increased sediment accumulation. Carbon, N and P accumulation rates had relatively constant ratios for each study site with few exceptions. Pipakallionsuo Loppi_2 and Loppi_8 and Uuhikonoja's UB_2022 had higher C and N relative to P accumulation rates compared to the other traps. Ritobäcken C2_C_2022 only had enrichment in C relative to P accumulation. For Ritobäcken and Uuhikonoja increased nutrient accumulation rates coincided with changes in elevation level (Figure 22).

Table 10. Sediment trap average sediment, C, N, and P accumulation rates. For comparison the phosphorus accumulation rate was calculated with HNO_3 digested phosphorus (TP) and sequential extraction calculated phosphorus (TP-SEDEX).

Site	Annual sediment accumulation, g $m^{-2}a^{-1}$	Annual C accumulation, g $m^{-2}a^{-1}$	Annual N accumulation, g $m^{-2}a^{-1}$	Annual TP accumulation, g $m^{-2}a^{-1}$	Annual TP-SEDEX accumulation, g $m^{-2}a^{-1}$
Ritobäcken	2474.4	93.78	7.42	1.48	1.98
Pipakallionsuo	230.1	8.72	0.69	0.14	0.18
Uuhikonoja*	6378.1	241.73	19.13	3.83	5.10

*Sediment and nutrient accumulation rates were calculated without UT_2022 trap that was considered anomalous deposition from bank erosion.

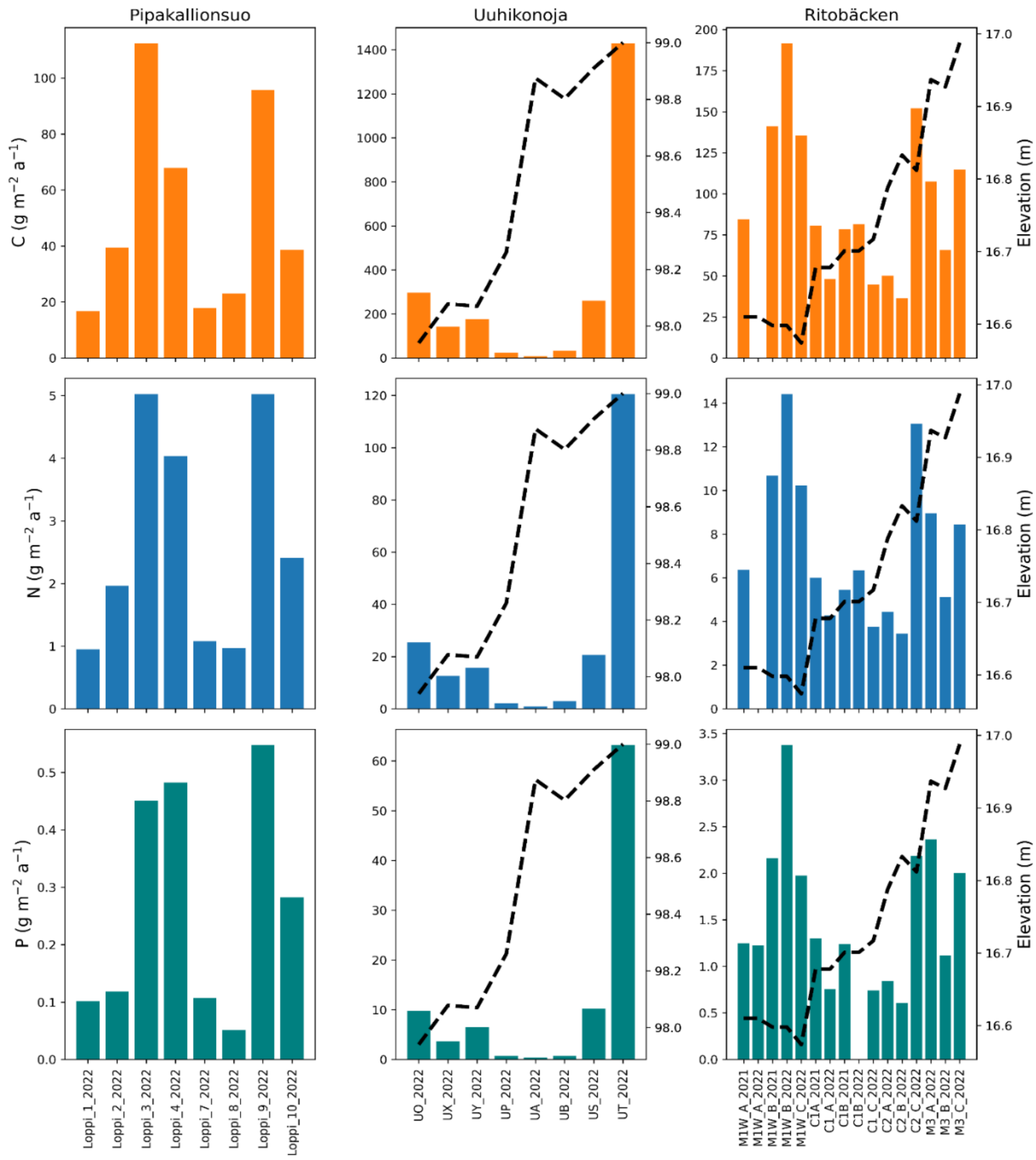

Figure 22. Sediment traps C, N, and P annual accumulation rates spatial distribution. Phosphorus accumulation rates calculated from the HNO_3 digestion (section 3.2.1.). Sediment traps are in order from downstream (left) to upstream (right). In Ritobäcken samples M1W_B_2022 for C and N has no values due to failed analysis. For Ritobäcken and Uuhikonoja the measured surface elevation is included on the secondary y-axis (black dashed line). Note the different vertical scales for each plot, especially in Uuhikonoja.

4.2.2. Spatial variability in sediment traps and sediment core geochemistry

Ritobäcken sediment trap geochemistry was compared to Andelin (2019) sediment cores topsoil (<3 cm depth) using Kruskal Wallis test on clr transformed data. To account for sediment traps temporal variability due to different sampling periods, only MP1, MP2, and MP4 were selected for the test. Sediment cores were from three different sampling locations, channel bank (B), floodplain (FP), and main channel (MC). Across all sampling locations the sediment core topsoil was similarly distributed in Al, K, and Zn. Conversely all sediment core sampling locations were significantly different in Fe and Mg. Sediment traps shared a similar distribution with FP cores in S and Mn, and with MC cores in P. For sediment traps seasonal variability, all measuring periods (MP1–4) shared a similar distribution of Fe and Zn. Most notable differences between measuring periods were found between MP1 and MP3, where significant differences were found in Al, K, P, S, and Mn. Floodplain sediment core profiles for whole core length show decrease in Mn, Zn, and P with increasing depth, and increase in Mg, Al, K, S, and Fe with increasing depth (see section 4.2.2.).

Principal component analysis was made from Mg, Al, K, Fe, P, S, Zn, and Mn that were analysed for both Ritobäcken sediment trap and sediment core samples (Figure 23). The first two principal components (PC) explain 78.7% of the total variance where PC1 and PC2 explain 46.2% and 32.5% of the variation respectively and first six PCs account for 99.4% of total variance. First principal component has high variable factor loadings for Al, Fe, Zn, and S (Figure 24). Closer inspection on PC1 shows that FP, B, sediment traps, and the upper layers of MC cores are grouped together, while MC cores deeper layers plot on opposite side of the PC1 axis. The second principal component has high variable factor loadings for K, and Mn. Sediment cores from FP and B locations are arranged across the PC2 based on their respective sampling depth, where surface layers are closer to sediment traps (fresh deposition) composition. Sediment traps sampled in MP3 plot slightly separately from traps sampled in MP1, 2, and 4. Principal component analysis factor loadings presented for first six principal components in Appendix 2. Biplot between PC1 and PC2 shows correlation between Fe and Al, and between Zn, Mg, and S. Biplot for PC2 and PC3 shows correlation between Al, Fe, S and Mn, and between P and K (not shown).

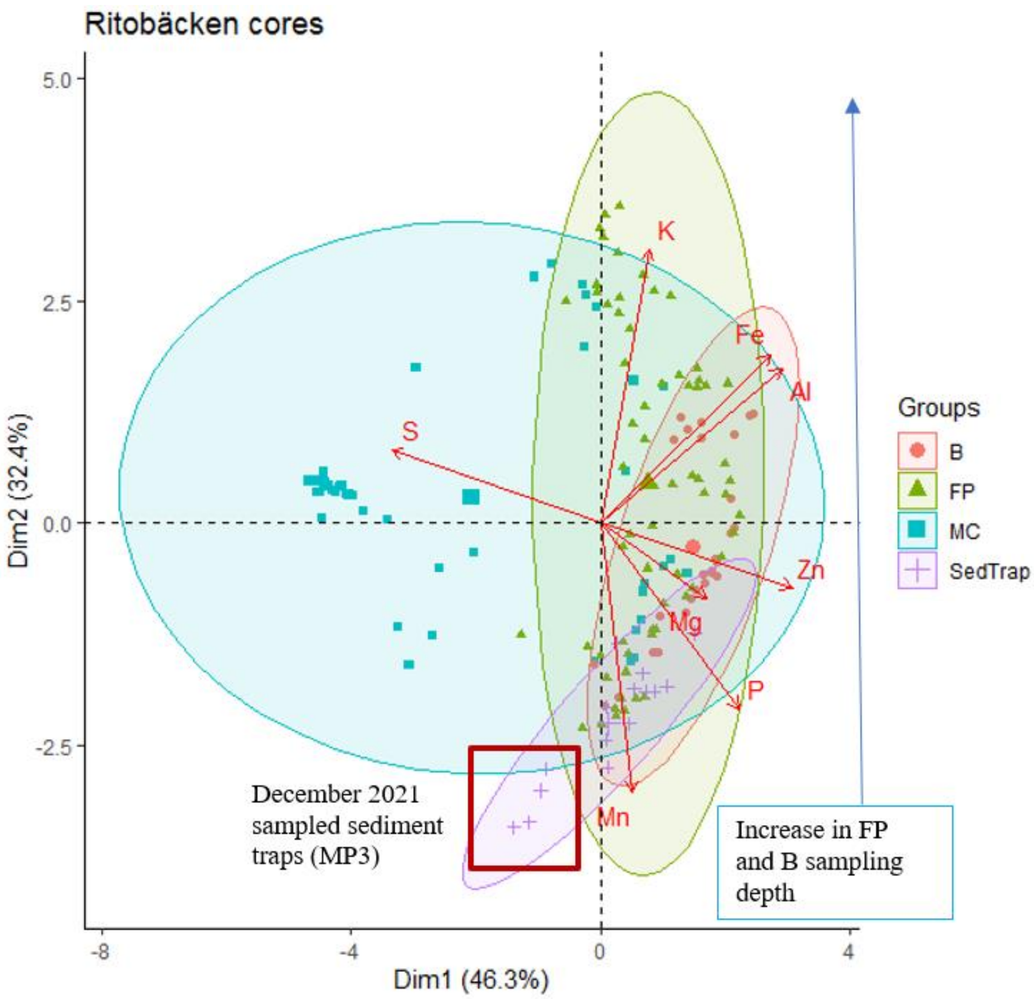

Figure 23. Principal component analysis (PCA) biplot with Ritobäcken sediment core and sediment trap geochemistry (Al, Mg, K, Fe, P, S, Zn, Mn). Sampling locations include bank (B) = red circles, floodplain (FP) = green triangles, main channel (MC) = blue square, and sediment traps (SedTrap) = purple plus sign. Red rectangle indicates four sediment traps from MP3 sampled in December 2021 (see text). Blue arrow shows increase in B and FP cores sampling depth along the second principal component axis (Dim2). Ellipses show different sampling location groups.

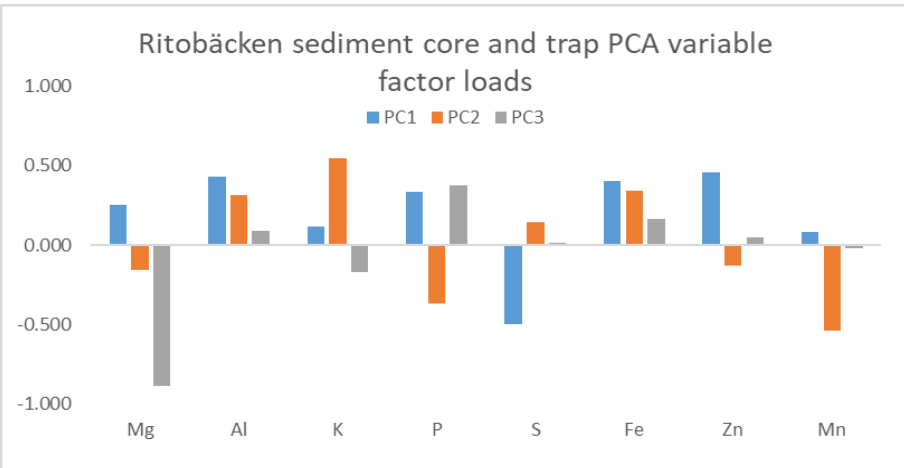

Figure 24. The first three principal components variable factor loadings for Ritobäcken sediment core and sediment traps in Figure 23.

Hierarchical cluster analysis (HCA) for sediment trap geochemistry and P-speciation (section 4.3.) identified two major clusters with Uuhikonoja and Ritobäcken samples placed in cluster A and Pipakallionsuo samples in cluster B (Figure 25). Cluster A had three secondary clusters which split into 1) Ritobäcken winter sampled traps (MP3) forming one cluster, 2) Ritobäcken May sampled traps (MP1, MP2, and MP4), and 3) Uuhikonoja sediment traps, with exception to UB_2022 that was identified as similar to Ritobäcken samples. Cluster B with Pipakallionsuo sediment traps was split into two secondary clusters with two trap transects in each group, Loppi_3, Loppi_4, Loppi_9, and Loppi_10 forming first group and Loppi_1, Loppi_2, Loppi_7, and Loppi_8 forming the second group.

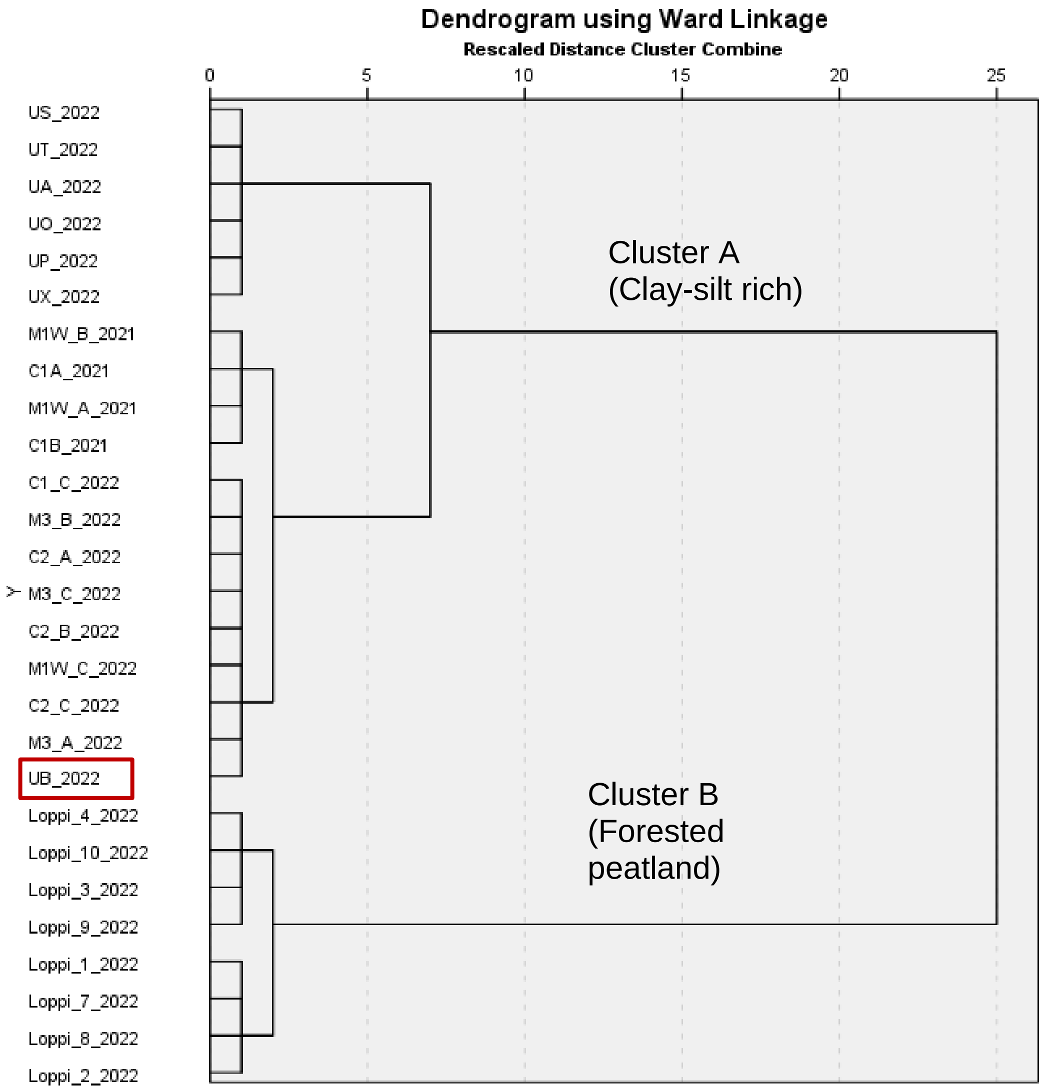

Figure 25. Hierarchical cluster analysis performed for sediment trap samples analysed elements and P-species. Wards method with squared Euclidian distance. Data was centre-log-ratio transformed prior to analysis to normalize cases around geometric mean. Red square highlights the Uuhikonoja sediment trap grouped together with Ritobäcken traps.

4.3. Phosphorus speciation

4.3.1. Sediment trap P-species spatial and temporal variability over different sampling locations

Sediment trap P speciation is dominated by Fe-P in all sites, with the lower proportions for species of Al-P, Ca-P, and Res.org-P varying in each study site (Figure 26). Second highest P species in Pipakallionsuo was Al-P, while at Ritobäcken and Uuhikonoja it was Ca-P. Ritobäcken and Uuhikonoja have very similar P speciation, with higher Res.Org-P in Uuhikonoja (Figure 26). Lowest concentrations in all sites were observed in exchangeable P, that was below method detection limit in all but one sample in Pipakallionsuo and not included in further statistical analyses. For all sites the highest variance was observed in Fe-P concentrations, changing from 330 mg kg^{-1} to 1130 mg kg^{-1}.

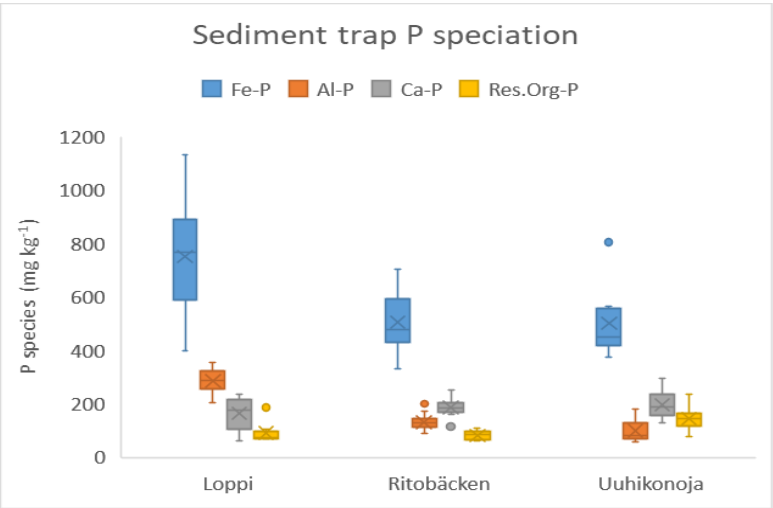

Figure 26. Comparison between study sites sediment trap P-speciation. Clear visual on P species ranking which changes between sites. Pipakallionsuo has the second highest species of Al-P, while Ritobäcken and Uuhikonoja it is Ca-P. Uuhikonoja has higher Res.Org-P relative to Ritobäcken and Pipakallionsuo. Largest variability in concentrations visible in Pipakallionsuo.

Total phosphorus calculated from the sum of all extracted P-species (TP-sedex) was on average 20% higher compared to HNO_3 acid digestion in Ritobäcken and approximately 10% higher for Uuhikonoja and Pipakallionsuo sediment traps (Table 11). Sediment traps TP-sedex was on average 840 mg kg^{-1}, 941 mg kg^{-1}, and 1298 mg kg^{-1} for Ritobäcken, Uuhikonoja and Pipakallionsuo respectively. For reference in 2021 Pipakallionsuo sediment trap samples the mean TP-sedex concentration was 933 mg kg^{-1}. Kruskal-

Wallis test shows that sediment traps at different study sites have significant differences in Al-P, Res.Org-P and TP-sedex (Table 11).

Table 11. Sediment trap average concentrations for each P species, including total phosphorus as a sum of P species (TP-sedex) and HNO_3 acid digested, TP (HNO_3). Letters indicates significant difference in P species distribution between study site based on Kruskal-Wallis test.

Site	Fe-P	Al-P	Ca-P	Res.Org-P	TP-Sedex	TP (HNO_3)
Ritobäcken	506.6	131.5^a	187.1	82.6^b	840.2^b	648.8^b
Uuhikonoja	501.6	98.8^a	195.8	145.1^{ab}	941.2^a	798.7^a
Pipakallionsuo	752.2	286.6^a	165.2	91.3^a	1297.6^{ab}	1168.7^{ab}

Ritobäcken sediment core profiles P speciation is nearly identical to the spatial variation presented by sediment traps. Sediment cores from FP have higher Fe-P concentrations closer to the surface that decrease with increasing depth, while MC N-core has low concentrations even at topsoil (Figure 27). Ritobäcken sediment traps show no distinct spatial variability across the floodplain reach length aside from MP3 samples with higher concentrations across all species that did not change P speciation (Figure 28). Ritobäcken MC sediment cores P-species was available only from two sediment cores (N and J) that were sampled for 0–3 cm depth, with 712 mg kg^{-1} average TP-sedex being slightly lower compared to floodplain cores.

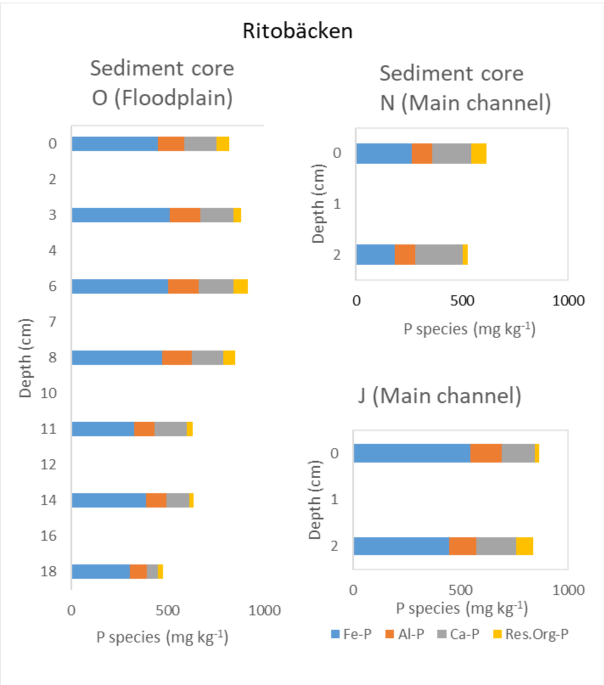

Figure 27. Comparison between sediment cores phosphorus speciation from Ritobäcken floodplain (FP) and main channel (MC) sediment cores.

Figure 28. Ritobäcken (left) and Uuhikonoja (right) sediment trap P speciation variability shown as concentrations (top) and proportions (bottom).

Uuhikonoja's floodplain sediment cores sampled in 2020, have higher distribution of Res.Org-P and lower Ca-P respective to sediment trap samples from 2022 (Figure 28 and Figure 29). Total phosphorus concentrations in floodplain sediment cores in Uuhikonoja and Ritobäcken were on average 958 mg kg^{-1}, and 779 mg kg^{-1} respectively. Floodplain sediment cores topsoil above 3 cm depth in Uuhikonoja and Ritobäcken have average TP-sedex of 905 mg kg^{-1}, and 878 mg kg^{-1}, respectively. Comparison between sediment traps and sediment cores from Ritobäcken and Uuhikonoja show slight change in P species with increasing depth (Figure 30). Both Ritobäcken and Uuhikonoja had significant differences between FP cores and sediment trap samples in Ca-P and Res.Org-P species. Additionally, Ritobäcken sediment traps and MC cores were significantly different in Res.Org-P.

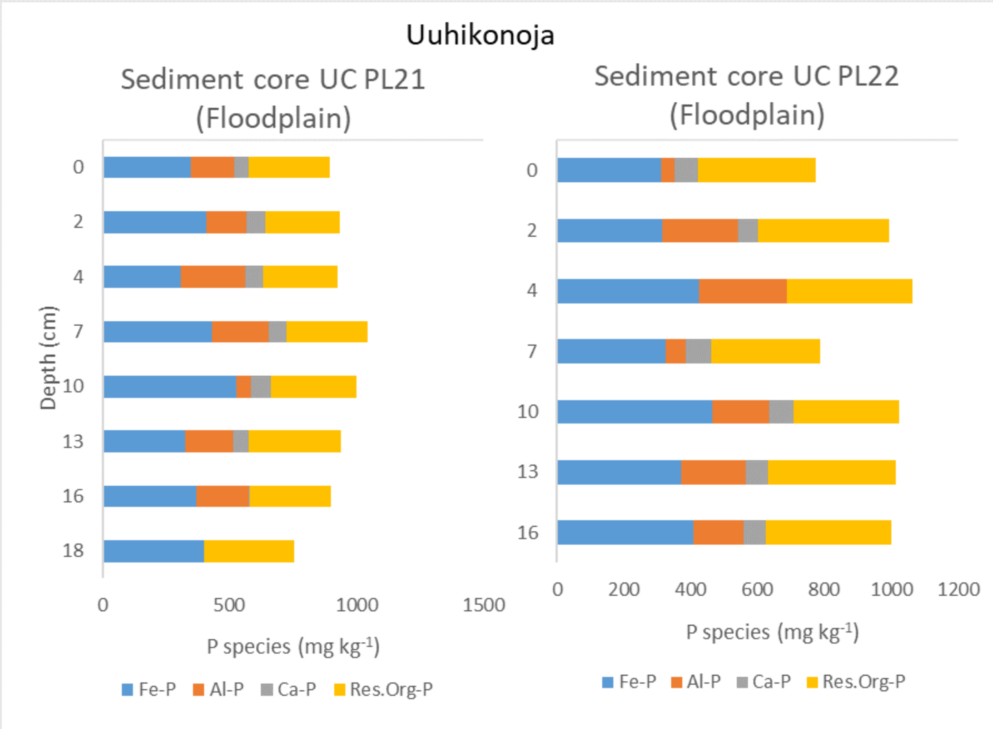

Figure 29. Uuhikonoja phosphorus speciation sediment core profiles sampled in 2020 from freshly excavated floodplain.

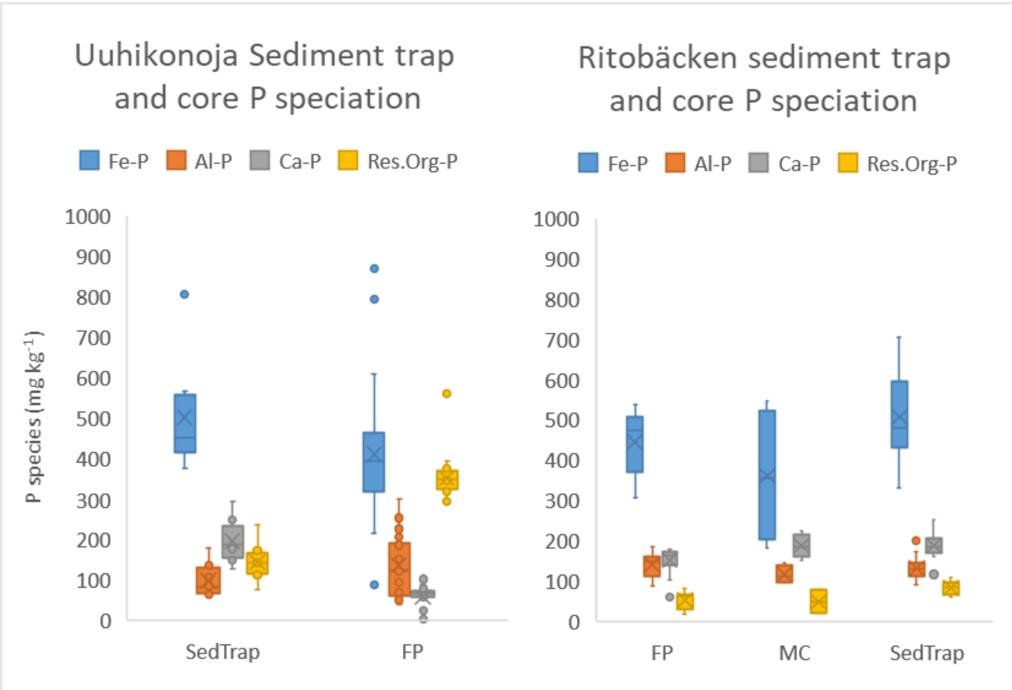

Figure 30. Uuhikonoja and Ritobäcken sediment trap and sediment core P-species distributions based on their sampling location 1) SedTrap = Sediment trap, 2) FP = Floodplain, 3) MC = Main channel. Uuhikonoja sediment cores sampled in 2020 show much higher Res.org-P and lower Ca-P relative to 2022 sampled sediment traps. Ritobäcken sediment traps and core P-species distributions are similar, with MC showing higher variation in Fe-P. Sediment cores maximum sampling depths varied between 18–26 cm in Uuhikonoja FP cores (4 cores), and between 5–21 cm for FP (2 cores) and 3 cm for MC (2 cores) in Ritobäcken.

Pipakallionsuo sediment trap speciation remained relatively similar between two sampling years (Figure 31). Total phosphorus concentrations were on average 45 % higher in 2022 but generally follow similar trend in spatial distribution, except for Loppi_4 that shows over two-fold increase in TP concentrations. Speciation also changed between the years where Fe-P contribution decreased but was not significant, with an increase observed in Al-P and Ca-P proportions. Mann Whittney U test found significant differences between sampling years in Al-P, Ca-P and Res.Org-P.

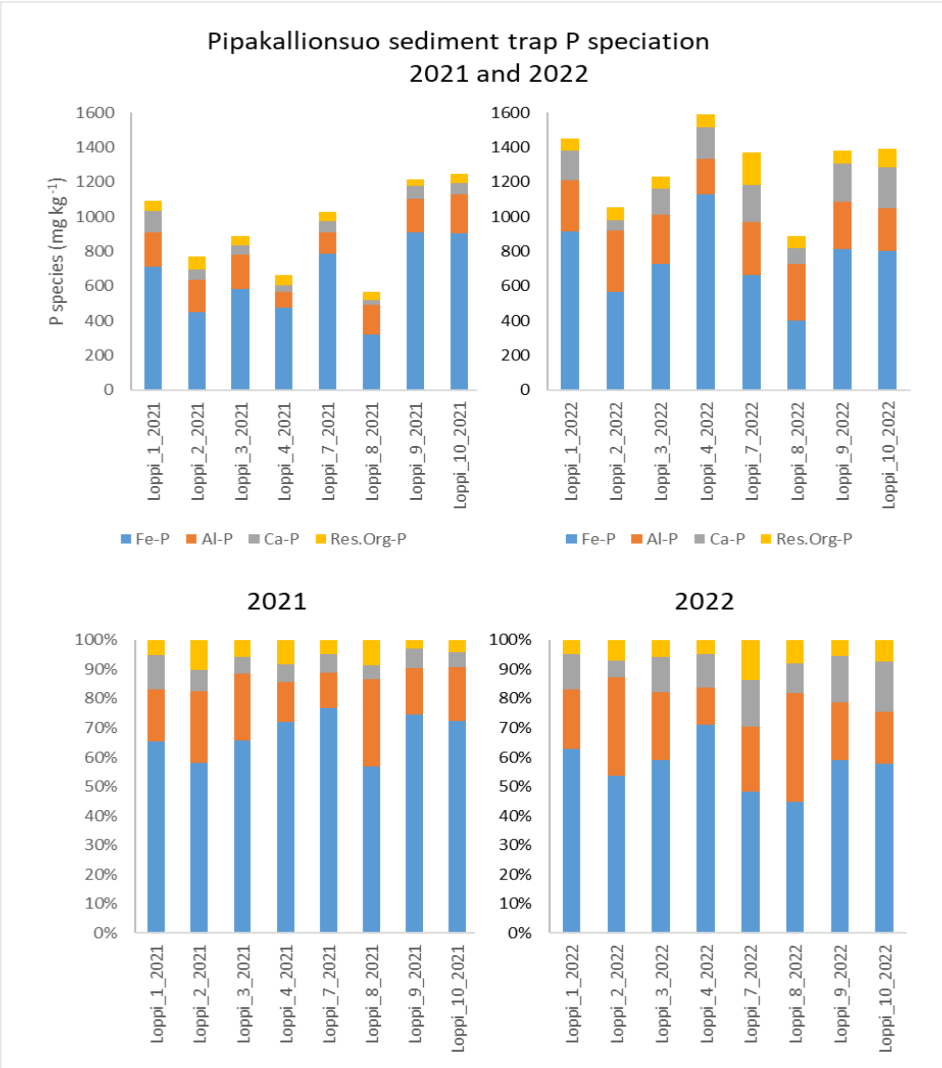

Figure 31. Pipakallionsuo sediment trap phosphorus speciation for year 2021 (left) and 2022 (right) as concentrations (top) and proportions (bottom).

4.3.2. Principal component analysis between sediment trap P species and geochemistry

Principal component analysis for sediment traps plots each study site in their own clusters with spatial variability in geochemical composition visible in linear shape of the clusters across the principal component axes (Figure 32). Uuhikonoja and Ritobäcken sediment traps are loosely arranged by their spatial proximity along the floodplain, forming linear pattern. Pipakallionsuo sediment traps did not follow similar floodplain scale spatial distribution, but instead sediment traps were paired with traps with similar proximity to the main channel. For example, Loppi_4 and Loppi_10, which were both further from the main channel, plotted closely and similarly Loppi_9 and Loppi_3 that were closer to main channel.

The first two principal components explain 75.6 % of total variance, with PC1 and PC2 explaining 63.5 % and 12.2 %, respectively. First principal component is split with small negative loading for Na, Mg, Al, K, Ti, V, Fe, Co, Ni, Cu, and Zr, while positive loadings are high on C, N, Mo, S, and Al-P. Ritobäcken and Uuhikonoja are grouped together on the opposite side of PC1 axis respective to Pipakallionsuo. The second principal component has the highest positive factor loading for Cr, Sr, U, C, and N, while highest negative factor loadings are for S, Mn, Co, and Ca-P. All study sites show greater variability across PC2, indicated by the elongated ellipses in Figure 32. Temporal variability was visible in Ritobäcken with sediment traps sampled in December 2021 (MP3) being slightly separated from the May 2022 sampled traps (MP1, MP2, and MP4). First five principal components account for 90.8 % of total variance, and variable factor loadings for first five PCs are presented in
Appendix 3.

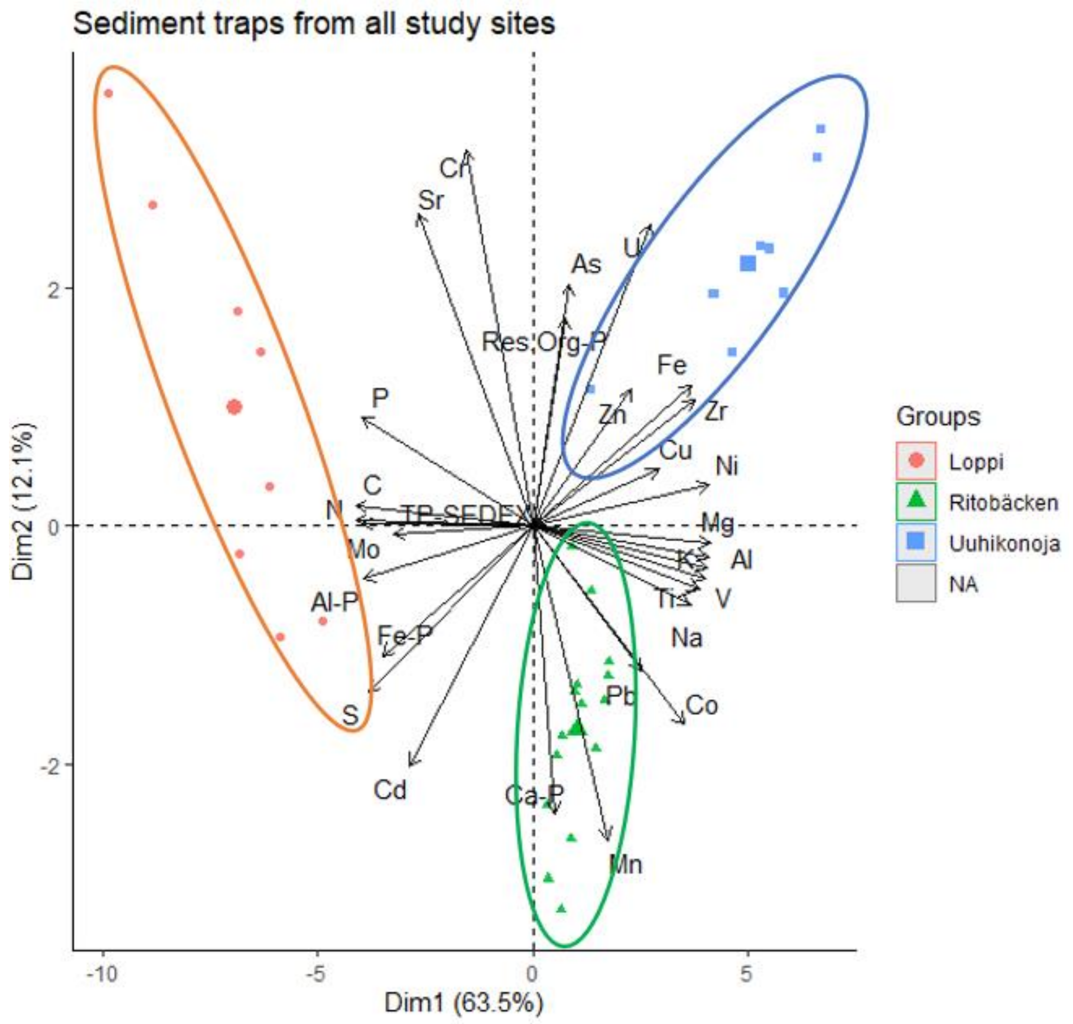

Figure 32. Principal component (PCA) for sediment trap geochemistry and P speciation from Pipakallionsuo (Red circles), Uuhikonoja (Blue squares) and Ritobäcken (Green triangles). Each study site plots in their respective groups with spatial variability highlighted with coloured ellipses. Black vectors are the variable factor loadings for analysed components.

5. DISCUSSION

5.1. Sediment accumulation

5.1.1. Factors affecting sediment transport in TSC floodplain

All TSCs show net sediment deposition on the floodplain, where clay-rich sites Uuhikonoja and Ritobäcken had more sediment deposition compared to forested peatland in Pipakallionsuo. Sediment traps had higher sediment accumulation in lower elevations or areas closer to the MC (Figure 11, Figure 12, and Table 5). At Pipakallionsuo, three out of four sediment trap pairs (transects) displayed higher accumulation close to MC with on average 53.6% higher accumulation rates.

Differences in sediment accumulation rates in rewetted areas such as floodplains are often related to the hydrology, channel stability, vegetation, soil compositional, and preferential flow path variables (Kronvang et al. 2007, Forsmann and Kjaergaard 2014). Kronvang et al. (2007) studied sediment and particulate phosphorus accumulation on inundating natural and restored river floodplains using sediment traps for direct sedimentation measurements. Their study results indicated that sediment accumulation was greatest at the areas where most of the flood water inflow enters the floodplain and generally decreased with increasing distance from the main channel (Asselman and Middelkoop 1995, Kronvang et al. 2007). Similar results were obtained in Pipakallionsuo where the transect at start of the TSC had highest sediment accumulation, suggesting highest inflow to floodplain at start of the TSC. Oppositely, Pipakallionsuo also had high sediment accumulation rates in middle sections of the floodplain adjacent to two transects with lower accumulation rates implying difference in inundation conditions or preferential flow paths. Conclusions about relationship of high sediment accumulation and high flood water inflow routes at start of the TSC floodplain in Ritobäcken and Uuhikonoja could not be made as the floodplain extends higher upstream. Sediment traps high sediment accumulation at the TSC upstream sections in Ritobäcken and Uuhikonoja suggested influence of vegetation management or increased erosional transport respectively (Figure 11). Modelled inundation extent in Ritobäcken show that water level enters the floodplain in the downstream lower elevated areas but gives no information on how the flow pattern changes as inundation extends further upstream (Figure 15).

By identifying the horizon corresponding to TSC excavation from sediment cores in Ritobäcken, Andelin (2019) showed that sediment accumulation rates decrease with increasing distance to MC. Thus, the results of Andelin (2019) support those of the present study. Lambert and Walling (1987) described heterogeneity in floodplains topography that captures flood water and its suspended sediments, settling them in disconnected depressions. They also had novel experiment at placing sediment traps in various topographically different locations, such as ebb channels, depressions, bank breaches, in areas close to vegetation, or no vegetation to investigate local scale depositional variation. In their study the trap location had no substantial effect on sediment accumulation but was mostly driven by changes in elevation. Hoffman et al. (2009) reported resuspension of main channel unconsolidated sediments as the main sediment transport mechanism in their study, while Baldan et al. (2021) discussed bank erosion as the primary factor in river setting. Kronvang et al. (2007) also reported increased bank erosional transport from freshly excavated channels. Established vegetation in TSC floodplains reduces erosion by increasing channel stability and can contribute to the nutrient uptake from floodplain soils (Powell et al. 2007, Davis et al. 2015, Krider et al. 2017). Floodplain sediments phosphorus deposition is mostly associated with particulate sediment transport (Noe and Hupp 2005). This was in-line with Kruskal-Wallis test results for Ritobäcken, showing similar P distribution between MC sediment cores and sediment traps, suggesting that fresh floodplain sediment deposition originates from the eroded upstream MC sediment pool, while the surface layers of FP and B sediments get enriched in P over time due to biogeochemical processes in the vadose zone. Significant differences interpreted from Kruskal-Wallis test between Ritobäcken sediment cores and sediment traps are potentially influenced by the different analysis methods and should be taken with suspicion.

Uuhikonoja TSC was excavated in 2020 and its relatively high sediment accumulation rates could be attributed to channel instability before vegetation is established on the excavated floodplain. Hence, sediment accumulation is expected to decrease in the future. Climate observations also indicated that in 2021–2022 Southern Finland had more precipitation relative to FMI reference period, that increases soil erosion especially without protective vegetation cover (Puustinen et al. 2007). Two sediment traps in Uuhikonoja with anomalously high sediment accumulation were connected to nearby slope erosion, supporting the thought of recently excavated TSCs instability. Additionally, even when excluding the traps with anomalous accumulation Uuhikonoja had multiple times higher sediment accumulation rates relative to Ritobäcken or Pipakallionsuo, suggesting increased erosional transport in freshly excavated floodplains as was observed by Mahl et al. (2015).

5.1.2. Ritobäcken inundation extent and sediment accumulation in floodplain

Ritobäcken was the only site with continuous water level and stream load observations allowing better estimate of the extent of inundation, inundation duration and TSS load, that is necessary to estimate floodplain sedimentation (Lambert and Walling 1987). A simple approach to estimate flooding extent during 14.10.2021–25.5.2022 (223 days) was used to estimate 2.3–3.2 tons of sediment (3–4% of stream TSS load) retained by the studied floodplain (Figures 14-18). Floodplain sediment accumulation mainly occurs during inundation events where increased stream flow velocity greatly dissipates when entering the floodplain, allowing suspended stream solids to settle (e.g. Walling and Bradley 1989, Jensen et al. 1992, Kronvang et al. 2007). Walling and Bradley (1989) reported that only 4 % of stream sediment was removed during baseflow conditions and majority (28%) of removal occurred during storm events (bankfull stage). Kronvang et al. (2007) reported similar high average sediment removal efficiency of 28% using conveyance losses from stream load, that is much higher than the estimate obtained in this thesis using sediment trap accumulations and average inundation extent. However, these studies are from much larger catchment sizes with much higher discharge in streams, making the smaller retention of 2–3% from short section in small agricultural stream catchment relatively positive result.

Modelled water levels for Ritobäcken inundation were used to show overbank flooding occurring during the study period and visualize inundation extent evolution in the floodplain (Figure 15A-F). As floodplain inundation starts to dissipate the downstream sections floodplains remained fully inundated as the upstream sections started to form disconnected pools into depressions as they were drained (Figure 15D and E). Modelled floodplain inundation does not show how quickly these pools are drained and in clayey soils they could be maintained relatively long periods, potentially affecting the redox conditions and thus, soil geochemistry.

Floodplain topography heterogeneity visible in Figure 15 and highly variable flooding extent makes the sediment deposition very hard to predict and it is highly possible that few sediment traps might not give reliable information on total floodplain sedimentation, and other methods such as stream TSS conveyance loss measurements should be preferred for more accurate measurement (Walling and Bradley 1989). Similar conclusions were made by Baborowski et al. (2007), who found sediment trap deposition to be highly variable due to complex flow patterns associated with inundation. Additionally, sediment transport in the main channel during baseflow conditions and during overbank flooding, as was observed on 19.2.2023 in Ritobäcken, is not measured by the sediment traps. Regardless, sediment traps provide valuable information on the fresh material being deposited on the floodplains allowing better interpretation of source and composition of the deposited material (Walling and Bradley 1989), and insight on how the deposited sediment changes in respective to longer timescale sediment core profiles.

5.1.2. Effect of vegetation and climate

Ritobäcken site had the vegetation management experiment showing that mowed sections accumulated on average 73.4% more sediment compared to control sections. Mowing the entire studied floodplain was estimated to increase the sediment deposition to 2.9–4.1 tons of sediment (3.32–4.69% of TSS) over the 223-day measuring period (MP2). Effects of vegetation on sediment deposition and difficulties in modelling are discussed extensively in literature (e.g., Västilä et al. 2016), where rigid vegetation causes flow resistance, and slower flow velocities relate to increased deposition of suspended sediments. Complexity can increase due to preferential flow paths affecting sediment transport (Kronvang et al. 2007, Forsmann and Kjaergaard 2014). The discrepancy found between TSS and water level increase (flooding) during February and March implies that there was no significant sediment deposition on the floodplain during this period despite high water stage. During this period soil was impermeable due to soil frost and thick snow cover significantly reduced soil erosion (Rekolainen and Posch 1993), as can be seen from climate data for this period (Figure 7). Experimental study by Bai and Sun (2021) on floodplain hydrology with snow and ice cover shows slower stream flow velocity and increased water retention time that increased the sediment retention in TSC. During winter the evapotranspiration decreases, leading to increase in groundwater portion of the base flow, with lower dissolved oxygen concentrations and increased water residence time, that could mobilize redox sensitive elements and nutrients (e.g. van der Grift et al. 2018).

5.2. Factors controlling sediment geochemistry and P-speciation

5.2.1. Soil type explaining different study site geochemistry (first principal component)

Most of the geochemical variability between study sites was explained by soil type. Sediments surrounding the main channel are generally linked to the underlying regional and local soil and bedrock geochemistry (e.g. Lahermo et al. 1996, Caritat and Mann 2019). Uuhikonoja and Pipakallionsuo locations are relatively close to each other in Tammela upland area and located in the same geological province which led to expectation of relatively similar bedrock geochemistry that forms the baseline for soil geochemistry. On the contrary the fresh sediment deposition transported to floodplains was found to reflect the surficial soil composition, biogeochemical reactions, and land use. Pipakallionsuo with till dominated catchment in forested peatland had high content of elements associated with organic matter (C, N, P, Mo, and S), while soils in the clay-rich agricultural catchment Uuhikonoja were composed mainly of minerogenic elements (e.g., K, Mg, Al, Fe, V, and Ni). Ritobäcken's clay and bedrock outcrop rich catchment was closer to Uuhikonoja in geochemical composition, but with higher contents of elements associated to organic matter (C, N, Mo, S, Co, and Cd). First principal component of the PCA for sediment trap geochemistry (Figure 32) was interpreted as the difference in topsoil minerogenic and organic matter associated content, which explains most of the variation in geochemistry (65.8%) between the three study sites. High minerogenic content in Ritobäcken and Uuhikonoja was expected for the clay-rich sites, where sediments deposited during Littorina Sea stages are ongoing weathering and erosional transport seen in stream sediments (Lahermo et al. 1996).

Both PCA and HCA both identified similar groupings based on sediment trap geochemistry, where sites were split between the general soil types of mineral and organic soils. Sediment trap UB_2022 from Uuhikonoja that was identified to have similar geochemistry to Ritobäcken site is suggested to be related to richer floodplain vegetation based on field observations (Appendix 4). Higher vegetation at UB_2022 location relative to other traps could capture sediment more efficiently and most likely from larger range of particle sizes, making it similar to Ritobäckens established vegetated floodplain. Sediment trap UB_2022 could foreshadow the change in floodplain deposited sediment composition after vegetation is established on the floodplain.

Pipakallionsuo sediment traps with higher sediment accumulation were more similar in geochemistry relative to traps with low accumulation. Sediment accumulation rates were not used in the PCA or HCA as variables, meaning that there is clear difference associated with higher sediment accumulation in Pipakallionsuo. Both HCA and PCA placed sediment traps Loppi_3, Loppi_4, Loppi_9, and Loppi_10 with higher minerogenic components in their own group, which most likely indicates erosional sediment transport to the inundated floodplain. Interestingly these four traps with high sediment accumulation were on two transects not adjacent to each other, implying that water level does not rise evenly across the floodplain, or the smaller drainage ditches connected to MC (see Figure 4) might have effect on the sediment transport rates.

Comparison between different sampling locations along the Ritobäcken TSC shows how the horizontal and vertical variability is heavily influenced by the potential acid sulphate soils that have remained waterlogged, indicated by high S concentrations in main channel cores deeper layers (Boman et al. 2010, Andelin 2019). Soils that have been drained and oxidized show shift from organic matter associated element enriched topsoil (<3 cm) to higher minerogenic element composition as the sampling depth increases (Figure 28).

5.2.2. Manganese as explanatory variable for spatial distribution (second principal component)

Second principal component shows that Mn has strong influence on the spatial variability of the fresh sediment deposited onto the floodplain (Figure 32), including vertical variability in Ritobäcken (Figure 23). Manganese is redox reactive element that behaves like Fe, by precipitating and dissolving in oxidized and anoxic conditions respectively (e.g., Davison 1993, Lahermo et al. 1996). However, Mn requires higher oxidation potential than Fe, this feature can be used to identify oxidized depositional conditions indicated by high Mn:Fe ratio (Naeher et al. 2013, Gravina et al. 2022). Scholtysik et al. (2020) reported opposite results where high Mn:Fe ratios were interpreted as anoxic conditions in lake basin sediments that formed authigenic reduction resisting Mn mineral, rhodochrosite (Mn(Ca)(CO_3)), after Mn oxide burial. Their study results also highlighted the importance of Mn oxide precipitation in surface sediments and required presence of oxygenised water column, that takes part in the formation of rhodochrosite.

Sediment traps represent horizontal and sediment core profiles vertical variability that was used to identify changes in redox conditions and geochemical composition. Both sediment trap and core samples indicate higher Mn:Fe ratios in topsoil, while Ritobäcken sediment traps could also detect seasonal variation with higher ratios in autumn-winter period (MP3), and lower in the annual deposition (MP1, MP2, and MP4). In winter anoxic groundwaters with dissolved Mn and Fe loads can contribute more to the stream baseflow (Björkvald et al. 2008), that precipitate as they discharge to oxidized floodplain. Finnish groundwaters have dissolved Mn concentrations in every season, controlled by the dissolved oxygen levels (Kousa et al. 2021). Microbial activity that consumes oxygen is reduced during cold temperatures outside the growth season (Vepraskas et al. 1999), which can explain the high Mn:Fe ratios in MP3 Ritobäcken sediment traps. Microbial oxidation can strongly influence the Mn sorption and precipitation as oxides (Yang et al. 2022), increasing the Mn:Fe ratio. Three out of four sediment trap transects in Pipakallionsuo had lower Mn:Fe ratios closer to MC and higher ratios further from the MC. Wetlands are prone to have more anoxic discharge that could dissolve Mn (e.g. Björkvald et al. 2008), coupled with sediment traps closer to MC which are most likely inundated more frequently than further traps. Transect of Loppi_7 and Loppi_8 sediment traps had same low Mn:Fe ratio, interpreted as similar higher inundation frequency and more anoxic conditions compared to higher Mn:Fe ratio traps.

A significant negative correlation was found between Mn:Fe and surface elevation in sediment traps in Ritobäcken and Uuhikonoja. Lower elevated areas are more frequently inundated which can lead to hypoxic or anoxic conditions as the floodplains organic matter degrades (Baldwin and Mitchell 2000). This suggests that higher Mn:Fe ratios observed in Uuhikonoja and Ritobäcken with more frequently inundated sections at lower elevation have remained oxidized in the floodplain. This is supported by higher Mn:Fe ratios in topsoil (<3 cm depth) in FP cores and lower ratios in MC cores in Ritobäcken (Figure 19). Sediment traps with low sediment accumulation coupled with higher Mn:Fe ratios are similarly interpreted as more oxidized conditions. Low Mn:Fe ratios observed in sediments deposited from eroded slope in Uuhikonoja (UT_2022 and US_2022, Figure 21) suggests that high Mn concentrations in other sediment traps originate from stream, either as stream erosional transport or precipitation of dissolved Mn. In all study sites higher Mn:Fe ratios were associated with higher Mg, Al, K, P, S, Fe, Co, and Mn concentrations.

5.2.3. Phosphorus speciation in cultivated Littorina clay soils

Phosphorus speciation distribution in sediment traps show practically no variation along the studied reach length in Ritobäcken or Uuhikonoja, even if TP concentrations varied between 664–1177 mg kg^{-1} and 696–1469 mg kg^{-1} for each site respectively (Figure 28). Two-stage channels floodplain deposited material was dominated by Fe-P in all sites, and clay-silt rich cultivated sites, Ritobäcken and Uuhikonoja, had second highest fraction in Ca-P. High Ca-P concentrations can be attributed to relatively little chemical weathering in Littorina Sea clays (Kaila 1963), which is redeposited to floodplains by fluvial transport.

Several studies have showcased that stream P transport is largely dominated by particulate transport, which coincides with SRP being readily removed from the water column by precipitation and sorption processes. Littorina Sea clays Ca-P can be weathered and dissolved by microbial activity to release bioavailable soluble P assimilated into organic matter fraction (Res.Org-P) that upon degradation is bound as Fe-P (Kaila 1963). Study by van der Grift et al. (2018) identified anoxic groundwater discharge as a source dissolved Fe in oxidized agricultural catchment, which rapidly precipitates as Fe-hydroxides and sorbs SRP to Fe-P fraction. Additionally frequent dry-wetting cycles increase the breakdown of floodplain organic matter and release its bound phosphorus (Lahermo et al. 1996, Soinne et al. 2010), redistributing it into Fe-P fraction. Neubauer et al. (2013) detected formation of Fe (oxy)hydroxide aggregates over 0.2 µm in stream waters with higher pH (>6 pH) that limit the Fe mobility as larger aggregate particles are settled to stream bed, supporting the theory of Fe precipitation and its potential to immobilize associated Fe-P.

Soluble reactive phosphorus retention is strongly controlled by the reactive Fe availability for Fe-P binding, that has been studied using Fe:P ratio (e.g., Jensen et al. 1992, Forsmann and Kjaergaard 2014, Trentman et al. 2020). Different Fe:P ratios have been reported to have sufficient available Fe surfaces for high SRP sorption rates, >15 for lake sediments (Jensen et al. 1992), >10 (bicarbonate dithionite extractable Fe and P) for wetlands (Forsmann and Kjaergaard 2014), and >3–6 for TSC floodplains (Trentman et al. 2020). Vegetated floodplain soils are generally oxidized during baseflow conditions due to direct contact with atmospheric oxygen and change to anoxic conditions under prolonged inundation, that can reduce the reactive Fe in the soils (Forsmann and Kjaergaard 2014, Trentman et al. 2020). When oxidized conditions are retained the incoming SRP is sorbed by the Fe and can be up taken by the vegetation, freeing more Fe surfaces for SRP sorption (Trentman et al. 2020). Sah and Mikkelsen (1986) found that flooding and drying sequence increases the soil P sorption capacity that remained increased for up to 119 days after flooding and was higher than in unflooded soils. Iron can be also reduced by microbial activity that is mediated by presence of soil carbon (Vepraskas et al. 1999). Sah and Mikkelsen (1989) reports that in amorphous Fe rich soils with insufficient soil carbon the oxidized conditions are preserved during flooded conditions and the amorphous Fe was not reduced, but the flood-drying sequence induced increase in P sorption would also not occur. When they added organic matter to the carbon poor soil the reducing conditions with associated Fe reduction, and increased P sorption was observed. Iron bound P release from soils can also be inhibited by humic substances (Tammeorg et al. 2022), making soil P saturation possible. Baldan et al. (2021) raised concerns of P saturated soil depositing in TSC floodplains inhibiting further SRP retention during new inundation events. High Fe:P ratios observed in the study sites implies that the risk of floodplain P saturation is not imminent but needs to be considered in long-term planning on TSC management. Lower average Fe:P ratios (22.3) were observed in organic soils of Pipakallionsuo, which has been suggested to indicate higher P saturation (Kjaergaard et al. 2012). Mowing and removing the vegetation from floodplain as was experimented in Ritobäcken should be considered as a measure to reduce floodplain soils P saturation as the vegetation will consume some of the floodplain retained nutrients.

Sediment core profiles from Ritobäcken and Uuhikonoja displayed highly variable P fractionation with the newly excavated TSC floodplain in Uuhikonoja (excavated in

2020) cores having noticeably higher Res.Org-P concentrations that differed from the 2021–2022 deposited sediment trap speciation. Older TSC in Ritobäcken (excavated 2010) sediment core and trap speciation's were close to identical in topsoil (Figure 27 and Figure 28). High Res.Org-P in Uuhikonoja before TSC excavation shows the drastic influence caused by immediate sediment water interface in floodplain that enhances the nutrient cycling. Previously conventionally dredged ditch banks were most likely not as influenced by the main channel and P speciation reflected more of the cultivated soil, where Res.Org-P burial was the dominating fraction (Kaila 1964). Uuhikonoja's floodplain sediment traps with lower Res.Org-P fraction are most likely going through faster remineralization to form Fe-P as rewetting enhances the dissolution of organic matter. Similar efficient remineralization of Res.Org-P is thought to occur in Ritobäcken where floodplain vegetation is already established and low Res.Org-P concentrations are observed.

5.3.4. Phosphorus speciation in drained organic soil

Pipakallionsuo's organic soils were expected to have higher Res.Org-P concentrations, but instead they were dominated by Fe-P similar to clay rich sites, followed by high Al-P. Strong positive correlation was found between minerogenic content and Fe-P and Ca-P, suggesting particulate transport to floodplains. Negative correlation between for P, S, C, and N for Ca-P and Fe-P, coincided with positive correlation with Al-P for the same list of elements, suggesting that Al-P is associated with organic matter content. Floodplain deposited Ca-P and Fe-P from particulate transport will go through either microbially enhanced weathering, reductive dissolution by anoxic conditions, or microbial reduction, while Al-P is less soluble in reductive conditions (Litaor et al. 2005). Heiberg et al. (2012) found similar observations in organic soils where Fe reduction from humic substances was replaced by an increase in Al-P and Ca-P fractions. Found low Ex-P concentrations are suspected to have been redistributed to Fe- and Al-P fractions in field setting or during the sample drying process, where rinsed sediments were inundated for over a week in standing water-sediment solution. Nieminen and Penttilä (2004) found that high productivity peatland soils had high P sorption capacity which easily resorbs any released P from Ex-P fraction.

Heiberg et al. (2012) incubation study found dissolution of humic (OM) bound Fe during inundation, while goethite associated Fe was largely unaffected. The released P concentrations from dissolved Fe peaked after 30 to 35 days of inundation and then decreased close to the oxidized conditions level that was attributed to resorption to Al-rich particles in sandy soil (Heiberg et al. 2012). They also found that sandy soils P sorption capacity was not affected by anoxic conditions during long inundation periods. Gressel et al. (1996) found a strong correlation between P and C in forest soils and interpreted it as mineralization of P related to breakdown of organic matter. Sah and Mikkelsen (1989) displayed that organic matter addition to rewetted soils increased P sorption and attributed it to the soil carbon initiated reduction as decomposition consumes oxygen and dissolves amorphous Fe that will precipitate in oxidized conditions and bind P after flooding ends. Darke and Walbridge (2000) noticed loss of Al and Fe hydroxides in forest floodplain during flood events, which recharged back to original levels after flooding was over. They could account the Fe recharge to sediment transport, but portion of Al recharge was left unidentified, proposed to be related to either dissolved Al input from groundwater discharge or fertilizer induced Al mobilization. Humic bound Al solubilization was found to increase at above 5.4 pH and release associated P (Darke and Walbridge 2000).

In addition to erosional particulate transport from upstream catchment, the subsoils in Pipakallionsuo are likely to be hypoxic or anoxic due to waterlogged peatland. Reducing conditions from oxygen deprived soils and groundwater can bring dissolved metals (e.g., Fe, Al, and Mn) and nutrients to oxidized sediment water interface and precipitate. Pipakallionsuo organic soils with large portion of sandy soils in upstream of the catchment coupled with found higher Al-P concentrations hint at similar findings to above literature, 1) reductive dissolution of Fe by anoxic conditions or microbial activity, 2) continuous breakdown of organic matter 3) release of metal and organic matter associated P 4) resorption or co-precipitation of P to Fe in oxidized and to Al in oxygen deprived conditions. More wet climate conditions in 2022 relative to previous year could explain the decrease in Fe-P proportion in Pipakallionsuo sediment traps (Figure 31) if it led to increased anoxic inundation on the floodplain. Low Mn:Fe ratio observed from 2022 sediment traps suggested less oxidized conditions for four traps (Figure 20) but P speciation shows no clear trends between these traps. However, some compositional difference most likely exists as HCA and PCA could identify two separate groups with high or low sediment accumulation rate (Figure 25 and Figure 32), even if it was not included in the analysis. These compositional differences suggest either different floodplain conditions or different sources of deposited material. Sandy soils resisting anoxic dissolution as described by Heiberg et al. (2012) could increase Pipakallionsuo potential to work as P sink but would require more thorough study on sediment properties in the area.

5.3. TSC carbon, nitrogen, and phosphorus accumulation

Two-stage channel floodplains captured nutrient rich sediments from the streams following closely the sediment accumulation rates and changes in elevation level (Figure 11 and Figure 22). Forested peatland catchment with mostly sandy till and organic soils had significantly lower sediment accumulation compared to clay-silt rich sites and was reflected in absolute nutrient retention amount (Table 10). Forested peatlands low sediment accumulation was slightly compensated by the higher nutrient concentrations. Floodplain deposited sediments C and N concentrations were consistent with observations from Finnish cultivated mineral soils (Lahermo et al. 1996, Heikkinen et al. 2021, Manninen et al. 2023) and river floodplain deposition in other studies (Noe and Hupp 2005, Baborowski et al. 2007). In floodplain sediments N is associated with OM deposition, while P is mostly associated with particulate sediment transport (Noe and Hupp 2005). Majority of C and N transported in Finnish streams is in dissolved phase while the remaining solid phase is highly resistant to degradation and could act as a sink after deposition in submerged conditions (Manninen et al. 2023). Two-stage channel floodplains frequent wet-drying cycle may increase the degradation of the resistant C and N solid phase, in addition to the floodplain vegetation being degraded. Particulate P accumulation in floodplains is highest close to agricultural fields due to loss of P from cultivated soils, but also shows the importance of floodplains in retaining SRP from streams during flooding conditions (Noe and Hupp 2005).

With a few exceptions C, N, and P accumulation rates had very stable ratios within each site. Enrichment of C and N relative to P accumulations observed in Pipakallionsuo

(Loppi_2_2022 and Loppi_8_2022) and Uuhikonoja (UB_2022) traps are explained by their higher OM content respective to other traps (>70% OM for Pipakallionsuo and >10% OM for Uuhikonoja) suggesting less particulate sediment deposition. Similar findings were observed by Noe and Hupp (2005) in groundwater fed headwater stream floodplains and was interpreted as lower nutrient availability. Ritobäckens had C and N enrichment relative to P accumulation in C2_C_2022 trap with no similar high OM content but had low Mn:Fe ratio and was inundated more frequently to other upstream traps (Figure 17), suggesting more anoxic conditions and reductive dissolution of P from sediments. Closer look on C2_C_2022 trap P speciation shows lower Ca-P concentration matching the below average TP concentration (Figure 28), further indicating that P release occurred from Ca-P fraction by weathering or microbial reduction.

Annual nutrient retention by floodplains shows much higher deposition in freshly excavated TSC floodplain in Uuhikonoja but the sediment accumulation controlled nutrient retention will most likely decrease as the channel stabilizes. Stable clay rich site Ritobäcken suggests that cultivated mineral soils still have higher C, N, and P accumulation after stabilization relative to the organic peatland in Pipakallionsuo. Nutrient accumulation rates are similar in magnitude to other sediment traps utilizing studies (Noe and Hupp 2005, Kjaergaard et al. 2012), but are manyfold higher when compared to nutrient retention estimated from stream suspended sediments (Kortelainen et al. 2006, Puustinen et al. 2007, Manninen et al. 2023). Geranmayeh et al. (2018) suggests that higher sediment and nutrient loads observed in sediment traps when compared to stream TSS derived loads are indicators of local sediment bed erosion and transport by resuspension. This means that nutrient accumulation rates from sediment traps might heavily overestimate nutrient retention in floodplains due to capturing erosional sediments from floodplain, bank, and main channel in addition to suspended solids.

6. CONCLUSIONS

Three two-stage channels in southern Finland were studied for sediment deposition using sediment traps and analyzed for major and trace elements, carbon, nitrogen, and phosphorus species. Sediment accumulation and associated nutrients retained by floodplain were used to study spatial variability and compared with previous studies with following key conclusions:

- Ritobäcken and Uuhikonoja with cultivated clay rich mineral soils had higher sediment accumulation rates relative to Pipakallionsuo with organic soils in forested peatland catchment. Factors affecting the sediment accumulation and spatial variability identified in the thesis included changes in surface topography, floodplain inundation extent, channel stability, floodplain morphology, and vegetation management.
- Mowing floodplain vegetation to 5–10 cm length significantly increased sediment accumulation rates in Ritobäcken. Modelled water level and inundation extent estimated total sediment deposition of 3–4 % of TSS load (2.3–3.2 tons) retained when approximately half of the floodplain was mowed over 14.10.2021–25.5.2022 period, and 3.3–4.7% of TSS load (2.9–4.1 tons) if vegetation management would have been applied to entire studied 250 m floodplain length. Sediment traps include erosional sediment transport which might lead to overestimation of sediment accumulation when compared to estimates from stream TSS conveyance losses.
- Most of the variation in sediment trap geochemistry was explained by differences in minerogenic material and organic matter associated with surficial soil type (PC1). Independent of PC1, redox sensitive Mn was found to explain spatial variability between sediment trap samples (PC2), when using Mn:Fe ratios. High Mn:Fe ratios in sediment traps coincided with high ratios in floodplain and main channel surface sediments from core samples, that started to decrease with increasing depth as hypoxic or anoxic conditions are expected to be predominant. The presence of redox sensitive metals and phosphorus species agreed with high Mn:Fe being a good predictor of changes in oxidizing conditions in cultivated

mineral soils. In peatland organic soils Mn:Fe ratio performed worse at explaining changes in reducible elements and oxidizing conditions. In mineral soil sites Mn:Fe ratios were higher in lower elevated areas with more frequent inundation, suggesting that floodplains remained oxidized during inundation.

- Phosphorus speciation was relatively uniform between the study sites despite the differences in geochemistry, land use, or surficial soil composition. Iron bound phosphorus was the dominant species in all sites followed by Al-P for Pipakallionsuo, and Ca-P for Ritobäcken and Uuhikonoja, indicating differences in soil types. Two-stage channel excavation has not changed the P speciation significantly as the results agree with previous studies for Finnish cultivated mineral soils and organic soils.
- Two-stage channels decrease stream nutrient loads by accumulating nutrient rich sediments to floodplains that might make them susceptible for P saturation. However, high Fe:P ratios in all study sites indicate that no P saturation is yet observed but could affect long term TSC management. It is unclear if Fe-P rich floodplain sediments can be re-excavated as a part of TSC management, without risking the release of the redox sensitive P species and should be studied further.

7. ACKNOWLEDGEMENTS

I wish to thank my supervisor Tom Jilbert and Kaisa Västilä for guiding me through the thesis process and introducing me to a very interesting thesis topic. I am thankful to Valumavesi project and other project associates for providing the sample materials and additional materials that allowed different perspectives to be studied in the thesis. Thank you for Tiina Ronkainen from Tapio Oy for collecting the Pipakallionsuo sediment traps and additional information on the Pipakallionsuo site conditions. Additional thanks to Tom Jilbert and Mareike Paul for taking the time to comment on the thesis drafts.

I wish to thank all Helsinki Geoscience Laboratories HelLabs personnel, especially Hanna Reijola, Tuija Vaahtojärvi and Juhani Virkanen who supervised and provided all the necessary help in the sample processing and laboratory analyses. Thank you to Siqi

Zhao for guidance in phosphorus speciation analysis using tailored sequential extraction scheme, and University of Helsinki EcoEnv labs research laboratory technician Heini Ali-Kovero for conducting carbon and nitrogen content analyses. Finally thank you to all the hydrogeology and environmental geology study track students for peer support and special thanks to faculty members Niina Kuosmanen and Seija Kultti for organizing thesis workshop to support thesis writing process.

8. REFERENCES

Aho, S., Antikainen, J., Bäcklund, P., Colpaert, A., Heikkilä, E., Heikkinen, O., Heininen, L., Husso, K., Hyyryläinen, T., Häkkilä, M., Häkli, J., Jahkola, M., Jukarainen, P., Jussila, H., Jutila, H., Kaila, K., Kalliola, R., Karppi, I., Kauppinen, J., Kivikkokangas-Sandgren, R., Kortelainen, J., Kultalahti, O., Kumpula, J., Lehtinen, A.A., Löytönen, M., Maaranen, P., Maasilta, P., Magga, T., Mikkonen, K., Muilu, T., Naukkarinen, A., Nieminen, M., Norio, R., Oksanen, J., Paasi, A., Palomäki, M., Raento, P., Raivio, P.J., Rikkinen, K., Rusanen, J., Schulman, H., Seppä, H., Siirilä, S., Suihkonen, P., Suojanen, I., Tiitta, A., Tikkanen, M., Tuovinen, M., Tykkyläinen, M., Vaattovaara, M., Valtakari, M., Vartiainen, P., Westerholm, J., Viitala, P., Vuorela, N. and Vuoristo, K.V. 1999. Suomen kartasto 1999: 100-vuotisjuhlakartasto. Suomen maantieteellinen seura ry ja WSOY, Porvoo, Helsinki, Juva, 207 p.

Aitchison, J. 1986. The statistical analysis of compositional data / J. Aitchison. Chapman and Hall, London, 416 p.

Andelin, M. 2019. Development of experimental methods for investigating sediment and nutrient transport in vegetated flows. Master's thesis, Aalto University, 74 p.

Asselman, N.E.M. and Middelkoop, H. 1995. Floodplain sedimentation: Quantities, patterns and processes. Earth surface processes and landforms 20, 481-499, doi: 10.1002/esp.3290200602.

Baborowski, M., Büttner, O., Morgenstern, P., Krüger, F., Lobe, I., Rupp, H. and Tümpling, W.v. 2007. Spatial and temporal variability of sediment deposition on artificial-lawn traps in a floodplain of the River Elbe. Environmental pollution 148, 770-778, doi: 10.1016/j.envpol.2007.01.032.

Bai, Y. and Sun, G. 2021. The streamwise velocity distribution in a two-stage channel with ice cover. Water Supply 22, 981-989, doi: 10.2166/ws.2021.225.

Baldan, D., Pucher, M., Akbari, E., Hein, T. and Weigelhofer, G. 2021. Effects of Two-Stage Ditch and Natural Floodplains on Sediment Processes Driven by Different Hydrological Conditions. Water 13, 2046.

Baldwin, D.S. and Mitchell, A.M. 2000. The effects of drying and re-flooding on the sediment and soil nutrient dynamics of lowland river-floodplain systems: a synthesis. Regulated rivers 16, 457-467, doi: 10.1002/1099-1646(200009/10)16:5<457::AID-RRR597>3.0.CO;2-B.

Barrow, N.J., Sen, A., Roy, N. and Debnath, A. 2021. The soil phosphate fractionation fallacy. Plant & Soil 459, 1-11, doi: 10.1007/s11104-020-04476-6.

Björkvald, L., Buffam, I., Laudon, H. and Mörth, C.-M. 2008. Hydrogeochemistry of Fe and Mn in small boreal streams: The role of seasonality, landscape type and scale. Geochimica et Cosmochimica Acta 72, 2789-2804, doi: 10.1016/j.gca.2008.03.024.

Boman, A., Fröjdö, S., Backlund, K. and Åström, M.E. 2010. Impact of isostatic land uplift and artificial drainage on oxidation of brackish-water sediments rich in metastable iron sulfide. Geochimica et cosmochimica acta 74, 1268-1281, doi: 10.1016/j.gca.2009.11.026.

Caritat, P.d. and Mann, A. 2019. An improved method for assessing the degree of geochemical similarity (DOGS2) between samples from multi-element geochemical datasets. Geochemistry: Exploration, Environment, Analysis 19, 58-73, doi: doi:10.1144/geochem2018-021.

Chang, S.C. and Jackson, M.L. 1957. FRACTIONATION OF SOIL PHOSPHORUS. Soil Science 84, 133-144.

Darke, A.K. and Walbridge, M.R. 2000. Al and Fe Biogeochemistry in a Floodplain Forest: Implications for P Retention. Biogeochemistry 51, 1-32.

Davis, R.T., Tank, J.L., Mahl, U.H., Winikoff, S.G. and Roley, S.S. 2015. The Influence of Two-Stage Ditches with Constructed Floodplains on Water Column Nutrients and Sediments in Agricultural Streams. JAWRA Journal of the American Water Resources Association 51, 941-955, doi: 10.1111/1752-1688.12341.

Davison, W. 1993. Iron and manganese in lakes. Earth-Science Reviews 34, 119-163, doi: 10.1016/0012-8252(93)90029-7.

Dee, M.M. and Tank, J.L. 2020. Inundation time mediates denitrification end products and carbon limitation in constructed floodplains of an agricultural stream. Biogeochemistry 149, 141-158, doi: 10.1007/s10533-020-00670-x.

Dieter, D., Herzog, C. and Hupfer, M. 2015. Effects of drying on phosphorus uptake in re-flooded lake sediments. Environmental Science and Pollution Research 22, 17065-17081, doi: 10.1007/s11356-015-4904-x.

Esri and National Land Survey of Finland. Light Gray Canvas Reference basemap. Accessed 20 August 2023. https://www.arcgis.com/home/item.html?id=1768e8369a214dfab4e2167d5c5f2454.

Esri. 2023a. ArcGIS Pro Flow Direction function documentation. Accessed 16 June 2023. https://pro.arcgis.com/en/pro-app/3.0/help/analysis/raster-functions/flow-direction-raster-function.htm.

Esri. 2023b. ArcGIS Pro Shaded Relief function documentation. Accessed 16 June 2023. https://pro.arcgis.com/en/pro-app/3.0/help/analysis/raster-functions/shaded-relief-function.htm.

Finnish Environment Institute 2018. CORINE Land Cover 2018 dataset 20 m. Accessed 16 June 2023. https://ckan.ymparisto.fi/dataset/%7B0B4B2FAC-ADF1-43A1-A829-70F02BF0C0E5%7D.

Finnish Environment Institute, SYKE. 2023. Valumavesi-project. Accessed 30 November 2023, https://www.syke.fi/hankkeet/valumavesi.

Finnish Meteorological Institute 2023. Open data, weather observations from Helsinki-Vantaa airport. Accessed 26 September 2023. https://www.ilmatieteenlaitos.fi/havaintojen-lataus.

Forsmann, D.M. and Kjaergaard, C. 2014. Phosphorus release from anaerobic peat soils during convective discharge — Effect of soil Fe:P molar ratio and preferential flow. Geoderma 223-225, 21-32, doi: 10.1016/j.geoderma.2014.01.025.

Geological Survey of Finland Hakku service, 2021. Superficial deposits 1:20 000/1:50 000. Accessed 24 November 2022, http://hakku.gtk.fi.

Geranmayeh, P., Johannesson, K.M., Ulén, B. and Tonderski, K.S. 2018. Particle deposition, resuspension and phosphorus accumulation in small constructed wetlands. Ambio 47, S134-S145.

Gong, X. and Richman, M.B. 1995. On the Application of Cluster Analysis to Growing Season Precipitation Data in North America East of the Rockies. Journal of climate 8, 897-931, doi: 10.1175/1520-0442(1995)008<0897:otaoca>2.0.co;2.

Gravina, P., Ludovisi, A., Moroni, B., Vivani, R., Selvaggi, R., Petroselli, C. and Cappelletti, D. 2022. Geochemical Proxies and Mineralogical Fingerprints of Sedimentary Processes in a Closed Shallow Lake Basin Since 1850. Aquatic Geochemistry 28, 43-62, doi: 10.1007/s10498-022-09403-y.

Gressel, N., McColl, J.G., Preston, C.M., Newman, R.H. and Powers, R.F. 1996. Linkages between Phosphorus Transformations and Carbon Decomposition in a Forest Soil. Biogeochemistry 33, 97-123.

Grunsky, E.C. 2010. The interpretation of geochemical survey data. Geochemistry: Exploration, Environment, Analysis 10, 27-74, doi:10.1144/1467-7873/09-210.

Haavisto-Hyvärinen, M., Sten, C.G. and Kaija, J. 1990a. Läyliäinen. Maaperäkartan 2042 08 selitys, 1 p.

Haavisto-Hyvärinen, M., Sten, C.G. and Kaija, J. 1990b. Loppi. Maaperäkartan 2042 09 selitys, 1 p.

Heiberg, L., Koch, C.B., Kjaergaard, C., Jensen, H.S. and Hansen, H.C.B. 2012. Vivianite Precipitation and Phosphate Sorption following Iron Reduction in Anoxic Soils. Journal of Environmental Quality 41, 938-949, doi: 10.2134/jeq2011.0067.

Heikkinen, J., Keskinen, R., Regina, K., Honkanen, H. and Nuutinen, V. 2021. Estimation of carbon stocks in boreal cropland soils - methodological considerations. European Journal of Soil Science 72, 934-945, doi: 10.1111/ejss.13033.

HELCOM. 2022. Assessment of sources of nutrient inputs to the Baltic Sea in 2017. Journal, 113.

Hodaj, A., Bowling, L.C., Frankenberger, J.R. and Chaubey, I. 2017. Impact of a two-stage ditch on channel water quality. Agricultural Water Management 192, 126-137, doi: 10.1016/j.agwat.2017.07.006.

Hoffman, A.R., Armstrong, D.E., Lathrop, R.C. and Penn, M.R. 2009. Characteristics and Influence of Phosphorus Accumulated in the Bed Sediments of a Stream Located in an Agricultural Watershed. Aquatic Geochemistry 15, 371-389, doi: 10.1007/s10498-008-9043-2.

Hoffmann, E.d. 2007. Mass Spectrometry : Principles and Applications. John Wiley & Sons, Incorporated, Newark, UNITED STATES, 503 p.

Howard, E.T. 2001. Inductively Coupled Plasma-Mass Spectrometry : Practices and Techniques. Academic Press, San Diego, p.

Jensen, H.S., Kristensen, P., Jeppesen, E. and Skytthe, A. 1992. Iron:phosphorus ratio in surface sediment as an indicator of phosphate release from aerobic sediments in shallow lakes. Hydrobiologia 235, 731-743, doi: 10.1007/BF00026261.

Jensen, J.L., Christensen, B.T., Schjønning, P., Watts, C.W. and Munkholm, L.J. 2018. Converting loss-on-ignition to organic carbon content in arable topsoil: pitfalls and proposed procedure. Eur J Soil Sci 69, 604-612, doi: 10.1111/ejss.12558.

Kaila, A. 1963. Phosphorus conditions at various depths in some mineral soils. Agricultural and Food Science 35, 69-79, doi: 10.23986/afsci.71598.

Kaila, A. 1964. Fractions of inorganic phosphorus in Finnish mineral soils. Agricultural and Food Science 36, 1-13, doi: 10.23986/afsci.71607.

Kallio, R.M. 2010. Evaluation of Channel Evolution and Extreme Event Routing for Two-Stage Ditches in a Tri-State Region of the USA. Master's thesis The Ohio State University, 261 p.

Kassambara, A. and Mundt, F. 2020. Factoextra: Extract and Visualize the Results of Multivariate Data Analyses. Accessed 16 November 2023. https://CRAN.R-project.org/package=factoextra.

Kielosto, S., Lindroos, P., Mäkilä, M. and Herola, E. 1998. Östersundomin kartta-alueen maaperä, 14 p.

Kindervater, E. and Steinman, A.D. 2019. Two-Stage Agricultural Ditch Sediments Act as Phosphorus Sinks in West Michigan. JAWRA Journal of the American Water Resources Association 55, 1183-1195, doi: 10.1111/1752-1688.12763.

Kjaergaard, C., Heiberg, L., Jensen, H.S. and Hansen, H.C.B. 2012. Phosphorus mobilization in rewetted peat and sand at variable flow rate and redox regimes. Geoderma 173-174, 311-321, doi: 10.1016/j.geoderma.2011.12.029.

Kortelainen, P., Mattsson, T., Finér, L., Ahtiainen, M., Saukkonen, S. and Sallantaus, T. 2006. Controls on the export of C, N, P and Fe from undisturbed boreal catchments, Finland. Aquatic Sciences 68, 453-468, doi: 10.1007/s00027-006-0833-6.

Kousa, A., Komulainen, H., Hatakka, T., Backman, B. and Hartikainen, S. 2021. Variation in groundwater manganese in Finland. Environmental Geochemistry and Health 43, 1193-1211, doi: 10.1007/s10653-020-00643-x.

Krider, L., Magner, J., Hansen, B., Wilson, B., Kramer, G., Peterson, J. and Nieber, J. 2017. Improvements in Fluvial Stability Associated with Two-Stage Ditch Construction in Mower County, Minnesota. JAWRA Journal of the American Water Resources Association 53, 886-902, doi: 10.1111/1752-1688.12541.

Kronvang, B., Andersen, I.K., Hoffmann, C.C., Pedersen, M.L., Ovesen, N.B. and Andersen, H.E. 2007. Water Exchange and Deposition of Sediment and Phosphorus during Inundation of Natural and Restored Lowland Floodplains. Water, Air, and Soil Pollution 181, 115-121, doi: 10.1007/s11270-006-9283-y.

Laakso, J., Uusitalo, R., Leppänen, J. and Yli-Halla, M. 2017. Sediment from Agricultural Constructed Wetland Immobilizes Soil Phosphorus. Journal of Environmental Quality 46, 356-363, doi: 10.2134/jeq2016.09.0336.

Lahermo, P., Väänänen, P., Tarvainen, T. and Salminen, R. 1996. Geochemical Atlas of Finland, Part 3: Environmental geochemistry - stream waters and sediments, 149 p.

Lambert, C.P. and Walling, D.E. 1987. Floodplain Sedimentation: A Preliminary Investigation of Contemporary Deposition within the Lower Reaches of the River Culm, Devon, UK. Geografiska Annaler. Series A, Physical Geography 69, 393-404, doi: 10.2307/521353.

Lê, S., Josse, J. and Husson, F. 2008. FactoMineR: An R Package for Multivariate Analysis. Journal of Statistical Software 25, 1 - 18, doi: 10.18637/jss.v025.i01.

Link, D.D., Walter, P.J. and Kingston, H.M. 1998. Development and Validation of the New EPA Microwave-Assisted Leach Method 3051A. Environmental Science & Technology 32, 3628-3632, doi: 10.1021/es980559n.

Litaor, M.I., Reichmann, O., Haim, A., Auerswald, K. and Shenker, M. 2005. Sorption Characteristics of Phosphorus in Peat Soils of a Semiarid Altered Wetland. Soil Science Society of America Journal 69, 1658-1665, doi: 10.2136/sssaj2005.0068.

Lunkka, J.P., Palmu, J.-P. and Seppänen, A. 2021. Deglaciation dynamics of the Scandinavian Ice Sheet in the Salpausselkä zone, southern Finland. Boreas 50, 404-418, doi: 10.1111/bor.12502.

Mahl, U.H., Tank, J.L., Roley, S.S. and Davis, R.T. 2015. Two-Stage Ditch Floodplains Enhance N-Removal Capacity and Reduce Turbidity and Dissolved P in Agricultural Streams. Journal of the American Water Resources Association 51, 923-940, doi: 10.1111/1752-1688.12340.

Manninen, N., Kanerva, S., Lemola, R., Turtola, E. and Soinne, H. 2023. Contribution of water erosion to organic carbon and total nitrogen loads in agricultural discharge from boreal mineral soils. The Science of the total environment 905, 167300, doi: 10.1016/j.scitotenv.2023.167300.

Moisanen, M. 2014. Abstract: The peatlands and peat resources of Loppi, southern Finland. Part 2: Geological Survey of Finland, 133p.

Naeher, S., Gilli, A., North, R.P., Hamann, Y. and Schubert, C.J. 2013. Tracing bottom water oxygenation with sedimentary Mn/Fe ratios in Lake Zurich, Switzerland. Chemical Geology 352, 125-133, doi: 10.1016/j.chemgeo.2013.06.006.

Neubauer, E., Köhler, S.J., von der Kammer, F., Laudon, H. and Hofmann, T. 2013. Effect of pH and Stream Order on Iron and Arsenic Speciation in Boreal Catchments. Environmental Science & Technology 47, 7120-7128, doi: 10.1021/es401193j.

Nieminen, M. and Penttilä, T. 2004. Inorganic and organic phosphorus fractions in peat from drained mires in northern Finland Silva Fennica. 38, 243-251, doi: 10.14214/sf.413.

Nifong, R.L. and Taylor, J.M. 2021. Vegetation and Residence Time Interact to Influence Metabolism and Net Nutrient Uptake in Experimental Agricultural Drainage Systems. Journal 13. 1416, doi: 10.3390/w13101416.

Noe, G.B. and Hupp, C.R. 2005. Carbon, Nitrogen, and Phosphorus Accumulation in Floodplains of Atlantic Coastal Plain Rivers, USA. Ecological Applications 15, 1178-1190.

Palmu, J.-P. 1999. Sedimentary environment of the Second Salpausselkä ice marginal deposits in the Karkkila-Loppi area in soutwestern Finland. Geologian tutkimuskeskus, Espoo. Tutkimusraportti / Geologian tutkimuskeskus, 148, p.

Powell, E.G., Andrew, W.D., Daniel, M.E., Joe, D. and William, W. 2007. Two-stage channel systems: Part 2, case studies. Journal of Soil and Water Conservation 62, 286.

Putkinen, N., Eyles, N., Putkinen, S., Ojala, A.E.K., Palmu, J.P., Sarala, P., Väänänen, T., Räisänen, J., Saarelainen, J., Ahtonen, N., Rönty, H., Kiiskinen, A., Rauhaniemi, T. and Tervo, T. 2017. High-resolution LiDAR mapping of glacial landforms and ice stream lobes in Finland. Bulletin of the Geological Society of Finland 89, 64-81, doi: 10.17741/bgsf/89.2.001.

Puustinen, M., Tattari, S., Koskiaho, J. and Linjama, J. 2007. Influence of seasonal and annual hydrological variations on erosion and phosphorus transport from arable areas in Finland. Soil and Tillage Research 93, 44-55, doi: 10.1016/j.still.2006.03.011.

R Core Team. 2023. R: A Language and Environment for Statistical Computing. R Foundation for Statistical Computing. Vienna, Austria. https://www.R-project.org/.

Rekolainen, S. and Posch, M. 1993. Adapting the CREAMS Model for Finnish Conditions. Hydrology Research 24, 309-322, doi: 10.2166/nh.1993.10.

Richardson, A.E. and Simpson, R.J. 2011. Soil Microorganisms Mediating Phosphorus Availability Update on Microbial Phosphorus. Plant Physiology 156, 989-996, doi: 10.1104/pp.111.175448.

Roley, S.S., Tank, J.L., Stephen, M.L., Johnson, L.T., Beaulieu, J.J. and Witter, J.D. 2012a. Floodplain restoration enhances denitrification and reach-scale nitrogen removal in an agricultural stream. Ecological Applications 22, 281-297, doi: 10.1890/11-0381.1.

Roley, S.S., Tank, J.L. and Williams, M.A. 2012b. Hydrologic connectivity increases denitrification in the hyporheic zone and restored floodplains of an agricultural stream. Journal of Geophysical Research-Biogeosciences 117, doi: 10.1029/2012jg001950.

Ruban, V., López-Sánchez, J., Pardo, P., Rauret, G., Muntau, H. and Quevauviller, P. 2001. Harmonized protocol and certified reference material for the determination of extractable contents of phosphorus in freshwater sediments–A synthesis of recent works. Fresenius' journal of analytical chemistry 370, 224-228, doi: 10.1007/s002160100753.

Ruban, V., López-Sánchez, J.F., Pardo, P., Rauret, G., Muntau, H. and Quevauviller, P. 1999. Selection and evaluation of sequential extraction procedures for the determination of phosphorus forms in lake sediment. Journal of Environmental Monitoring 1, 51-56, doi: 10.1039/A807778I.

Ruttenberg, K.C. 1992. Development of a Sequential Extraction Method for Different Forms of Phosphorus in Marine Sediments. Limnology and Oceanography 37, 1460-1482.

Ryan, P. 2014. Environmental and low temperature geochemistry. WILEY, Hoboken, 426 p.

Saarnisto, M. 2000. Shoreline displacement and emergence of lake basins. Special Paper of the Geological Survey of Finland 29, 25-34.

Sah, R.N. and Mikkelsen, D.S. 1986. Sorption and bioavailability of phosphorus during the drainage period of flooded-drained soils. Plant and Soil 92, 265-278.

Sah, R.N. and Mikkelsen, D.S. 1989. Phosphorus Behavior in Flooded-Drained Soils. I. Effects on Phosphorus Sorption. Soil Science Society of America Journal 53, 1718-1722, doi: 10.2136/sssaj1989.03615995005300060018x.

Scholtysik, G., Dellwig, O., Roeser, P., Arz, H.W., Casper, P., Herzog, C., Goldhammer, T. and Hupfer, M. 2020. Geochemical focusing and sequestration of manganese during eutrophication of Lake Stechlin (NE Germany). Biogeochemistry 151, 313-334, doi: 10.1007/s10533-020-00729-9.

SFS3008. 1981. Veden, lietteen ja sedimentin kuiva-aineen ja hehkutusjäännöksen määritys. Finnish Standards Associations SFS, 2 p.

SFS6878. 2004. Water quality. Determination of phosphorus. Ammonium molybdate spectrometric method. Finnish Standards Association SFS, 24 p.

Smith, V.H. 2003. Eutrophication of freshwater and coastal marine ecosystems a global problem. Environmental Science and Pollution Research 10, 126-139, doi: 10.1065/espr2002.12.142.

Smith, V.H., Joye, S.B. and Howarth, R.W. 2006. Eutrophication of Freshwater and Marine Ecosystems. Limnology and Oceanography 51, 351-355.

Sohlenius, G. and Öborn, I. 2004. Geochemistry and partitioning of trace metals in acid sulphate soils in Sweden and Finland before and after sulphide oxidation. Geoderma 122, 167-175, doi: 10.1016/j.geoderma.2004.01.006.

Soinne, H., Räty, M. and Hartikainen, H. 2010. Effect of air-drying on phosphorus fractions in clay soil. Journal of Plant Nutrition and Soil Science 173, 332-336, doi: 10.1002/jpln.200900225.

SPSS Inc. 2021. IBM SPSS Statistics for Windows, Version 28.0. IBM Corporporation. Armonk, New York.

Tammeorg, O., Nürnberg, G.K., Nõges, P. and Niemistö, J. 2022. The role of humic substances in sediment phosphorus release in northern lakes. Science of The Total Environment 833, 155257, doi: 10.1016/j.scitotenv.2022.155257.

The National Land Survey of Finland, 2023. Elevation model 2 m. Accessed 23 April 2023. https://asiointi.maanmittauslaitos.fi/karttapaikka/tiedostopalvelu/korkeusmalli.

The National Land Survey of Finland, 2023. Laser scanning data 0,5 p. Accessed 23 April 2023. https://asiointi.maanmittauslaitos.fi/karttapaikka/tiedostopalvelu/laserkeilausaineisto_05

Tikkanen, M. and Oksanen, J. 2002. Late Weichselian and Holocene shore displacement history of the Baltic Sea in Finland. Fennia - International Journal of Geography 180, 9-20.

Trentman, M.T., Tank, J.L., Jones, S.E., McMillan, S.K. and Royer, T.V. 2020. Seasonal evaluation of biotic and abiotic factors suggests phosphorus retention in constructed floodplains in three agricultural streams. Science of The Total Environment 729, 138744, doi: 10.1016/j.scitotenv.2020.138744.

Uusitalo, R., Ylivainio, K., Hyväluoma, J., Rasa, K., Kaseva, J., Nylund, P., Pietola, L. and Turtola, E. 2012. The effects of gypsum on the transfer of phosphorus and other nutrients through clay soil monoliths. Agricultural and food science 21, 260-278, doi: 10.23986/afsci.4855.

van der Grift, B., Osté, L., Schot, P., Kratz, A., van Popta, E., Wassen, M. and Griffioen, J. 2018. Forms of phosphorus in suspended particulate matter in agriculture-dominated lowland catchments: Iron as phosphorus carrier. Science of The Total Environment 631-632, 115-129, doi: 10.1016/j.scitotenv.2018.02.266.

Västilä, K., Järvelä, J. and Koivusalo, H. 2016. Flow-Vegetation-Sediment Interaction in a Cohesive Compound Channel. Journal of Hydraulic Engineering 142, 11, doi: doi:10.1061/(ASCE)HY.1943-7900.0001058.

Vepraskas, M.J., Richardson, J.L., Tandarich, J.P. and Teets, S.J. 1999. Dynamics of hydric soil formation across the edge of a created deep marsh. Wetlands 19, 78-89, doi: 10.1007/BF03161736.

Walling, D.E. and Bradley, S.B. 1989. Rates and patterns of contemporary floodplain sedimentation: A case study of the river Culm, Devon, UK. GeoJournal 19, 53-62, doi: 10.1007/BF00620549.

Williams, L.L. and Lück-Vogel, M. 2020. Comparative assessment of the GIS based bathtub model and an enhanced bathtub model for coastal inundation. Journal of Coastal Conservation 24, 23, doi: 10.1007/s11852-020-00735-x.

Wyant, K.A., Corman, J.E. and Elser, J.J. 2013. Phosphorus, Food, and Our Future. Oxford University Press, New York, p.

Yang, F., Tang, Y., Mi, Y., Jiang, L., Luo, P. and Yang, Y. 2022. Mn(II) Sorption on Stream Sediments Sampled in Manganese Mining Area: Dynamics and Mechanisms. Journal 12, 3368. 10.3390/app12073368.

Yli-Halla, M., Puustinen, M. and Koskiaho, J. 1999. Area of cultivated acid sulfate soils in Finland. Soil Use and Management 15, 62-67, doi: 10.1111/j.1475-2743.1999.tb00065.x.

9. APPENDICES

Appendix 1. Sediment trap results for loss on ignition (LOI), C:LOI and C:N ratios. Very high organic matter content (LOI) relative to other traps with-in respective site and referred to in text are highlighted in bold.

Site	Sample	LOI	C:LOI	C:N
Pipakallionsuo	Loppi_1_2022	40.41	0.51	17.61
Pipakallionsuo	Loppi_2_2022	**78.68**	0.55	20.06
Pipakallionsuo	Loppi_3_2022	48.23	0.54	22.37
Pipakallionsuo	Loppi_4_2022	38.24	0.50	16.83
Pipakallionsuo	Loppi_7_2022	38.01	0.50	16.56
Pipakallionsuo	Loppi_8_2022	**70.49**	0.53	23.69
Pipakallionsuo	Loppi_9_2022	39.18	0.51	19.06
Pipakallionsuo	Loppi_10_2022	31.65	0.49	16.03
Ritobäcken	M1W_A_2022	11.18	No data	No data
Ritobäcken	M1W_A_2021	17.66	0.32	13.28
Ritobäcken	M1W_B_2022	7.14	0.45	13.30
Ritobäcken	M1W_B_2021	12.05	0.42	13.23
Ritobäcken	M1W_C_2022	10.92	0.36	13.26
Ritobäcken	C1_A_2022	10.89	0.35	11.19
Ritobäcken	C1A_2021	11.41	0.40	13.43
Ritobäcken	C1B_2021	11.65	0.43	14.37
Ritobäcken	C1_C_2022	10.50	0.34	11.88
Ritobäcken	C2_A_2022	10.23	0.35	11.32
Ritobäcken	C2_B_2022	10.92	0.36	10.57
Ritobäcken	C2_C_2022	9.28	0.45	11.64
Ritobäcken	M3_A_2022	6.50	0.43	12.03
Ritobäcken	M3_B_2022	9.65	0.39	12.85
Ritobäcken	M3_C_2022	7.62	0.41	13.56
Uuhikonoja	UO_2022	7.47	0.31	11.68
Uuhikonoja	UX_2022	8.05	0.31	11.23
Uuhikonoja	UY_2022	7.52	0.27	11.26
Uuhikonoja	UP_2022	9.48	0.33	11.50
Uuhikonoja	UA_2022	7.04	0.26	10.27
Uuhikonoja	UB_2022	**12.07**	0.41	11.26
Uuhikonoja	US_2022	6.22	0.27	12.61
Uuhikonoja	UT_2022	5.99	0.24	11.86

Appendix 2. Ritobäcken sediment core and sediment trap PCA factor loadings and cumulative variance explained for Figure 23. PCA was performed on centered-log-ratio (CLR) transformed variables.

	PC1	PC2	PC3	PC4	PC5	PC6
Mg	0.254	-0.154	-0.890	-0.268	0.149	0.026
Al	0.431	0.315	0.090	0.044	-0.165	0.325
K	0.113	0.547	-0.170	0.474	0.143	-0.617
P	0.332	-0.366	0.374	-0.340	0.420	-0.457

	PC1	PC2	PC3	PC4	PC5	PC6
S	-0.499	0.142	0.011	-0.222	-0.178	0.050
Fe	0.401	0.342	0.166	-0.074	0.342	0.453
Zn	0.459	-0.129	0.050	-0.068	-0.774	-0.217
Mn	0.081	-0.539	-0.023	0.726	0.077	0.220
Cumulative proportion	0.462	0.787	0.892	0.942	0.976	0.994

Appendix 3. Sediment trap PCA factor loadings and cumulative variance explained for Figure 33. PCA performed on centered-log-ratio (CLR) transformed data.

	PC1	PC2	PC3	PC4	PC5
Na	0.88	-0.16	-0.02	-0.20	-0.17
Mg	0.99	-0.04	0.07	0.06	0.03
Al	0.98	-0.06	0.09	0.05	0.05
K	0.97	-0.08	-0.04	0.14	-0.06
Ti	0.93	-0.13	0.15	0.25	0.07
P	-0.95	0.22	0.10	0.02	0.11
S	-0.92	-0.33	-0.08	0.05	-0.01
V	0.96	-0.11	0.18	0.05	0.09
Cr	-0.37	0.76	-0.36	0.10	0.12
Fe	0.88	0.28	0.24	0.09	0.13
Co	0.85	-0.40	0.04	-0.22	0.15
Ni	0.98	0.08	-0.08	0.06	0.00
Cu	0.70	0.11	-0.37	-0.36	-0.14
Zn	0.55	0.27	-0.64	0.34	0.06
Mn	0.42	-0.63	-0.13	-0.36	0.26
Sr	-0.64	0.63	-0.06	-0.12	0.29
Zr	0.90	0.25	-0.03	0.22	0.15
As	0.20	0.49	0.66	-0.12	0.40
Mo	-0.95	0.00	0.01	0.14	0.20
Cd	-0.69	-0.48	-0.15	0.22	0.21
Pb	0.60	-0.29	-0.38	0.39	0.43
U	0.66	0.61	0.27	-0.15	0.20
N	-0.99	0.01	-0.01	0.08	0.03
C	-0.99	0.04	-0.01	0.03	0.05
Fe-P	-0.84	-0.26	0.25	-0.05	0.17
Al-P	-0.94	-0.11	-0.05	0.17	0.04
Ca-P	0.12	-0.58	0.56	0.39	0.01
Res.Org-P	0.18	0.42	0.30	0.42	-0.47
TP-SEDEX	-0.78	-0.02	0.27	-0.03	-0.11
Cumulative % of variance	63.51	75.65	82.83	87.17	90.79

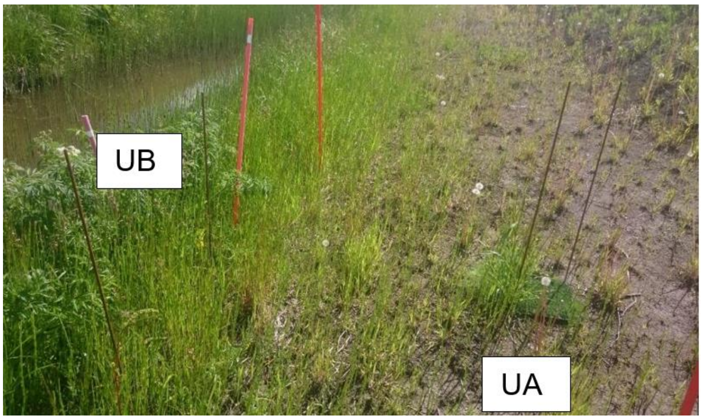

Appendix 4. Uuhikonoja sediment trap locations UB_2022 (left) and UA_2022 (right) before sample collection 21.6.2022. UB_2022 was the only sediment trap in Uuhikonoja covered by thick vegetation. Also, the sediment trap corner marking brown steel poles visible that could affect the sediment accumulation by trapping vegetation.